의학박사 학위논문

CITED2 의 뉴클레오린-AKT 신호전달 활성화를 통한 전립선암 전이 촉진

CITED2 enhances prostate cancer metastasis by activating nucleolin-AKT pathway

2019 년 2 월

서울대학교 대학원
의과학과 약리학전공
신 승 현

A thesis of the Degree of Doctor of Philosophy

CITED2 enhances prostate cancer metastasis by activating nucleolin-AKT pathway

CITED2 의 뉴클레오린-AKT 신호전달 활성화를 통한 전립선암 전이 촉진

February 2019

The Department of Biomedical Science,
Seoul National University
College of Medicine
Seung-Hyun Shin

ABSTRACT

Despite many efforts to develop hormone therapy and chemotherapy, no effective strategy to suppress prostate cancer metastasis has been established because the metastasis is not well understood. I here investigate a role of CBP/p300-interacting transactivator with E/D-rich carboxy-terminal domain-2 (CITED2) in prostate cancer metastasis. CITED2 is highly expressed in metastatic prostate cancer, and its expression is correlated with poor survival. The CITED2 gene is highly activated by ETS-related gene that is overexpressed due to chromosomal translocation. CITED2 acts as a molecular chaperone to guide PRMT5 and p300 to nucleolin, thereby activating nucleolin. Informatics and experimental data suggest that the CITED2-nucleolin axis is involved in prostate cancer metastasis. This axis stimulates cell migration through the epithelial–mesenchymal transition and promotes cancer metastasis in a xenograft mouse model. Our results suggest that CITED2 plays a metastasis-promoting role in prostate cancer and thus could be a target for preventing prostate cancer metastasis.

Keywords: Prostate cancer, Metastasis, CITED2, AKT, ETS-related gene, PRMT5, P300, Post-translational modification

Student number: 2013-21776

CONTENTS

LIST OF TABLES AND FIGURES

LIST OF ABBREVIATIONS

CITED2: Cbp/p300−interacting transactivator 2

ChIP: Chromatin immunoprecipitation

EMT: epithelial-mesenchymal transition

ERG: ETS−related gene

ETS: erythroblast transformation−specific

GSE: Genomic Spatial Event

GSEA: Gene Set Enrichment Analysis

NCL: Nucleolin

PRMT5: Protein arginine N−methyltransferase 5

PCR: polymerase chain reaction

RioK1: RIO kinase 1

SBP: Streptavidin−Binding Peptide

TCGA: The Cancer Genomic Atlas

WDR77: WD repeat−containing protein 77

INTRODUCTION

Prostate cancer is the most frequently diagnosed cancer and the second leading cause of cancer-related death among males. Despite many efforts to develop hormone therapy and chemotherapy, the prognoses of patients with advanced prostate cancer remains poor, because these treatments cannot control cancer metastasis (1, 2). One of the most distinct features of prostate cancer is that more than half of the patients display gene fusion between androgen-responsive gene TMPRSS2 and ETS transcription factor genes such as ERG and ETV1 (3). TMPRSS2-ERG fusion is reported to promote cancer progression (4, 5), but the downstream mechanism is not clearly known.

CBP/p300-interacting transactivator with E/D-rich carboxy-terminal domain 2 (CITED2, also known as MRG1 and p35srj) is a transcriptional coregulator together with the transcriptional coactivator p300/CBP. Depending on its target gene, it functions as a positive or negative regulator of gene expression. For example, CITED2 acts as a coactivator of AP-2 transcription factors by recruiting p300/CBP to AP-2 target

genes (6). In contrast, CITED2 inhibits hypoxia-induced gene expression by preventing p300/CBP recruitment to the hypoxia-inducible factor 1α (HIF-1 α) (7). CITED2 interacts with other components besides the aforementioned proteins. CITED2 expression is induced by hypoxia, lipopolysaccharides, growth factors, and proinflammatory cytokines (8). CITED2 also plays essential roles in embryonic stem cell differentiation (9) and development of diverse organs, including liver (10), lung (11), heart (12), and lens (13). Furthermore, adult hematopoietic stem cell (HSC) functions are maintained by CITED2 via lnk4a/Arf and Trp53 (14), and acute myeloid leukemia critically requires CITED2 expression (15). However, only a few investigations have been conducted on the role of CITED2 in tumor development during the last decade. CITED2 was reported to promote tumorigenesis of Rat1 cells (8) and growth of lung cancer cells (16). However, CITED2 inhibited proliferation of colon cancer cells (17), and low expression of CITED2 was associated with a poor prognosis in breast cancer (18). In particular, CITED2 is suspected to be extensively involved in prostate cancer, since its expression is induced by an ETS family member ELK1 (19), which has been reported to recruit AR to

activate growth signaling in prostate cancer cells (20). In this study, I performed co-immunoprecipitation and shotgun proteomics to discover a CITED2-interacting protein, and identified nucleolin. Nucleolin is an RNA-binding nulceolar protein, which has been reported to stimulate cancer progression and metastasis (21-23), although the exact underlying mechanism has not been determined.

Nucleolin is widely known to regulate rRNA transcription of the engrafting complex of pre-ribosomes. Nucleolin binds to non-transcribed spacers of rDNA transcription initiation sites or interacts with histone-1 to induce de-condensation of chromatin structures (24, 25). Nucleolin also forms the pre-rRNA processing complex by recruiting U3 snoRNP (26, 27). Moreover, Nucleolin promotes translation of target mRNAs by binding to their G-rich mRNA coding regions to facilitate polysome formation on transcripts (28). Nucleolin consists of three functional domains: the N-terminal domain composed of highly acidic regions intermixed with basic regions, the RNA-binding domain, and the glycine- and arginine-rich domain. Nucleolin is post-translationally modified by casein kinase 2 and $p43^{cdc2}$, which phosphorylate nucleolin at serine residues within the

acidic regions (29) and at threonine residues within the basic regions, respectively (30). These phosphorylation events of nucleolin are regulated throughout the cell cycle. Notably, P300-mediated acetylation (31) and PRMT5-mediated methylation (32) of nucleolin have also been reported, but no studies have been conducted on the oncogenic functional changes induced by these post-translational modifications of nucleolin.

In the present study, I found that CITED2 was highly expressed in metastatic prostate cancer because of *TMPRSS2-ERG* gene fusion, which promoted metastasis by activating nucleolin at the post-translational level. I also propose that the CITED2-nucleolin signaling pathway is a potential target for treating prostate cancer metastasis.

MATERIALS AND METHODS

Reagents and antibodies

Antibodies against CITED2, PRMT5, β-tubulin, WDR77, RioK1, p300, β-CTN, Vimentin, TWIST, Snail, N-Cad and ZEB1 were purchased from Santa Cruz Biotechnology (Santa Cruz, CA); anti-nucleolin, anti-dimethyl-arginine and anti-acetyl-lysine from Upstate Biotechnology (Lake Placid, NY); anti-p-AKT, anti-AKT and anti-E-cadherin from Cell Signaling (Danvers, MA); anti-FLAG, anti-MYC and anti-HA from Sigma-Aldrich (St. Louis, MO); anti-ERG and anti-α-SMA from Abcam (Cambridge, MA). MK2206 was purchased from Selleckchem. Human recombinant proteins of CITED2, PRMT5, P300, nucleolin were purchased from Origene. Fetal bovine serum (FBS), dithiothreitol (DTT), G418 disulfate salts (G418), EPZ015666, Leptomycin B, Bay-11-7082, LY294002, Cycloheximide, Wortmannin and others were obtained from Sigma-Aldrich.

siRNAs and plasmids

The nucleotide sequences (5' to 3') of siRNAs are;

UUAUGUCCUUGGUGAUAGATT for CITED2 (NM_006079), AGACUAUAGAGGUGGAAAGAAAGC for nucleolin (NM_005381), AUGAUGUUGAUAAAGCCU, CGUCCUCAGUUAGAUCCU and CCACGGUUAAUGCAUGCU for ERG #1~3 (NM_001136154), GGACUGGAAUACGCUAAU for PRMT5 (NM_001039619), GACAAAACCGUGGAAGUA for p300 (NM_001429), CCUCACAGCCCUGAAGUACUCUUTC for AKT (NM_005163) and AUGAACGUGAAUUGCUCAA for non-targeting control. The cDNAs of CITED2, nucleolin, luciferase, luciferase-CITED2 were cloned by reverse transcription and PCR using Pfu DNA polymerase, and the cDNAs were inserted into pcDNA, Myc-tagged, FLAG-tagged, HA-tagged, or FLAG/streptavidin-binding protein (SBP)-tagged vectors by blunt-end ligation. TRC lentiviral shRNA targeting CITED2 or nucleolin were purchased from Dharmacon (Lafayette, CO).

Cell lines and cell culture

HEK293T (human embryonic kidney) and human prostate cancer (PC3, DU145, VCaP, LNCaP, C42B, and 22RV1) cell lines were obtained from the American Type Culture Collection (Manassas, VA). Mycoplasma contamination was routinely

tested when cell growth or shape was changed. The cell lines were cultured in RPMI1640 or DMEM supplemented with 10% heat-inactivated FBS in a 5% CO_2 humidified atmosphere at 37° C. Luciferase-expressing and luciferase/CITED2-coexpressing PC3 stable cell lines were established from five G418-resistant clones per cell line. The expression of luciferase has been confirmed with luciferase assay.

Immunoblotting and immunoprecipitation

Cell lysates were separated on SDS-polyacrylamide gels, and transferred to Immobilon-P membranes (Millipore; Bedford, MA). Membranes were blocked with a Tris/saline solution containing 5% skim milk and 0.1% Tween-20 for 1 hour, and incubated with a primary antibody overnight at 4° C. Membranes were incubated with a horseradish peroxidase-conjugated secondary antibody for 1 hour, and visualized using the ECL kit (Thermo; Rockford, IL). To analyze protein interactions, cell lysates were incubated with anti-CITED2, anti-Flag or anti-Ac-K or dimethyl-R antibody for 4 hours at 4° C, and the immune complexes were precipitated with protein A/G beads (Santa Cruz, CA). Precipitated proteins were eluted in a

denaturing 2xSDS sample buffer, loaded on SDS-PAGE, and immunoblotted.

Immunohistochemistry (IHC) of Human Prostate Cancer Tissue array

Human prostate cancer tissue arrays were purchased from SuperBioChips Lab (Seoul, South Korea). Tumor staging was defined according to the AJCC cancer staging manual (7^{th} edition) (33). The array slides were dried for 1 hour in an oven at 60° C, dewaxed, and autoclaved in an antigen retrieval solution. Tissue sections were treated with 3% H_2O_2, and then incubated with a primary antibody (against CITED2, ERG or p-AKT) overnight at 4° C, and with a biotinylated secondary antibody for 1 hour at room temperature. The immune complexes were visualized using the Vectastatin ABC kit (Vector Laboratories, Burlingame, CA), and tissue slides were counterstained with hematoxylin for 10 min. The immune-stained cells were counted at 4 high-power fields for each tissue.

Immunofluorescence

Cells grown on cover slides were fixed with methanol for 30

min, permeabilized with 0.1% Triton X-100 for 10 min, blocked by 3% BSA for 2 h, and then incubated with a primary antibody in the dark overnight at 4° C. The slides were incubated with Alexa Flour® 488 IgG anti-mouse/rabbit (green, 1:200), Alexa Flour® 568 IgG anti-goat (red, 1:200), Alexa Flour® 647 IgG anti-mouse (purple, 1:200), or Alexa Flour® 633 phalloidin (F-actin) solution in the dark for 1 h. Then, nuclei were stained with 4',6-diamidino-2-phenylindole (DAPI) for 10 min. Fluorescence images were photographed using confocal microscopy.

Orthotopic Xenograft Mouse Model

All animal studies were carried out according to the proposed protocol approved by the Seoul National University Institutional Animal Care and Use Committee (No. 150629-4-1). PC3 prostate cancer cells were transfected with the luciferase-IRES-EGFP or the luciferase-IRES-CITED2 plasmid and treated with G418 to select stable cell lines. Male 8 weeks old Balb/cSlc-nu/nu mice are used for orthopotic xenografts. We opened the low midline abdomen of mouse with 3-4 mm incision, and smoothly pressed the bladder using sterile cotton swab to

find the prostate. The PC3 stable cell lines were injected into the ventral lobe of prostate. After 14 days, shRNA lentiviruses were injected into grafted tumors, and tumor growth and metastasis were monitored using Xenogen IVIS® Lumina.

Informatics analysis

Publicly available prostate cancer microarray dataset GSE6919 was analyzed to compare CITED2 and nucleolin mRNA levels between normal and cancer tissues. All tissues (n = 171) were grouped as four classes: normal prostate tissues free of any pathological alteration (n=18), normal prostate tissues adjacent to tumors (n=63), primary prostate tumors (n=65), and metastatic prostate tumors (n=25). The values of the 33113_at probe (corresponding to CITED2), the 32590_at (corresponding to nucleolin) on each group were calculated and compared between the four groups using the Pearson correlation. The prostate cancer gene set enrichment analysis (GSEA) was also performed using GSE6919 data set, and a formatted GCT file was used as input for the GSEA algorithm v2.0 (available from: http://www.broadinstitute.org/gsea). For grouping the GSE6919 data set, the values of the 33113 or 32590_at probe were used

as criteria standard for low expression and high expression group. CITED2 mRNA expression in 28 different type of cancer were obtained from using The Cancer Genome Atlas (TCGA), each cancer provisional data sets are based on generated by TCGA Research Network (http://cancergenome.nih.gov). The abbreviations used in Fig. 1a and the number of patients are as follows. ACC, Adrenocortical Carcinoma (n = 79); Bladder, Bladder Urothelial Carcinoma (n = 408); Glioma, Brain Lower Grade Glioma (n = 530); Breast, Breast Invasive Carcinoma (n = 1100); Cervical, Cervical Squamous Cell Carcinoma and Endocervical Adenocarcinoma (n = 306); Cholangiocarcinoma n = 36); Colorectal, Colorectal Adenocarcinoma (n = 382); GBM, Glioblastoma Multiforme (n = 166); Head & neck, Head and Neck Squamous Cell Carcinoma (n = 522); chRCC, Kidney Chromophobe (n = 66); ccRCC, Kidney Renal Clear Cell Carcinoma (n = 534); Liver, Liver Hepatocellular Carcinoma (n = 373); Lung adeno, Lung Adenocarcinoma (n = 517); Lung squ, Lung Squamous Cell Carcinoma (n = 501); DLBC, Lymphoid Neoplasm Diffuse Large B-cell Lymphoma (n = 48); Mesothelioma (n = 87); Ovarian, Ovarian Serous Cystadenocarcinoma (n = 307); Pancreas, Pancreatic

Adenocarcinoma (n = 179); PCPG, Pheochromocytoma and Paraganglioma (n = 184); Prostate, Prostate Adenocarcinoma (n = 498); Sarcoma (n = 263); Melanoma, Skin Cutaneous Melanoma (n = 472); Testicular Germ Cell, Testicular Germ Cell Cancer (n = 156); Thymoma (n = 120); Thyroid, Thyroid Carcinoma (n = 509); Uterine CS, Uterine Carcinosarcoma (n = 57); Uterine, Uterine Corpus Endometrial Carcinoma (n = 177); Uveal Melanoma (n = 80).

Fractionation of cytoplasmic and nuclear components

Cells were spun down at 800 x g for 5 min, and gently homogenized in a hypotonic solution containing 20 mM Tris/HCl (pH 7.8), 1.5 mM $MgCl_2$, 10 mM KCl, 0.2 mM EDTA, 0.5% NP-40, 0.5 mM dithiotheritol, and 0.5 mM PMSF. The cell lysates were centrifuged at 3000 x g for 10 min at 4° C, and the supernatant was collected as the cytosolic fraction. The pellet was resuspended in a hypertonic solution containing 20 mM Tris/HCl (pH 7.8), 400 mM NaCl, 1 mM EDTA, 1.5 mM $MgCl_2$, 10% glycerol, 0.5 mM dithiotheritol, and 0.5mM PMSF, and intermittently vortexed on ice for 30 min. After the suspension was centrifuged at 18000 x g for 20 min at 4° C, the supernatant

was collected as the nuclear fraction.

Cell viability assay

Cells were grown in 98-well culture plates, and incubated with 100 μL/well of the MTT labeling reagent (Sigma-Aldrich) for 3 h. Blue formazan crystals were solubilized with acidified isopropanol, and formazan levels were determined at 570 nm.

Fast protein liquid chromatography

FPLC analysis was performed on Preparative Biomolecular Purification System equipped with AKTA explorer 10 and Superdex 200 10/300 GL column (GE Healthcare, Uppsala, Sweden). After transfected with CITED2 or empty vector, the cells were centrifuged at 800 x g for 5 min, and resuspended with a lysis buffer consist of 20 mM Tris/HCl (pH 7.5), 150mM NaCl, 1 mM EDTA, 0.5% NP-40, 0.5 mM PMSF and protease inhibitor. The cell lysates were centrifugated at 4000 x g for 10 minutes to separate into pellet and supernatant. Transfer supernatant and collect it for FPLC analysis. 100μl of protein elusion was continuously monitored at 280 nm using a UV detector. To estimate molecular weight of proteins in each

fraction, the Sigma-Aldrich FPLC protein markers (29 kDa – 700 kDa) were run on FPLC in the same condition. All procedures were carried out at 4° C. Each elute was subjected to immunoblotting with antibodies against nucleolin, PRMT5, WDR77, CITED2, P300, and RioK1.

Migration and invasion assays

PC3 or DU145 cells were cultured in 24-well transwell plates with an 8.0-μm polycarbonate membrane which were purchased from Corning Life Science (Acton, MA). The lower chamber was filled with a culture medium containing 10% FBS as a chemo-attractant. For cell migration analysis, PC3 or DU145 cells in an FBS-free medium were seeded into the upper chamber and incubated at 37° C for 12 h. For cell invasion analysis, the polycarbonate membrane was coated with 0.5 mg/ml of Matrigel. Cells on the upper surface of the interface membrane were removed using a cotton swab. Migrating cells on the lower surface of the membrane were stained with hematoxylin and eosin, and counted under an optical microscope at a 100x magnification.

Quantitative RT-PCR

Total RNA was isolated using TRIZOL reagent (Invitrogen; Carlsbad, CA), and cDNA synthesis was carried out in a reaction mixture (Promega, Madison, WI) containing M-MLV Reverse Transcriptase, RNase inhibitor, dNTP, and random primers at 46° C for 1 h. Quantitative real-time PCR on 96-well optical plates was performed in the qPCR Mastermix (Enzynomics, Daejeon, Korea), and fluorescence emitting from dye-DNA complex was monitored in CFX Connect Real-Time Cycler (BIO-RAD, Hercules, CA). The mRNA values of targeted genes were calculated relative to GAPDH expression. All reactions were performed in triplicate. The nucleotide sequences of PCR primers are summarized in Table 2.

RNA inmunoprecipitation

RNA immunoprecipitation (RIP) was conducted using the Magna RIP™ RNA-binding protein immunoprecipitation kit (EMD Millipore, Billerica, MA). Cells were spun down and homogenized in a RIP lysis buffer containing a protease inhibitor cocktail and RNase inhibitor. After cell lysates were centrifuged at 18000 x g for 10 min, the supernatant was incubated with IgG or anti-

nucleolin antibody in RIP inmmunoprecipitation buffer overnight at 4° C, followed by incubation with protein A/G magnetic beads. The immune complexes were precipitated using a magnetic separator, and incubated in a protein degradation buffer containing 10% SDS and proteinase K at 55° C for 30 min. The samples were mixed with 400 μL of phenol:chloroform:isoamyl alcohol and centrifuged at 18000 x g for 10 min to separate the phases. The aqueous phase (350 μL) was mixed with 400 μL of chloroform, and centrifuge at 18000 x g for 10 min. The aqueous phase (300 μL) was mixed with 50 μL of salt solution I/II, 5 μL of precipitation enhancer and 850 μL of absolute ethanol, and centrifuged at 18000 x g for 30 min at 4° C. The pellet was washed with 80% ethanol, and resolved in 20 μL of RNase-free water. The level of AKT mRNA in the sample was quantified by RT-qPCR and represented as percentage of IP/input signal (% input). All reactions were performed in triplicate.

Chromatin immunoprecipitation (ChIP)

Cells were fixed with 37% formaldehyde at 37° C for 10 min, treated with 150 mM glycine. Fixed cells were lysed with 0.5% NP-40, and centrifuged at 800 x g at 4° C for 10 min to collect

crude nuclear fraction. Nucleus pellet was incubated with 1% SDS and sonicated to shear genomic DNAs into 300-500bp fragments. Soluble chromatin complexes were immunoprecipitated with IgG or anti-ERG antibody overnight at 4° C. Immune complexes were precipitated with protein A/G beads pre-blocked by salmon sperm DNA at 4° C for 4 h. The beads were sequentially washed with a low salt buffer, a high salt buffer, LiCl wash buffer, and TE buffer. The immunoprecipitation chromatin complexes were eluted in a ChIP direct elution buffer at 65° C for 30 min and incubated overnight at 65° C to cross-link chromatin complex. DNAs were isolated by phenol-chloroform-isoamylalcohol (25:24:1) and precipitated with ethanol and glycogen. The extracted DNAs were resolved in nuclease-free water and analyzed by real-time PCR (95° C/55° C/72° C, 30 sec at each phase).

Statistical analysis

All data were analyzed using Microsoft Excel 2013 software or Graph pad Prism 5 software, and results were expressed as means and standard deviations. I used the unpaired, two-sided Student t-test or Mann-Whitney U test to compare protein

expression level, mRNA expression level, cell viability, ROI flux, and cell numbers. Statistical significances were considered when P values were less than 0.05. And also, Protein or mRNA expression correlations were analyzed using a Spearman's p statistic, Survival rate analysis were performed by drawing curves and calculating log-rank P test using The Kaplan-Meier method.

Data availability

The authors declare that all data supporting the findings of this study are available within the article and its supplementary information files or from the corresponding author upon reasonable request. Raw data file for LC-MS/MS is included in Table 1. Raw data files for RNA-seq have been deposited in the NCBI Gene Expression Omnibus database under the accession code GSE119113.

RESULTS

CITED2 is highly expressed in metastatic prostate cancer.

I examined CITED2 expression in 28 different types of cancer using the TCGA database and found relatively high CITED2 mRNA levels in thyroid, kidney, ovarian, lung, prostate, breast, and lung cancers (Fig. 1A). I next compared CITED2 levels between normal and cancer tissues using the Genomic Spatial Event (GSE) database. Of six types of cancers evaluated, CITED2 was elevated only in prostate cancer compared with normal tissue (Fig. 1B). Prostate cancer patients from the TCGA database were categorized into CITED2_low and CITED2_high groups with respect to the median CITED2 expression value. Overall survival was lower in the CITED2_high group than in the CITED2_low group (Fig. 1C). In thyroid, ovarian, lung, and breast cancers, CITED2 expression was not correlated with overall survival (Fig. 2A). In renal cell carcinoma (RCC), the CITED2_high group showed a longer survival than that of the CITED2_low group. To examine the involvement of CITED2 in prostate cancer progression, I determined CITED2 expression in primary tumor and metastatic tumor tissues and found that CITED2 expression was increased in metastatic tumors (Fig.

1D). CITED2 expression in other types of cancers was not significantly increased with tumor stage (Fig. 2B). To evaluate CITED2 expression at the protein level, immunohistochemistry (IHC) using an anti-CITED2 antibody was performed in human prostate cancer tissues, which were categorized according to their Gleason score. Increased CITED2 protein levels were associated with an increasing Gleason score (Fig. 3A). When the prostate cancer tissues were divided into the CITED2_high and CITED2_low groups, a lower tumor-free survival was evident in CITED2_high compared with CITED2_low (Fig. 3B). CITED2 expression might correlate with poor prognosis in prostate cancer patients.

ERG increases CITED2 expression at transcription level in prostate cancer.

The ETS genes are fused to the promoters of the androgen receptor target genes, leading to their high expression in prostate cancer cells (3, 34). Because ELK1 in the ETS family has been reported to transactivate the *CITED2* gene (19, 35), I examined which member in the ETS family is responsible for *CITED2* gene activation in prostate cancer. I compared the

mRNA levels of ETS members between normal prostate and prostate cancer tissues using the GSE6919 prostate cancer data set (Fig. 4A). Among those mRNAs, the ETS-related gene (ERG) level increased to the greatest extent in cancer tissues (Fig. 4B). The rate of gene fusion was highest to ERG among the ETS members according to the TCGA mutation sequence data (Fig. 5A). Immunoblotting analysis in various prostate cancer cell lines showed an apparent correlation between ERG and CITED2 expressions (Fig. 5B). Of the examined cell lines, VCaP harboring the TMPRSS2-ERG gene fusion expressed both ERG and CITED2 in the highest levels. When ERG was knocked down using three different siRNAs, the CITED2 protein and mRNA expression were both significantly downregulated in three cell lines, indicating ERG-dependent expression of CITED2 (Fig. 5C, 5D). In prostate cancer cells harboring the TMPRSS2-ERG fusion, ERG expression is known to be highly induced by testosterone. As expected, testosterone robustly induced ERG expression in VCaP cells, where CITED2 expression was subsequently increased. Such effects of testosterone were not observed in DU145 cells without the TMPRSS2-ERG fusion (Fig. 6). To examine the ERG binding to the CITED2 promoter, I

performed chromatin immunoprecipitation and quantitative PCR analyses. Among the three regions within the promoter, the second region was identified as an ERG-binding site (Fig. 7A). I then constructed a luciferase reporter plasmid containing the CITED2 promoter. Compared to PC3 and DU145 with a lower level of ERG, three prostate cancer cell lines with high ERG expression had greater luciferase activity (Fig. 7B). In these cell lines, CITED2 promoter activity was diminished by knocking-down ERG or by mutating the putative ERG binding motif (Fig. 7C). Next, I performed IHC to characterize ERG expression in prostate cancer tissues. The ERG level in prostate cancer increased with the Gleason score (Fig. 8A). Tumor-free survival in the ERG_high group was significantly lower compared with the ERG_low group (Fig. 8B). Pearson's correlation analyses showed that CITED2 expression was positively correlated with ERG expression (Fig. 8C). Furthermore, I performed PCR using DNAs extracted from prostate cancer tissues and detected *TMPRSS2-ERG* gene fusion in 15 of 49 prostate cancers (Fig. 9A). A chi-square test revealed that *TMPRSS2-ERG* gene fusion is associated with a high Gleason score (Fig. 9B). ERG and CITED2 overexpression in the *TMPRSS2-ERG* gene fusion

samples (Fig. 9C) further support the ERG-driven overexpression of CITED2 in prostate cancer cells.

CITED2 binds to a multimeric complex consisting of nucleolin, p300, and PRMT5.

To identify the CITED2-interacting proteins, I pulled down the FLAG/SBP-tagged CITED2 construct that was overexpressed in HEK293T cells using anti-FLAG or streptavidin affinity beads, and analyzed the co-purified proteins using LC-MS/MS. Proteins pulled down commonly by anti-FLAG antibody (red) and streptavidin (blue) are listed in Table 1. In addition to p300 and CBP, the PRMT5 complex subunits PRMT5, WDR77, and RIOK1, as well as nucleolin were co-purified with CITED2 (Fig. 10A). The interaction between PRMT5 and CITED2 was verified by immunoprecipitation and immunoblotting using HEK293T cells co-expressing MYC-PRMT5 and Flag/SBP-CITED2 (Fig. 10B). I analyzed the interactions among endogenous PRMT5, nucleolin, WDR77, RIOK1, and CITED2 and found that CITED2 and PRMT5 both interacted with nucleolin, WDR77, and RIOK1 (Fig. 11A). These protein interactions were confirmed in the immunoprecipitates using nucleolin, WDR77, or RIOK1

antibodies (Fig. 11B). As previously shown in HEK293T cells, these interactions were also identified in all prostate cancer cell lines examined (Fig. 12). To verify the presence of this multimeric complex, I separated intracellular proteins using fast protein LC. Standard protein markers were used to determine the molecular weight of each fraction (Fig. 13A). CITED2, PRMT5, nucleolin, WDR77, Riok1, and p300 were detected in the ~500 kDa fraction. Importantly, when CITED2 was overexpressed, the complex was shifted to ~700 kDa (Fig. 13B), which suggested that CITED2 plays a role in attracting proteins to the complex. To examine if CITED2, nucleolin, P300, and PRMT5 are directly associated, an *in vitro* binding assay was conducted using recombinant proteins. CITED2 directly interacted with nucleolin, P300 and PRMT5, while PRMT5 did not bind to P300 and nucleolin. Nucleolin and P300 were also bound directly (Fig. 14). Next, I performed immunofluorescent staining to determine the subcellular location of the proteins. The subunits in the complex were co-localized mainly in the nuclei of PC3 (Fig. 15A) or HEK293T cells (Fig. 15B). The interaction between PRMT5 and CITED2 was further characterized by immunoprecipitation of the domain peptides of CITED2 and PRMT5. p300, PRMT5, and

nucleolin were identified to bind to the transactivation domain (TAD), the serine/glycine-rich junction (SRJ), and the cysteine/arginine-rich domain 3 (CR3) of CITED2, respectively (Fig. 16A, 16B). In addition, CITED2 interacted with the N-terminus of PRMT5 (Fig. 17). Since CITED2 provides different binding sites for p300, PRMT5 and nucleolin, these proteins could form a stable complex in a noncompetitive manner. Therefore, I hypothesized that CITED2 acts as an essential binder to make the multimeric complex.

CITED2 modulates translocation of nucleolin through methylation and acetylation.

To examine whether CITED2 affects the subcellular localization of these subunits by forming a complex, I evaluated each subunit in the nuclear and cytoplasmic fractions of HEK293T cells overexpressing CITED2. CITED2 overexpression reduced nuclear expression of nucleolin but enhanced cytoplasmic expression, which was attenuated by a nuclear export inhibitor Leptomycin B (Fig. 18). This suggests that CITED2 induces the nuclear export of nucleolin. To determine role of CITED2 in the PRMT5/p300/nucleolin complex, immunoprecipitation was

performed using HEK293T cells with either CITED2 overexpression or silencing. Notably, PRMT5 and p300 binding to nucleolin were potentiated by CITED2 overexpression but weakened by CITED2 knockdown (Fig. 19). This result prompted us to determine whether CITED2 acts as a molecular chaperone to guide PRMT5 and p300 to nucleolin. As expected, nucleolin was arginine-dimethylated and lysine-acetylated by PRMT5 and p300, respectively (Fig. 20A, 20B). More importantly, both modifications were dependent on CITED2 (Fig. 21A, 21B). The CITED2-dependent modifications of nucleolin were attenuated by PRMT5 and p300 knockdown (Fig. 22A, 22B), which supports our hypothesis that CITED2 promotes post-translational modifications of nucleolin by recruiting PRMT5 and p300. Our next objective was to determine the subcellular location where CITED2-facilitated nucleolin modification occurs. The CITED2-dependent modifications of nucleolin were detected in the nuclear fraction, which was expected since nucleolin is present mainly in the nucleus (Fig. 23). Although the level of nucleolin protein was low in the cytoplasmic fraction compare to nuclear fraction, surprisingly, the dimethylated and acetylated nucleolin forms were clearly

detected in the same fraction (Fig. 23). The nuclear export of nucleolin was promoted by CITED2 overexpression, which was reversed by a PRMT5 inhibitor EPZ015666 (Fig. 24). These results suggest that nucleolin is modified in the nucleus and then translocated to the cytoplasm in part. The EGR-CITED2-PRMT5/p300-nucleolin pathway is summarized in Fig. 25.

The CITED2-nucleolin axis positively regulates EMT and cell migration in prostate cancer.

The cellular consequences of the CITED2-nucleolin axis were examined using gene set enrichment analyses. Prostate cancer tissues in the GSE6919 dataset were divided into low and high expression groups based on the mean CITED2 and nucleolin expression values (Fig. 26A). I identified the gene sets that were enriched in the high group compared with the low group (Fig. 26B). Several metastasis-related gene sets were among the top 10 gene sets enriched in the CITED2_high and nucleolin_high groups. To determine the role of the CITED2-nucleolin axis in cellular processes, I searched for gene sets commonly associated with CITED2 and nucleolin. Five of the top 10 common gene sets were related to metastasis (Fig. 27A). The enrichment

profiles of two representative gene sets associated with CITED2 and nucleolin expression are shown in Fig. 27B and those of other gene sets in Fig. 28A, 28B. To support the patient-derived gene set enrichment data, I conducted RNA-seq analysis in PC3 cells. CITED2 was knocked down in PC3 cells using siRNAs (Fig. 29A). To observe changes in gene expression pattern by CITED2 knockdown, heat map clustering was performed (Fig. 29B). I found that metastasis-related gene sets were more enriched in the control group than in the CITED2 knockdown group (Fig. 29C). Based on these results, I evaluated whether the CITED2-nucleolin axis is involved in prostate cancer cell migration. In phalloidin-stained PC3 and DU145 cells, lamellipodia were formed depending on CITED2 expression (Fig. 30A). The CITED2 and nucleolin expression levels in the cells were verified by Western blotting (Fig. 30B). And then, In Transwell® migration and invasion assays, CITED2 stimulated cell migration and invasion in a nucleolin-dependent manner (Fig. 30C and Fig. 30D). In addition, CITED2 increased the protein and mRNA levels of mesenchymal markers but decreased those of epithelial markers, and these effects of CITED2 were attenuated by knocking-down nucleolin (Fig. 31A, 31B). However, CITED2 or

nucleolin expression did not affect cell growth or viability in prostate cancer cells (Fig 32A–C). Taken together, these results strongly suggest that the CITED2–nucleolin axis enhances the metastatic potential, rather than cell growth, in prostate cancer cells.

The CITED2–nucleolin axis promotes prostate cancer metastasis in mice.

To characterize the *in vivo* role of the CITED2–nucleolin axis in metastasis, I established stable PC3 cell lines and implanted them into the prostates of male athymic nude mice (Fig. 33A). CITED2 overexpression (Fig. 33B), luciferase activity (Fig. 33C), and the degree of cell migration (Fig. 33D) were assessed in PC3 stable cell lines. The gene–silencing efficacies of lentiviruses harboring five different shRNAs targeting CITED2 or nucleolin were evaluated by Western blotting (Fig. 33E). The abdomens of the mice were opened 2 months after cell implantation, revealing strong growth of the xenografted tumors in the prostates (Fig. 34A). In tumor tissue homogenates obtained from mouse xenograft, protein expressions of CITED2 and nucleolin were measured to verify the overexpression or

knockdown of CITED2 and nucleolin (Fig. 34B). I monitored the bioluminescence emitted from cancer cells each week to trace the metastatic growth of the prostate tumors (Fig. 35). Compared with the control group, metastasis was enhanced in the CITED2-overexpressing group but reduced in the CITED2 knockdown group. The metastasis-promoting effect of CITED2 overexpression was abolished by nucleolin knockdown (Fig. 36A). Integrated values of ROI luminescence were used in statistical analyses of tumor growth and metastasis. The results showed that prostate tumor growth was delayed by CITED2 or nucleolin knockdown (Fig. 36B). Metastasis was significantly enhanced by CITED2 overexpression, and this effect was reversed by nucleolin knockdown (Fig. 37A). Furthermore, mouse survival was decreased by CITED2 overexpression but rescued by CITED2 or nucleolin knockdown (Fig. 37B). The CITED2 overexpression group showed significant body weight loss, suggesting that these mice might be cachectic (Fig. 37C). Representative images of liver metastases are shown in Fig. 37D. Based on these results, the CITED2-nucleolin axis may activate signaling pathway(s) that strongly induce cancer metastasis.

CITED2-activated nucleolin promotes the AKT-driven EMT by enhancing translation of AKT mRNA.

To explore the signaling pathway responsible for nucleolin-mediated EMT, I performed proteomic analyses of phosphoproteins and found that phospho-AKT was reduced most in nucleolin-knockdown cells (Fig. 38A, 38B). Nucleolin knockdown downregulated the protein levels of total AKT as well as phospho-AKT in prostate cancer cells (Fig. 39A), which occurred without any change in AKT mRNA levels (Fig. 39B). The CITED2-nucleolin axis was shown to affect the levels of AKT and phospho-AKT (Fig. 39C, 39D). CITED2 overexpression facilitated de novo synthesis of the AKT protein (Fig. 40A) but did not stabilize the protein (Fig. 40B). Moreover, mRNA processing genes were enriched in cells with altered CITED2 or nucleolin expression (Fig. 41A). These results prompted us to evaluate whether the CITED2-nucleolin axis regulates the translation of AKT mRNA. I immunoprecipitated nucleolin using anti-nucleolin antibody and quantified the amount of co-precipitated AKT mRNA by quantitative RT-PCR. The nucleolin-AKT mRNA interaction was enhanced by CITED2 overexpression but reduced by CITED2 knockdown (Fig. 41B).

Glyceraldehyde-3-phosphate dehydrogenase (GAPDH) mRNA was used as a negative control to verify the specificity of RNA immunoprecipitation. Because the interaction between nucleolin protein and AKT mRNA was attenuated by silencing PRMT5 or P300 even under CITED2 overexpression (Fig. 41C), CITED2 may have enhanced the nucleolin-AKT mRNA interaction via PRMT5-mediated methylation and P300-mediated acetylation of nucleolin. To check whether cell migration was stimulated due to enhancement of AKT translation mediated by CITED2, migration assay was conducted with AKT knockdown and CITED2 overexpression (Fig. 42A). Compared to the control, CITED2 overexpression increased migration in PC3 and DU145 cells, which was attenuated by AKT knockdown (Fig. 42B). Using three different PI3K inhibitors (Wortmannin, LY294002, and MK2206), I examined whether the AKT signaling pathway mediates CITED2-induced cell migration. As previously shown in Fig. 30C, CITED2-dependent cell migration was almost completely attenuated by each of these inhibitors (Fig. 43). In a similar manner, mRNA markers (Fig. 44A) and EMT protein (Fig. 44B) were no longer regulated by CITED2. Because AKT signaling promotes SNAIL expression via NF-kB activation (36),

I examined whether NF-kB mediates the CITED2-AKT-EMT signaling. CITED2-dependent cell migration and invasion both were abolished by an NF-kB inhibitor Bay-11-7082 (Fig. 45). IHC was used to determine if AKT is activated in prostate cancer tissues. Phospho-AKT expression increased concomitantly with an increase in the Gleason score (Fig. 46A) and was associated with poor survival of patients with prostate cancer (Fig. 46B). Pearson's correlation analyses revealed a significant positive correlation between phospho-AKT and CITED2 levels (Fig. 46C).

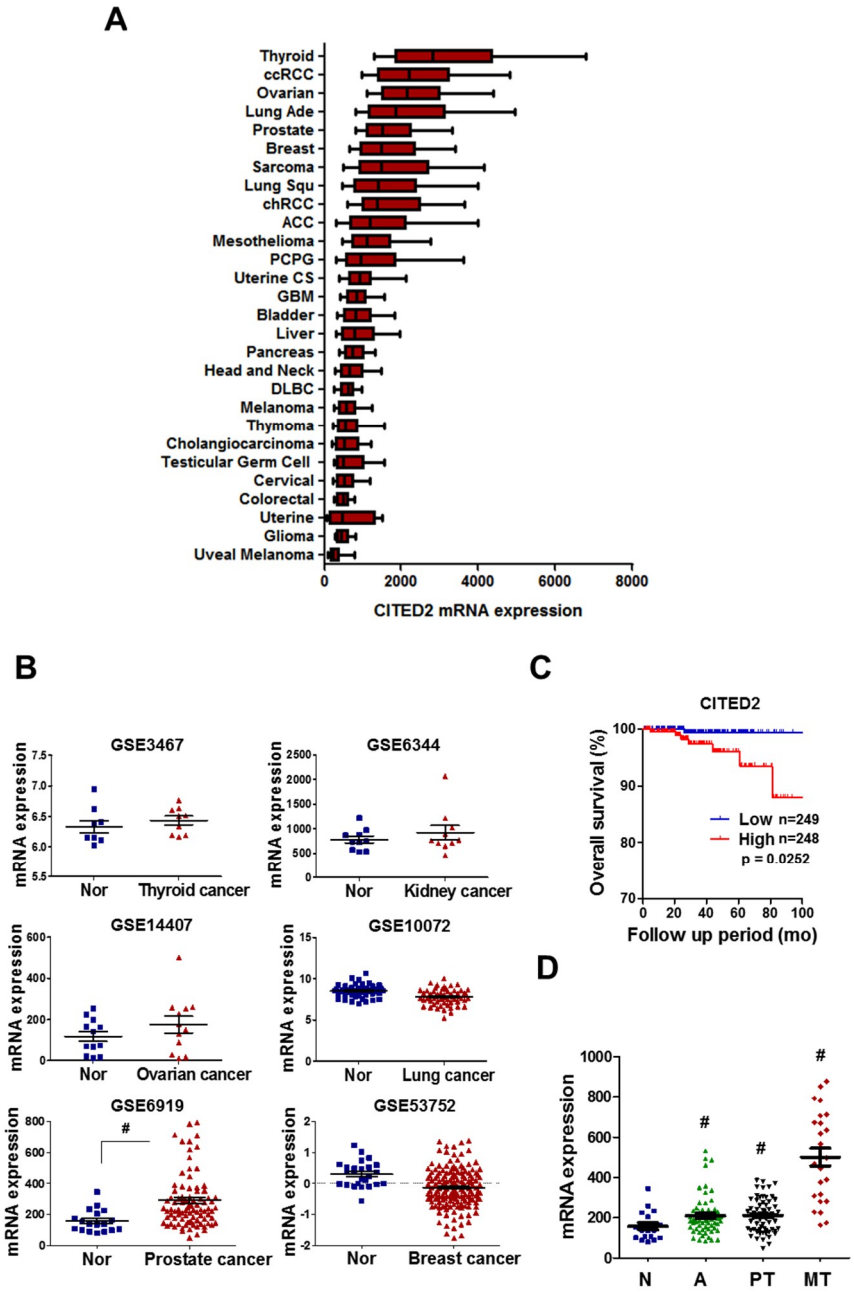

Figure 1. CITED2 is overexpressed in prostate cancer.

Figure 1. CITED2 is overexpressed in prostate cancer.

(A) CITED2 mRNA expression in 28 different type of cancer as determined by RNA Seq V2 RSEM. Box plots indicate the distribution of values and the middle thick line in the box shows mean value and whiskers represent 10-90 percentile. Results were obtained from using The Cancer Genome Atlas (TCGA), each cancer provisional data sets are based on generated by TCGA Research Network (http://cancergenome.nih.gov). The abbreviations and the number of patients are described in the method section. (B) CITED2 mRNA levels in normal (blue squares) and cancer tissues (red triangles) of thyroid, kidney, ovarian, lung, prostate, and breast (GSE datasets). (C) Kaplan-Meier overall survival analysis of prostate cancer patients on TCGA. P-value was calculated by Log-rank Test. (D) CITED2 mRNA levels in human prostate cancer tissues of data set GES6919. N, normal prostate tissue (blue squares); A, normal prostate tissue adjacent tumor tissue (green triangles); PT, prostate primary tumor tissue (black inverted triangles); MT, metastatic prostate tumor tissue (red diamond). The horizontal lines in all dot plots represent the means ± s.e.m. and # denotes $P < 0.05$ versus the normal tissue group by Mann-Whitney statistical analysis.

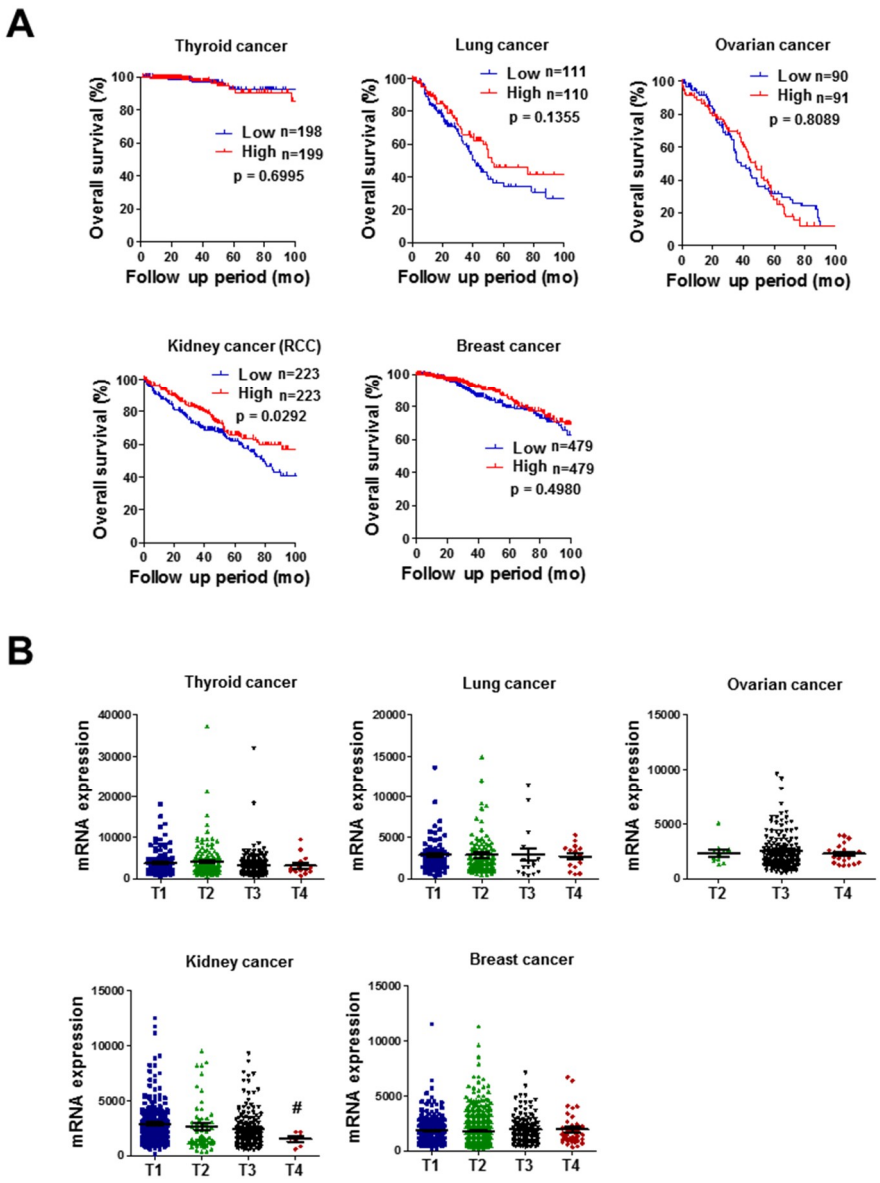

Figure 2. CITED2 expression does not correlate with the overall survival and the tumor stage in thyroid, ovarian, lung, and breast cancer.

Figure 2. CITED2 expression does not correlate with the overall survival and the tumor stage in thyroid, ovarian, lung, and breast cancer.

(A) Kaplan–Meier overall survival analysis of thyroid, lung, kidney, breast and ovarian cancer patients. P–value was calculated by Log–rank test. (B) CITED2 mRNA levels according to tumor stages in human thyroid, lung, kidney, breast, and ovarian cancer tissues. Dot plots indicate the distribution of values, and the horizontal lines are the mean ± s.e.m. # denotes $P < 0.05$ versus the T1 group by Mann–Whitney statistical analysis. T1, blue squares; T2, green triangles; T3, black inverted triangles; T4, red diamond. Data were obtained from using The Cancer Genome Atlas (TCGA).

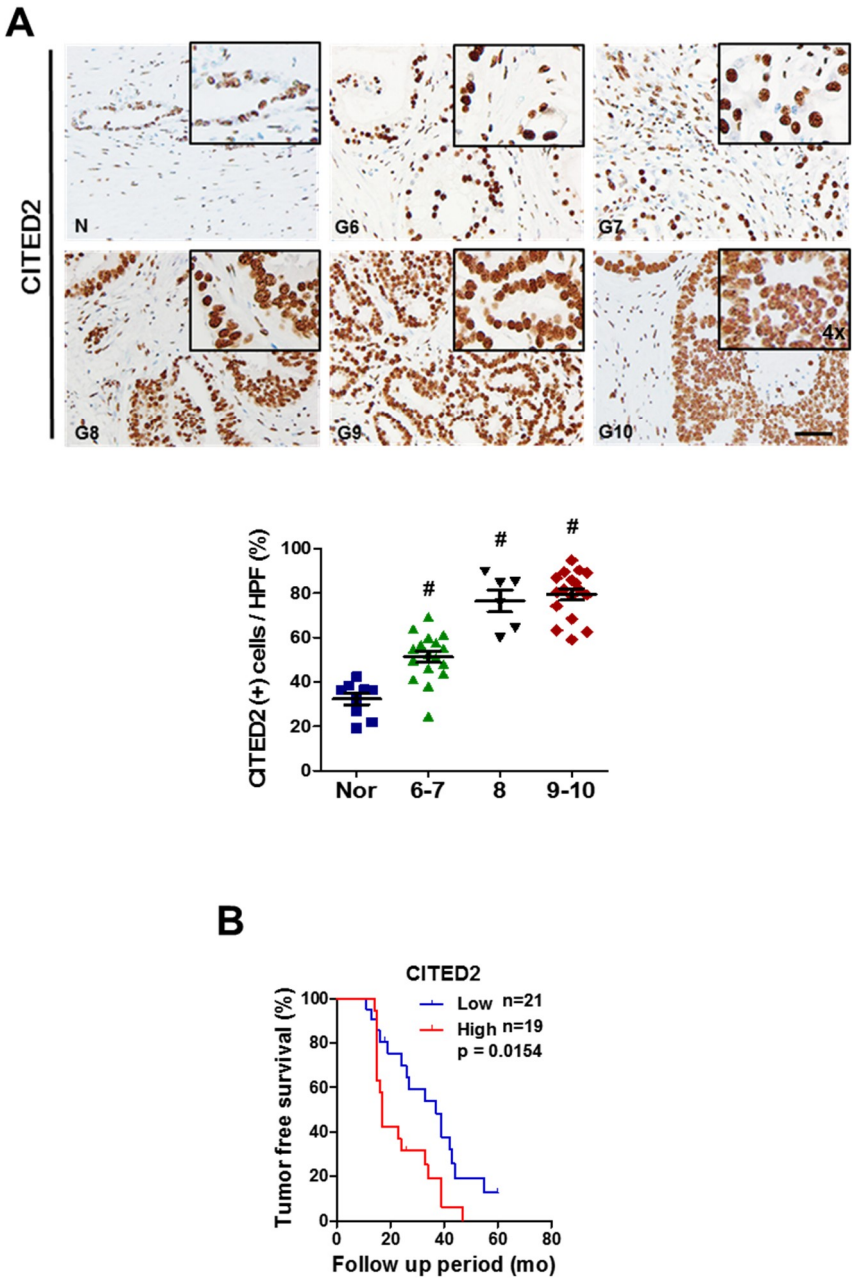

Figure 3. CITED2 protein expression is associated with poor prognosis in prostate cancer.

Figure 3. CITED2 protein expression is associated with poor prognosis in prostate cancer.

(A) Representative images of human prostate adenocarcinoma tissues immunostained with anti-CITED2 antibody. Abbreviations at the left bottoms of images: N, normal prostate tissue (blue squares); G6~10 (6-7, green triangles; 8, black inverted triangles; 9-10, red diamond) Gleason scores 6~10 of prostate cancer (left panel). The immunostaining scores were calculated by counting stained cells and presented as dot plots (right panel). The scale bar represents 50μm. (B) Kaplan-Meier tumor-free survival analysis of prostate cancer patients. P-value was calculated by Log-rank Test. The horizontal lines in all dot plots represent the means ± s.e.m. and # denotes $P < 0.05$ versus the normal tissue group by Mann-Whitney statistical analysis.

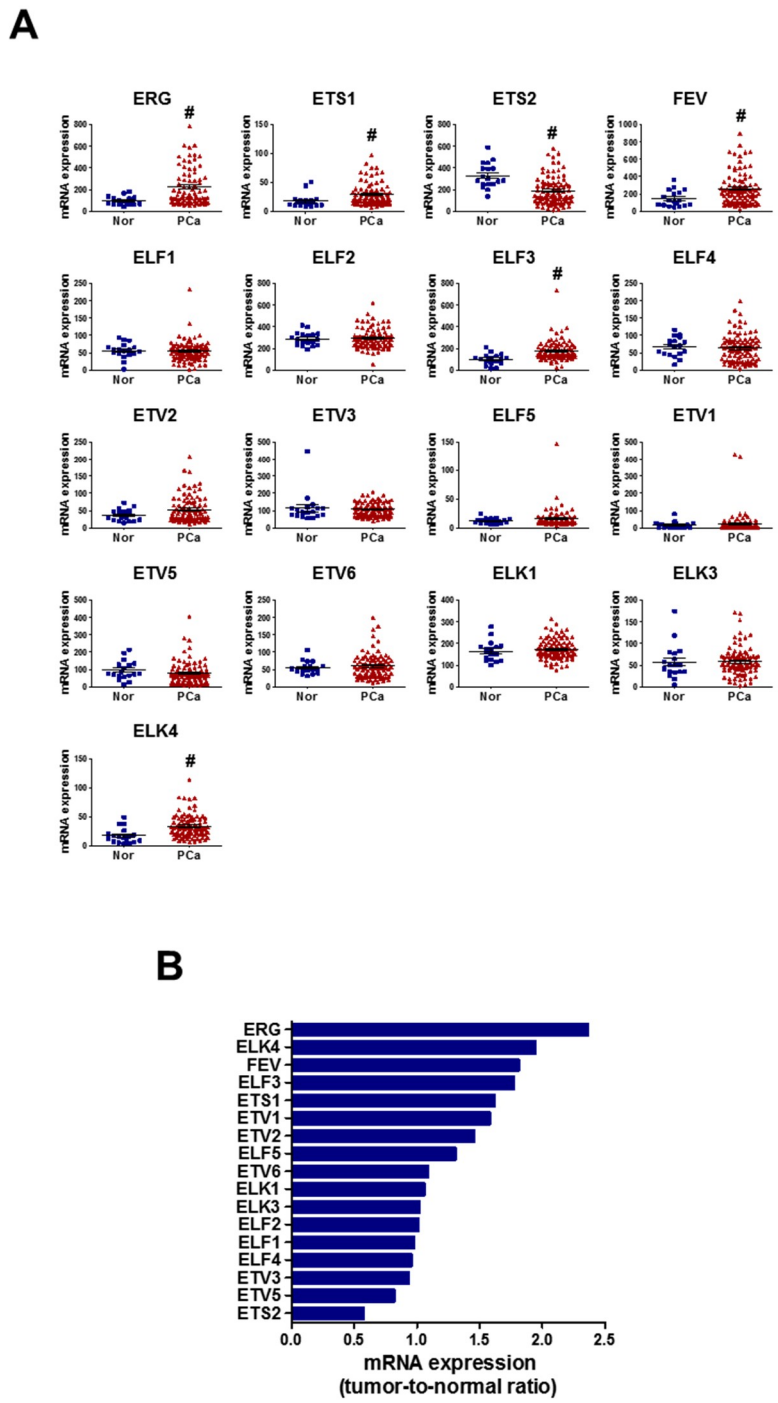

Figure 4. ERG level is the most increased in prostate cancer tissue.

Figure 4. ERG level is the most increased in prostate cancer tissue.

(A) The mRNA levels of the ETS family members in GSE6919 dataset. Each bar represents the ratio of tumor level to normal level. (B) Comparison of ETS gene family mRNA expression between normal and cancer prostate tissues, which were obtained from data set GES6919. Nor, normal prostate tissue (N = 19, blue squares); PCa, prostate tumor tissue (N = 90, red triangles). The horizontal lines represent the mean ± s.e.m., # denotes $P < 0.05$ versus the normal prostate group by Mann–Whitney statistical analysis.

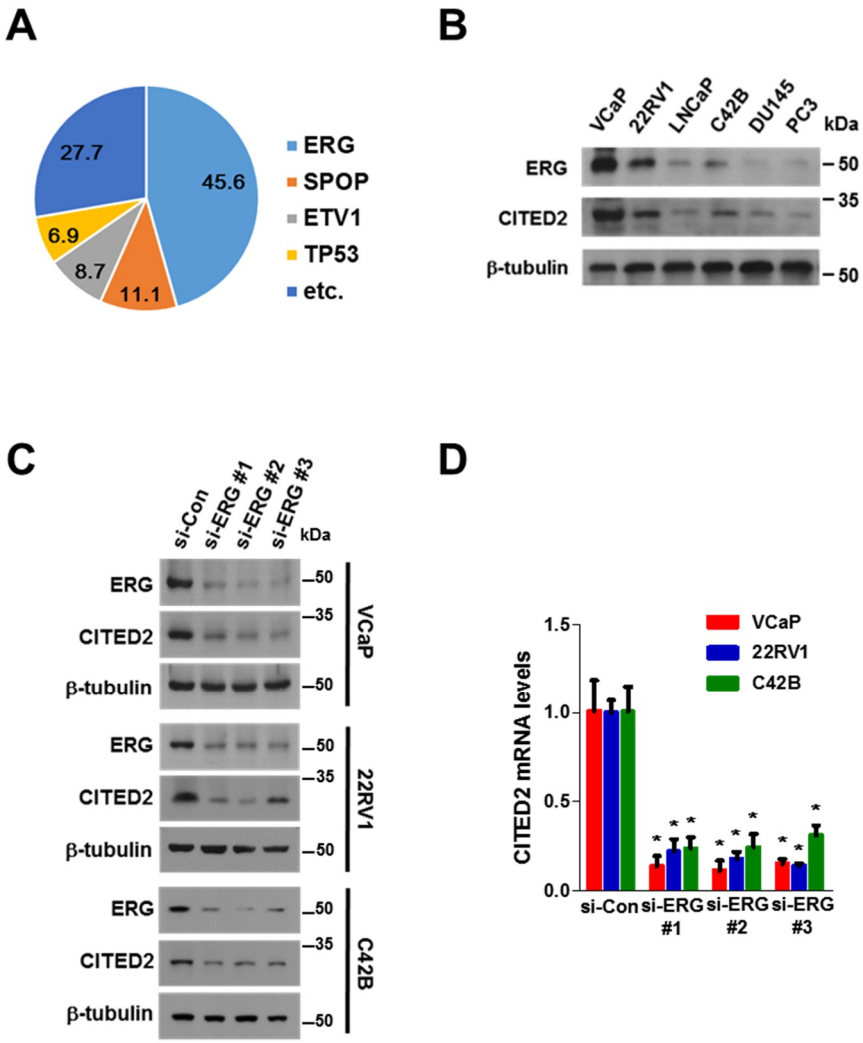

Figure 5. CITED2 is up-regulated due to the TMPRSS2-ERG gene fusion in prostate cancer.

Figure 5. CITED2 is up-regulated due to the TMPRSS2-ERG gene fusion in prostate cancer.

(A) The circular chart shows mutation subtypes identified in 333 prostate cancer patients. Data were obtained from TCGA (Prostate Adenocarcinoma, Cell 2015). (B) Lysates of prostate cancer cell lines were immunoblotted with anti-ERG, anti-CITED2, or anti-β-tubulin antibody. (C) Indicated cells were transfected with non-targeting siRNA (si-Con) or three different ERG-targeting siRNAs (si-ERG #1, #2 and #3) at an 80 nM concentration. Cell lysates were immunoblotted using the indicated antibodies. (D) RT-qPCR was performed to analyze CITED2 mRNA levels in prostate cancer cells transfected with the indicated siRNAs. Each bar represents the mean + s.d. (n=3). * denotes $P < 0.05$ versus the si-Con group by Student's t-test.

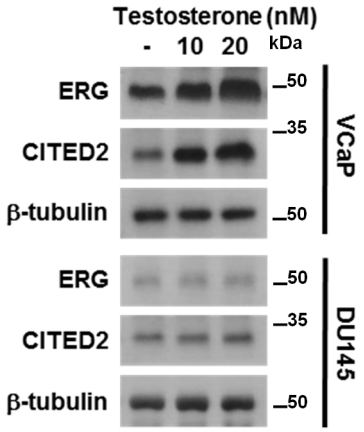

Figure 6. Testosterone induced CITED2 expression in VCaP cells.

VCaP and DU145 cells were treated with testosterone, and the cell lysates were immunoblotted with anti-ERG, anti-CITED2, or anti-β-tubulin antibody.

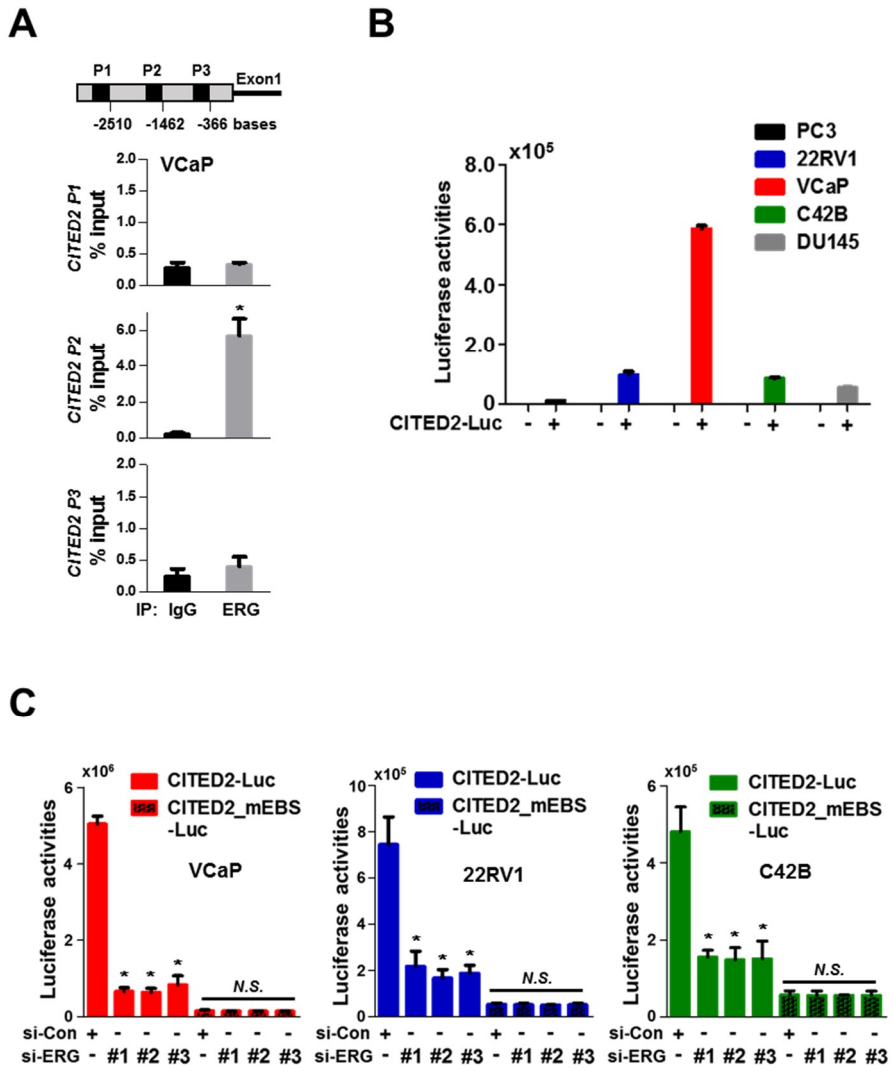

Figure 7. ERG binds and activates the CITED2 promoter.

Figure 7. ERG binds and activates the CITED2 promoter.

(A) The ERG binding to three CITED2 promotor regions (P1, P2 and P3) was detected by ChIP-qPCR using anti-ERG antiserum or non-immunized serum (IgG). The co-precipitated CITED2 promotor regions was quantified using RT-qPCR. Results (the mean ± s.d., n=3) were represented as percentages of IP signal/input signal (% input). * denote $P < 0.05$ versus the IgG control group. (B) The activities of the CITED2 promoter-luciferase reporter. Prostate cancer cells were transfected with the reporter plasmid. Luciferase activities (the mean + s.d., n=3) were measured by a luminometer. (C) The indicated siRNAs were co-transfected with the CITED2-luciferease or CITED2_mEBS (mutated ERG-binding sequence, patterned) reporter plasmid. Luciferase activities (mean + s.d., n=3) were measured by a luminometer. * denotes $P < 0.05$ versus the si-Con group by Student's t-test and N.S. does 'not significantly different' among the groups.

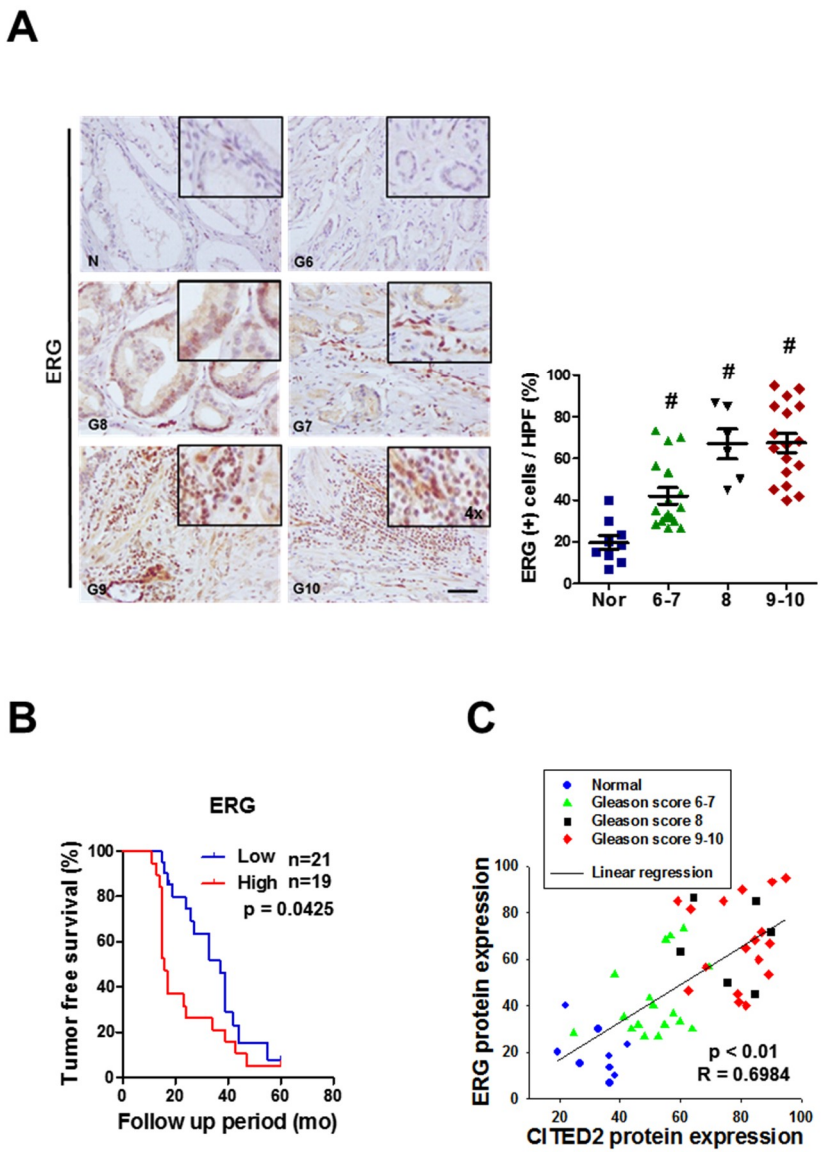

Figure 8. ERG protein expression is associated with poor prognosis in prostate cancer.

Figure 8. ERG protein expression is associated with poor prognosis in prostate cancer.

(A) Representative images of human prostate adenocarcinoma tissues immunostained with anti-ERG antibody. Abbreviations at the left bottoms of images: N, normal prostate tissue (blue squares); G6~10 (6-7, green triangles; 8, black inverted triangles; 9-10, red diamond) Gleason scores 6~10 of prostate cancer (left panel). The immunostaining scores were calculated by counting stained cells and presented as dot plots (right panel). The scale bar represents 50μm. The horizontal lines represent the mean ± s.e.m., # denotes $P < 0.05$ versus the normal prostate group by Mann-Whitney statistical analysis. (B) Kaplan-Meier tumor-free survival analysis of prostate cancer patients. P-value was calculated by Log-rank Test. (C) Protein expression scatter diagrams of ERG versus CITED2. Linear regression and correlation of ERG versus CITED2. R-square (R2) means coefficient of determination calculated by Pearson's correlation.

A

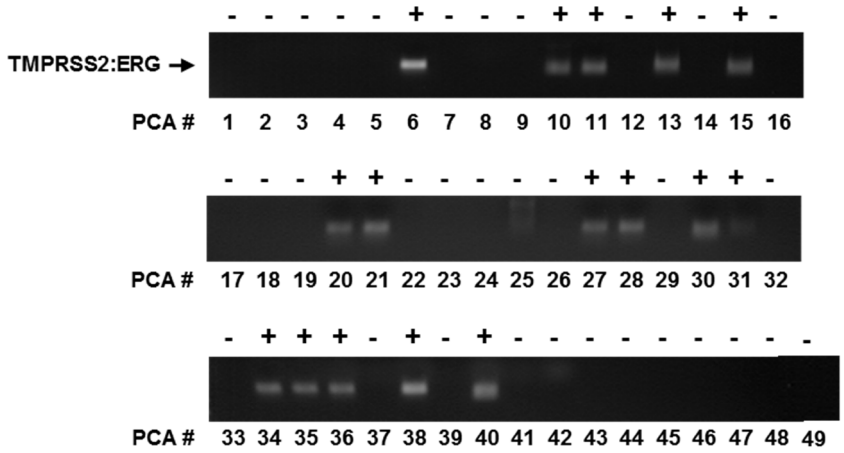

B

TMPRSS2:ERG	+	-
G6 ~ G7	4	13
G8 ~ G10	12	9
Chi^2	4.3545	
P-value	0.0369	

C

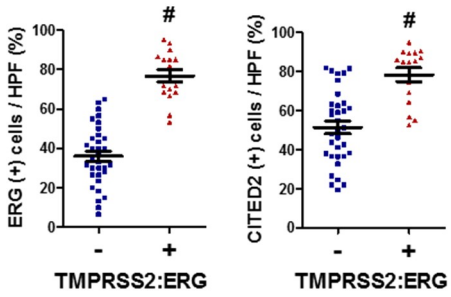

Figure 9. The TMPRSS2-ERG gene fusion support the ERG-driven overexpression of CITED2 in patient tissues.

Figure 9. The TMPRSS2-ERG gene fusion support the ERG-driven overexpression of CITED2 in patient tissues.

(A) DNAs extracted from prostate cancer tissues were subjected to PCR using a forward primer binding to the *TMPRSS2* promoter and a reverse primer binding to the *ERG* gene. The PCR products of the TMPRSS2-ERG fusion gene (+, positive; -, negative) are indicated as an arrow. (B) Distribution of the TMPRSS2:ERG fusion according to the prostate cancer Gleason score was statistically analyzed using chi-square test. (C) The immunostaining scores were calculated by counting stained cells. Blue and red symbols indicate ERG (right panel) and CITED2 (left panel) levels in the TMPRSS2-ERG fusion negative (blue squares) and positive (red triangles) group. The horizontal lines in all dot plots represent the means ± s.e.m. and # denotes $P < 0.05$ versus the normal group by Mann-Whitney statistical analysis.

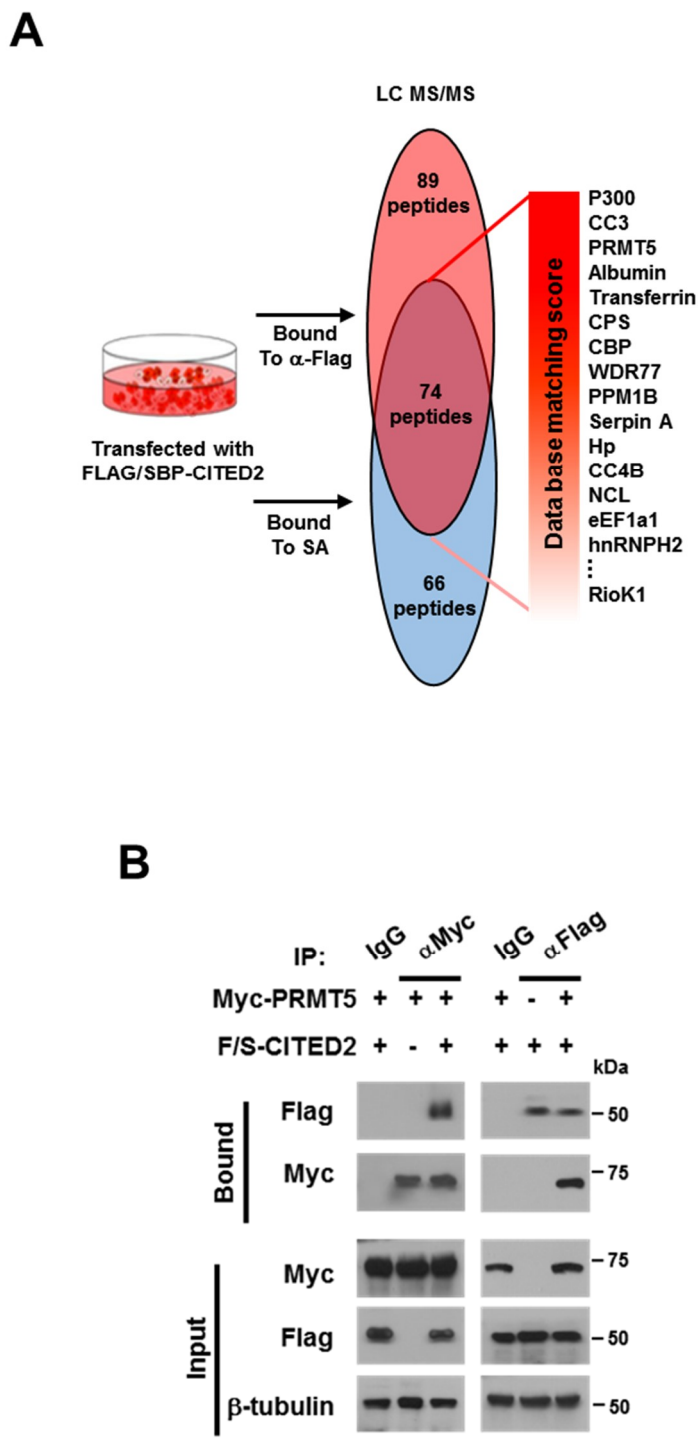

Figure 10. P300 and nucleolin, the PRMT5 complex subunits PRMT5, WDR77, and RIOK1 were co-purified with CITED2.

Figure 10. P300 and nucleolin, the PRMT5 complex subunits PRMT5, WDR77, and RIOK1 were co-purified with CITED2.

(A) HEK293T cells were transfected with the Flag/SBP-CITED2 plasmid. CITED2-interacting proteins were precipitated using anti-Flag tag antibody or streptavidin, and identified by LC-MS/MS analyses. The proteins identified commonly in two precipitates are listed.

(B) HEK293T cells were cotransfected with Flag/SBP-CITED2 and Myc-PRMT5. Proteins in cell lysates were immunoprecipitated with anti-Myc, anti-Flag, or IgG, and the precipitates were immunoblotted with the indicated antibodies.

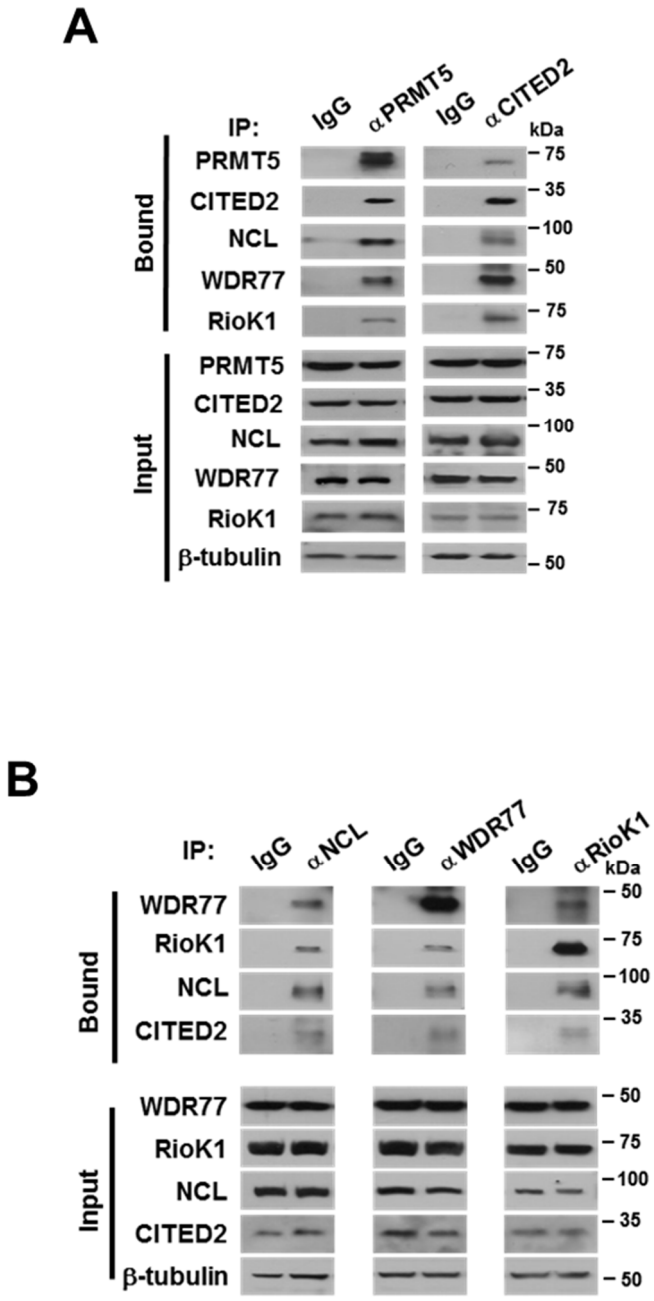

Figure 11. CITED2 is included in the multimeric complex of nucleolin.

Figure 11. CITED2 is included in the multimeric complex of nucleolin. (A) HEK293T cell lysates were immunoprecipitated with anti-PRMT5 antibody or anti-CITED2 or IgG, and the precipitates were immunoblotted with the indicated antibodies. (B) HEK293T cell lysates were immunoprecipitated with anti-nucleolin, anti-WDR77, anti-RioK1 antibody, or IgG, followed by immunoblotting with the indicated antibodies.

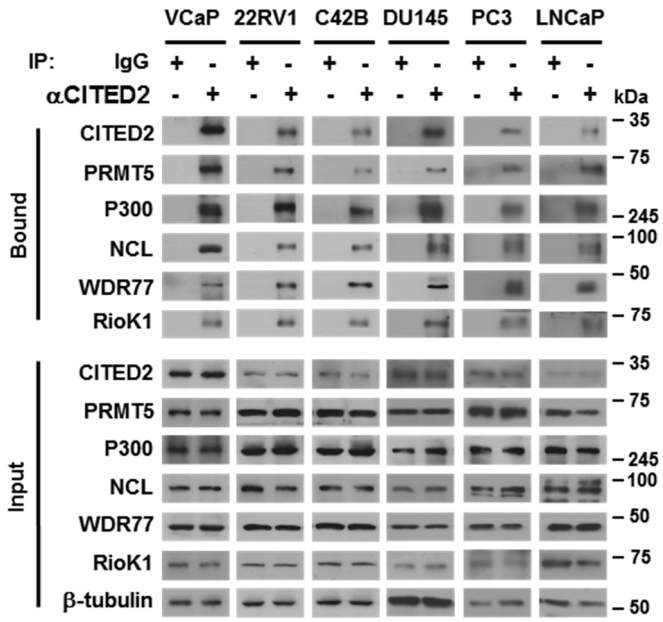

Figure 12. CITED2 interacts with P300 and PRMT5 complex in prostate cancer cells.

Prostate cancer cell lysates were immunoprecipitated with anti-CITED2 antibody or IgG, and the precipitates were immunoblotted with the indicated antibodies.

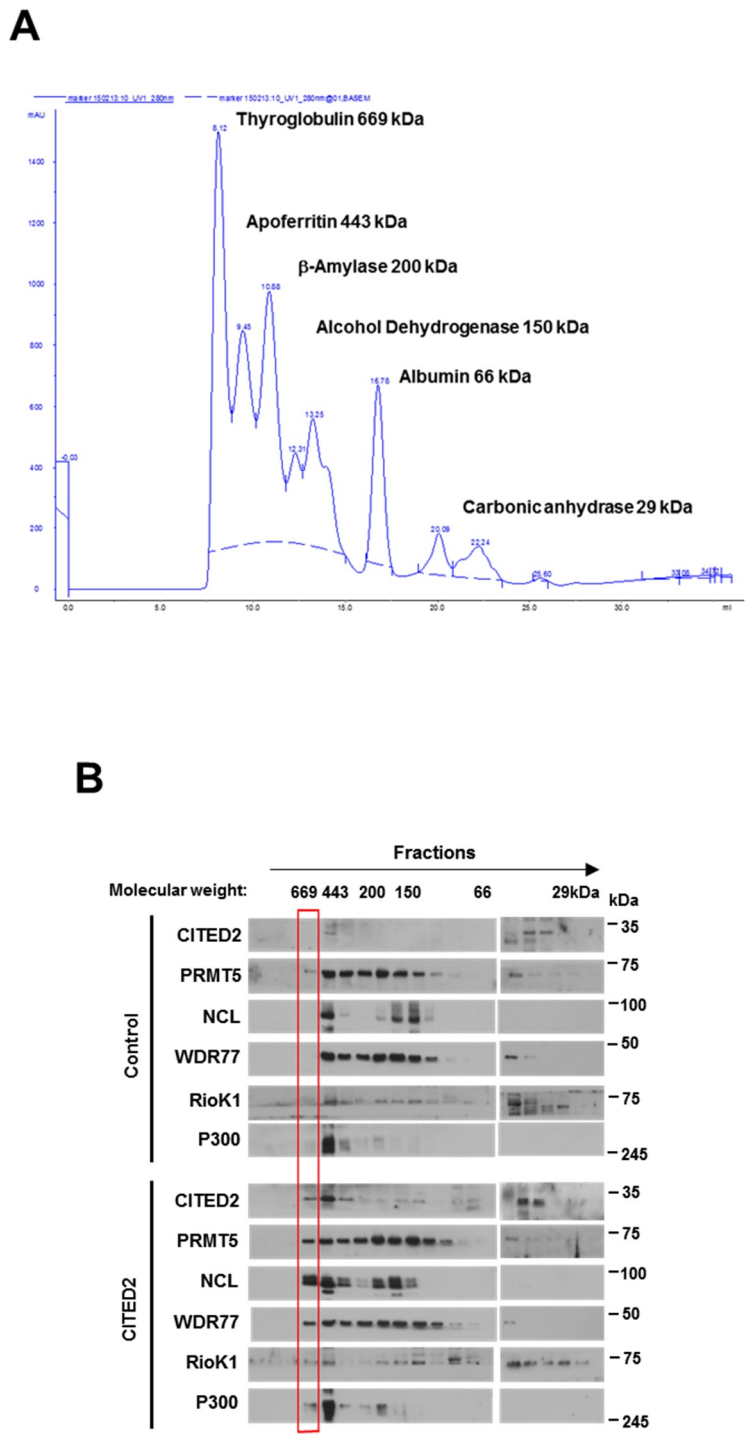

Figure 13. CITED2 forms a multimeric complex with nucleolin, p300, and PRMT5 subuints.

Figure 13. CITED2 forms a multimeric complex with nucleolin, p300, and PRMT5 subuints.

(A) Standard protein markers used for FPLC analysis with Superdex™ 200 column. (B) HEK293T cells were transfected with pcDNA or CITED2, and the cell lysates were subjected to FPLC. The FPLC elutes were immunoblotted with the indicated antibodies. The red box indicates a bigger-sized complex (600 to 700 kDa) that is formed by CITED2 overexpression.

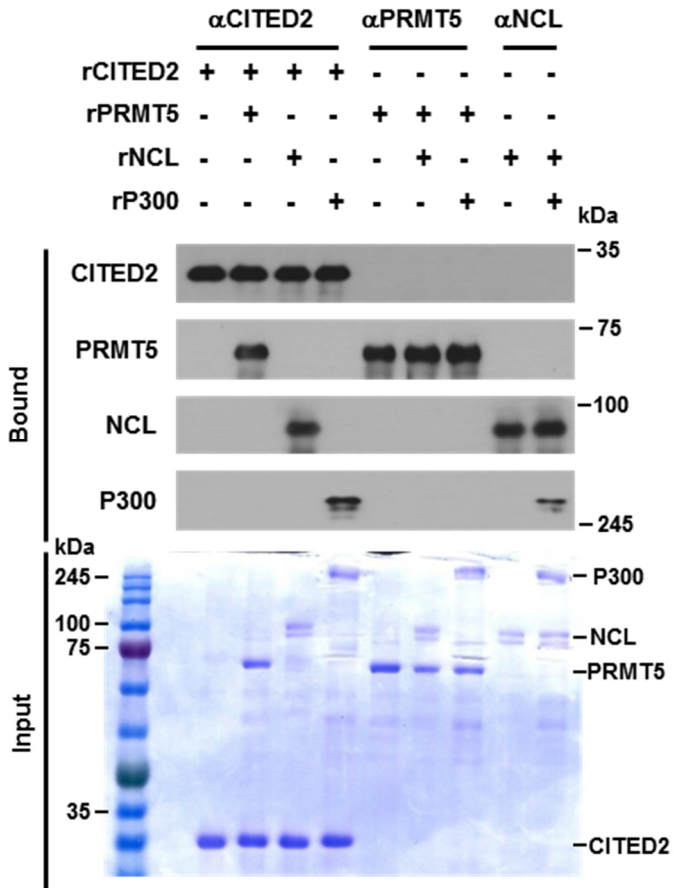

Figure 14. CITED2 directly interacted with nucleolin, P300 and PRMT5.

In vitro binding analysis. Recombinant protein CITED2, PRMT5, nucleolin, P300 were put together in a test tube. Proteins in tube were immunoprecipitated with indicated antibodies, and the precipitates were immunoblotted. Input levels were verified by electrophoresis and Coomassie staining.

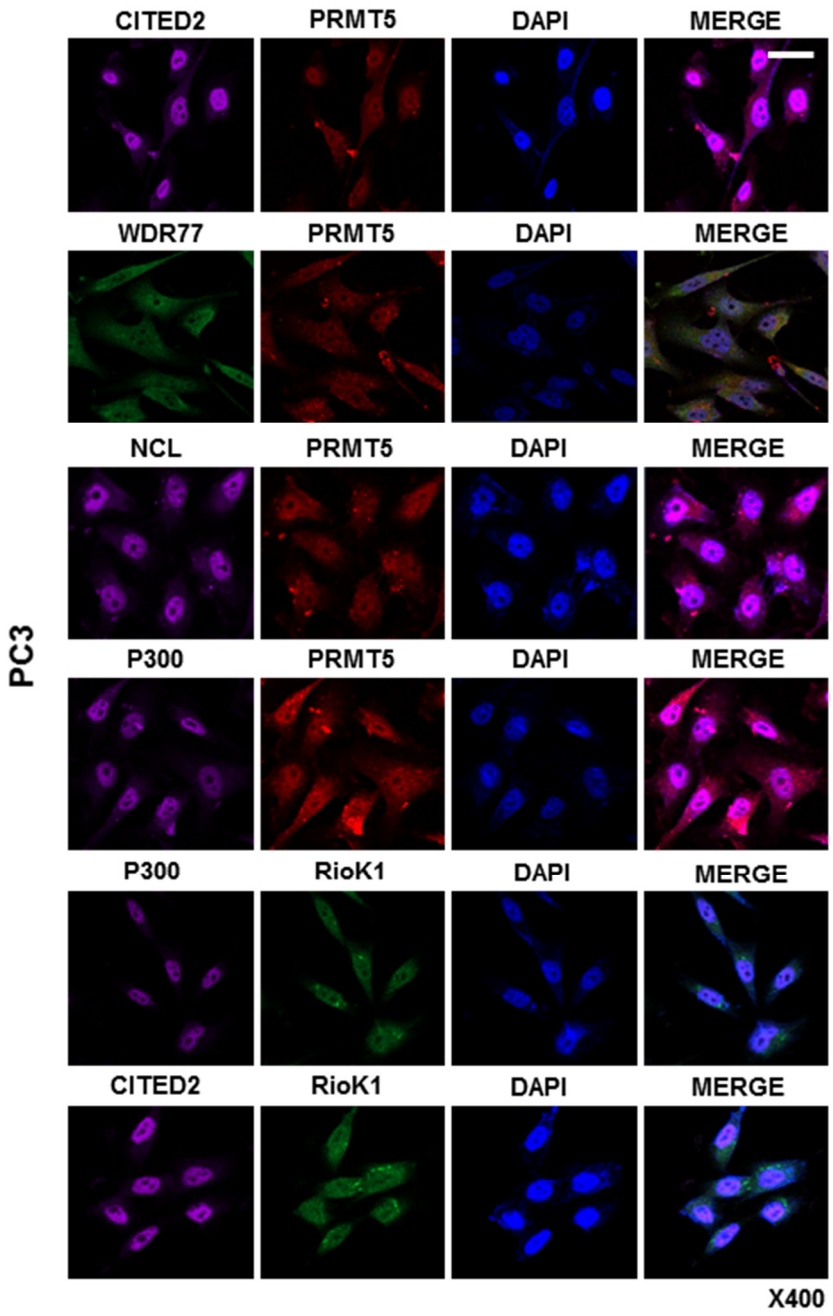

Figure 15. The subunits in the complex were co-localized mainly in the nuclei of PC3 and HEK293T cell.

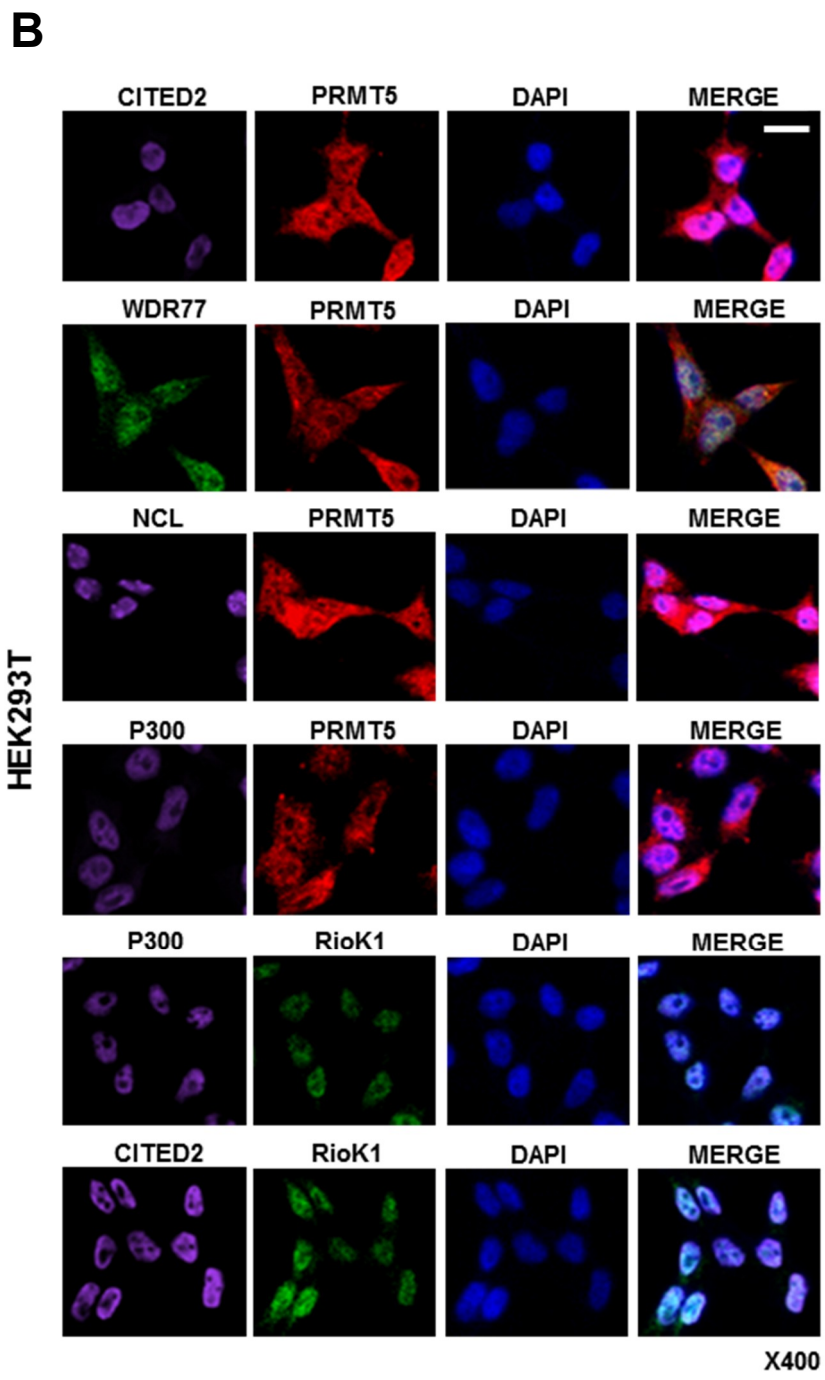

Figure 15. The subunits in the complex were co-localized mainly in the nuclei of PC3 and HEK293T cell.

Figure 15. The subunits in the complex were co-localized mainly in the nuclei of PC3 and HEK293T cell.

(A) Representative immunofluorescence images. PC3 cells were grown on coverslips, fixed with methanol, and stained with the indicated antibodies. All samples were stained with DAPI to visualize nuclei. The scale bar represents 20μm. (B) Representative immunofluorescence images. HEK293T cells were grown on coverslips, fixed with methanol, and stained with the indicated antibodies. All samples were stained with DAPI to visualize nuclei. The scale bar represents 20 μm.

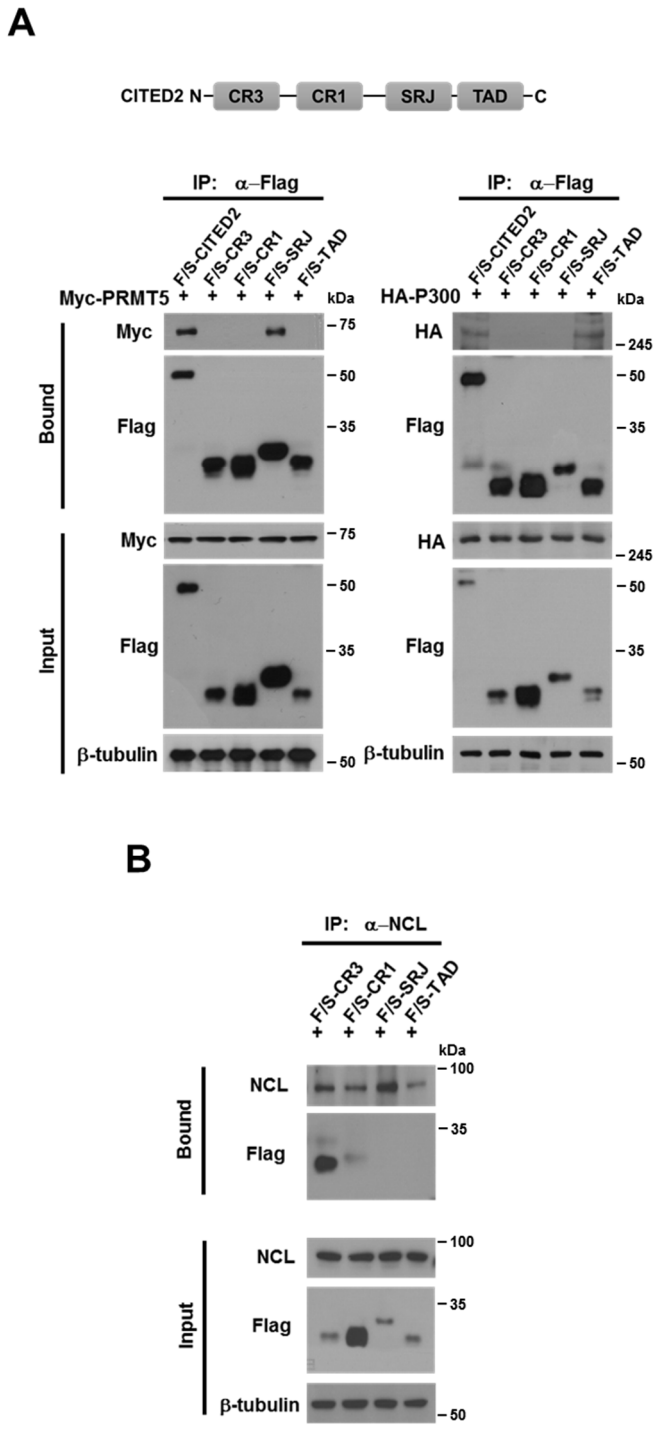

Figure 16. Different domain of CITED2 interacts with p300, PRMT5 and nucleolin.

Figure 16. Different domain of CITED2 interacts with p300, PRMT5 and nucleolin.

(A) The Flag/SBP-CITED2 constructs are shown in the top panel. HEK293T cells were cotransfected with one of the CITED2 constructs and Myc-PRMT5, HA-P300 and Flag/SBP-peptides were immunoprecipitated with anti-Flag and Myc-PRMT5 and HA-P300 were detected by Western blotting. (B) HEK293T cells were transfected with the CITED2 constructs, and cell lysates were immunoprecipitated with anti-nucleolin and Flag/SBP-CITED2 peptides were detected by Western blotting.

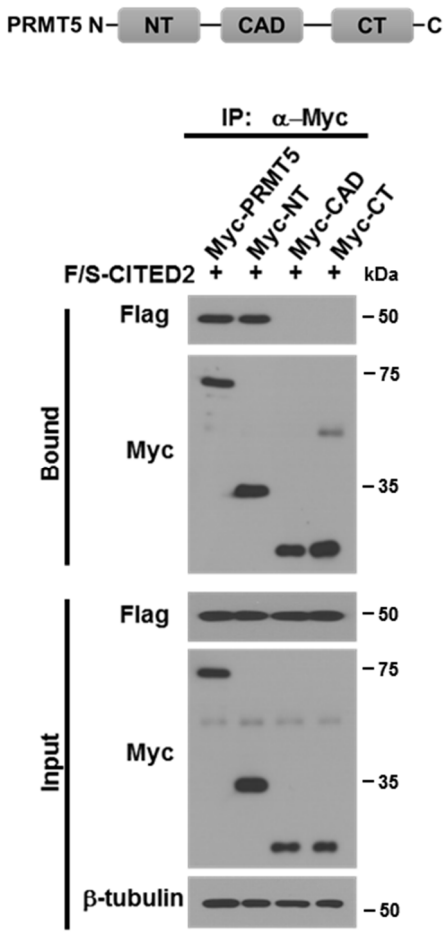

Figure 17. CITED2 interacted with the N-terminus of PRMT5.

The Myc-PRMT5 constructs are shown in the top panel. HEK293T cells were cotransfected with one of the PRMT5 construct and Flag/SBP-CITED2, and Myc-peptides were immunoprecipitated with anti-Myc and Flag/SBP-CITED2 were detected by Western blotting.

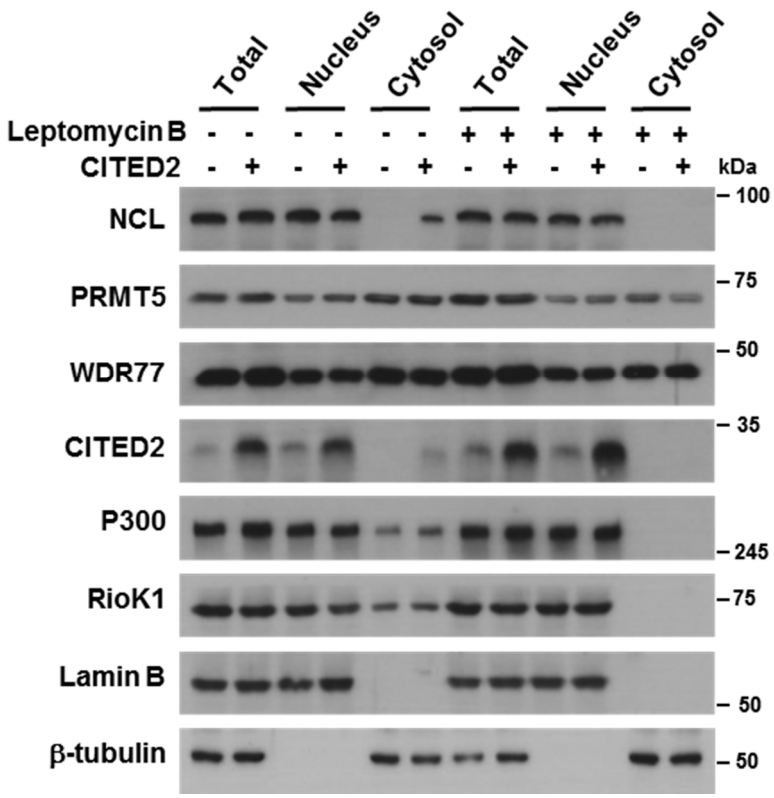

Figure 18. CITED2 overexpression enhanced cytoplasmic expression of nucleolin. HEK293T cells were transfected with pcDNA or CITED2 and treated with Leptomycin B (200 nM), and the cell lysates were fractionated to cytosoli and nuclear components. The cell fractions were immunoblotted with the indicated antibodies.

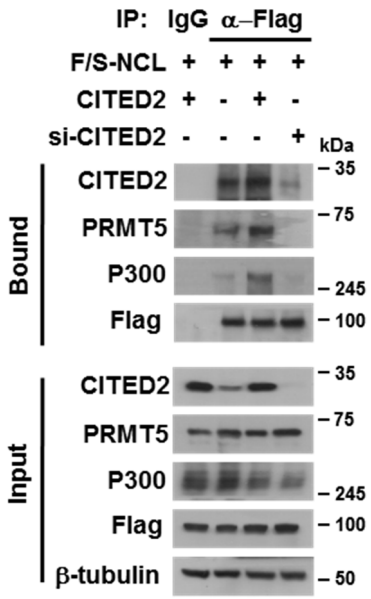

Figure 19. PRMT5 and p300 binding to nucleolin were potentiated by CITED2 overexpression.

HEK293T cells were cotransfected with Flag/SBP-nucleolin and CITED2 or si-CITED2. Cell lysates were immunoprecipitated with anti-Flag and immunoblotted with the indicated antibodies.

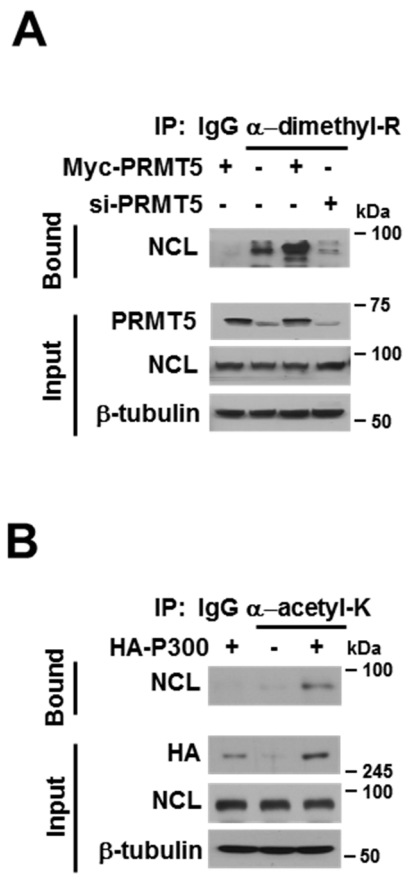

Figure 20. Nucleolin was arginine-dimethylated and lysine-acetylated by PRMT5 and p300.

(A) HEK293T cells were transfected with Myc-PRMT5 and/or si-PRMT5. Cell lysates were immunoprecipitated with anti-dimethyl arginine antibody and precipitated nucleolin was immunoblotted. (B) HEK293T cells were transfected with HA-p300. Cell lysates were immunoprecipitated with anti-acetyl lysine antibody and precipitated nucleolin was immunoblotted.

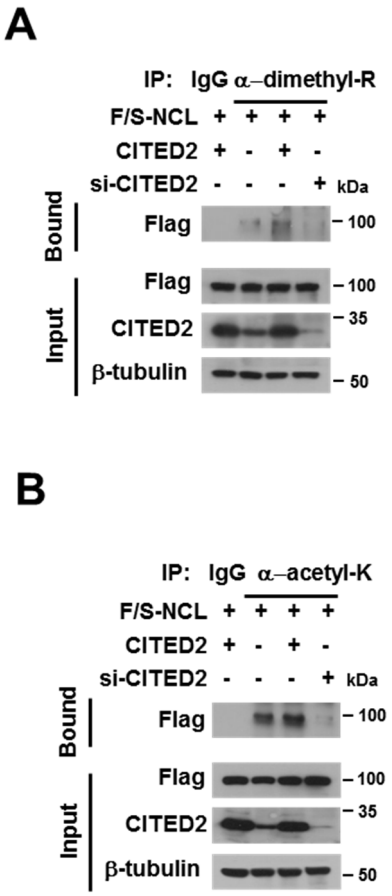

Figure 21. Post-translational modifications of nucleolin were dependent on CITED2.

(A) HEK293T cells were cotransfected with Flag/SBP-nucleolin and CITED2 or si-CITED2. Cell lysates were immunoprecipitated with anti-dimethyl arginine antibody and precipitated nucleolin was immunoblotted. (B) HEK293T cells were cotransfected with Flag/SBP-nucleolin and CITED2 or si-CITED2. Cell lysates were immunoprecipitated with anti-acetyl lysine antibody and precipitated nucleolin was immunoblotted.

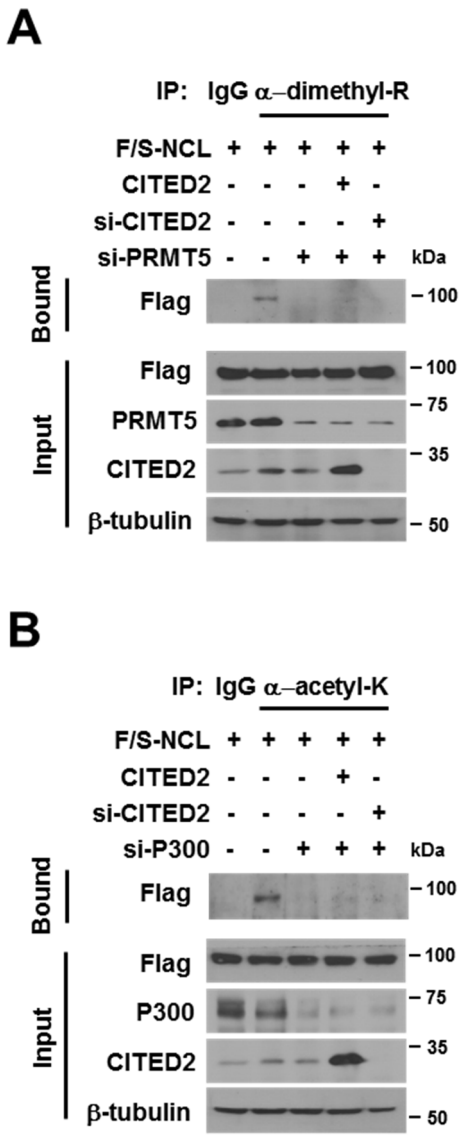

Figure 22. The CITED2–dependent modifications of nucleolin were attenuated by PRMT5 and p300 knockdown.

Figure 22. The CITED2-dependent modifications of nucleolin were attenuated by PRMT5 and p300 knockdown.

(A) HEK293T cells were cotransfected with the indicated plasmids and siRNAs. Cell lysates were immunoprecipitated with anti-dimethyl arginine antibody and precipitated nucleolin was immunoblotted. (B)HEK293T cells were cotransfected with the indicated plasmids and siRNAs. Cell lysates were immunoprecipitated with anti-acetyl lysine antibody and precipitated nucleolin was immunoblotted.

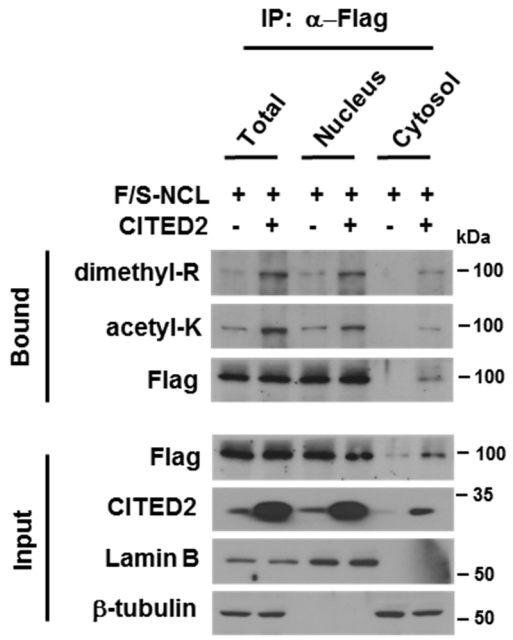

Figure 23. The dimethylated and acetylated nucleolin forms were detected in the cytoplasmic fraction.

HEK293T cells were cotransfected with Flag/SBP–nucleolin and CITED2, and the cell lysates were fractionated to cytosoli and nuclear components. The cell fractions were immunoprecipitated with anti–Flag antibody and immunoblotted with the indicated antibodies.

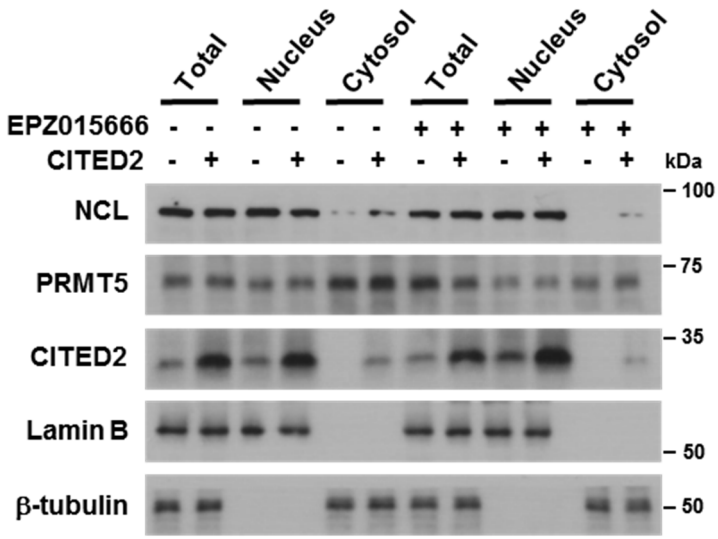

Figure 24. Translocation of nucleolin was decreased by a PRMT5 inhibitor.

HEK293T cells were transfected with pcDNA or CITED2 with EPZ015666 (5 μM), and the cell lysates were fractionated to cytosoli and nuclear components. The cell fractions were immunoblotted with the indicated antibodies.

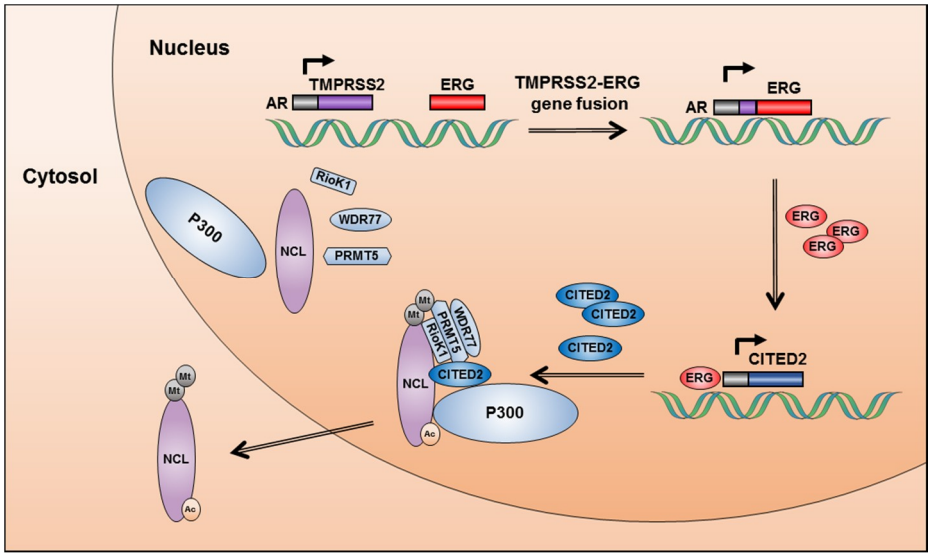

Figure 25. Graphical summary of The EGR-CITED2-PRMT5/p300-nucleolin pathway in prostate cancer.

ERG is upregulated due to the TMPRSS2-ERG gene fusion and transactivates the CITED2 gene in prostate cancer cells. Overexpressed CITED2 induces the methylation and acetylation of nucleolin in the nucleus by recruiting PRMT5 and p300, then modified nucleolin is translocated to the cytoplasm.

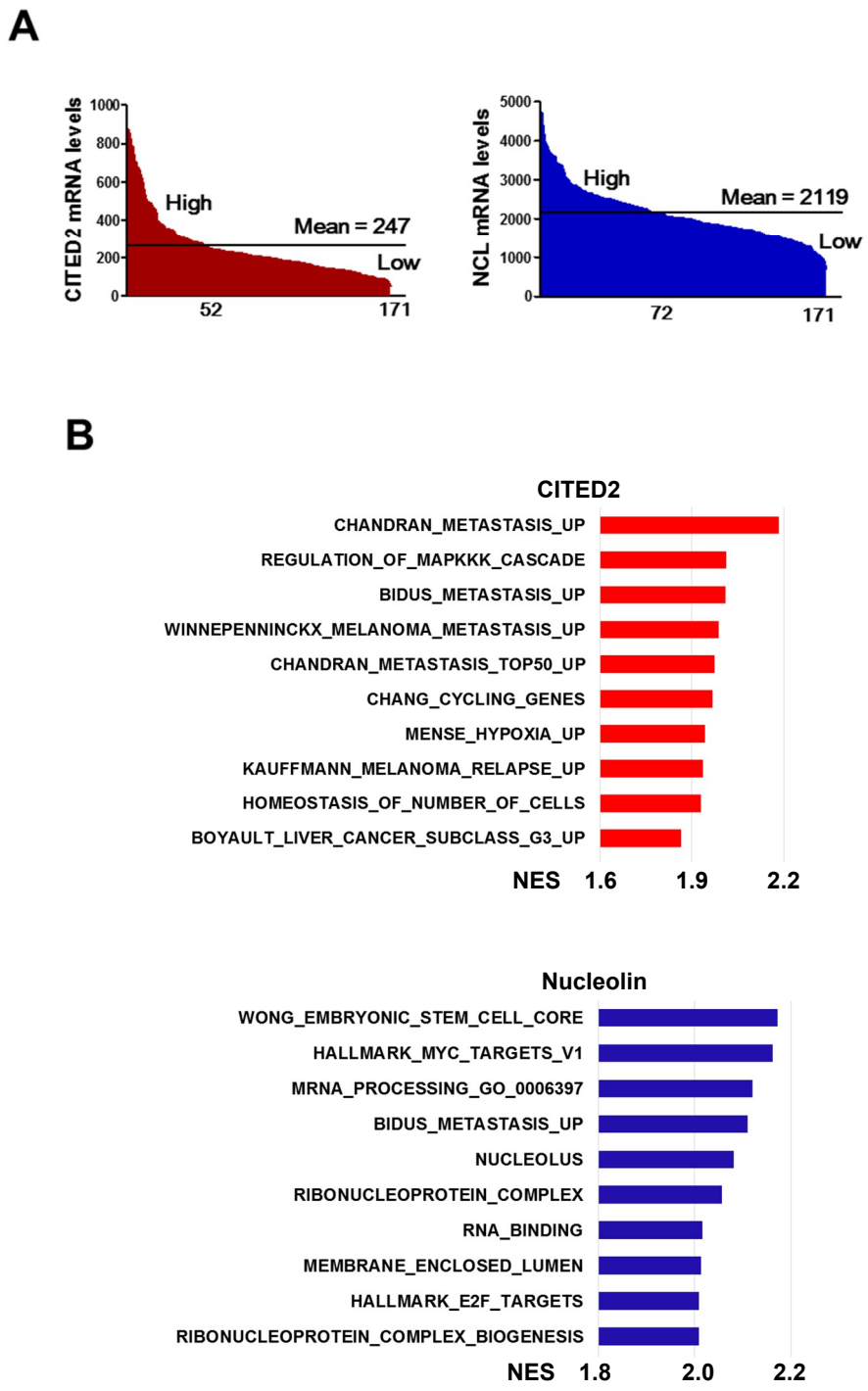

Figure 26. CITED2 and nucleolin both are positively associated with high expression of metastasis-related gene sets.

Figure 26. CITED2 and nucleolin both are positively associated with high expression of metastasis-related gene sets.

(A) Distribution of CITED2 (left) or nucleolin (right) mRNA levels in 171 human prostate tissues (data set GSE6919). Based on the mean values, the prostate cancer tissues were divided into high and low groups. The numbers of cancers are 52 in the CITED2 high, 119 in the CITED2 low, 72 in the nucleolin high, and 99 in the nucleolin low group. (B) Top 10 gene sets showing a positive correlation with CITED2 or nucleolin are ranked.

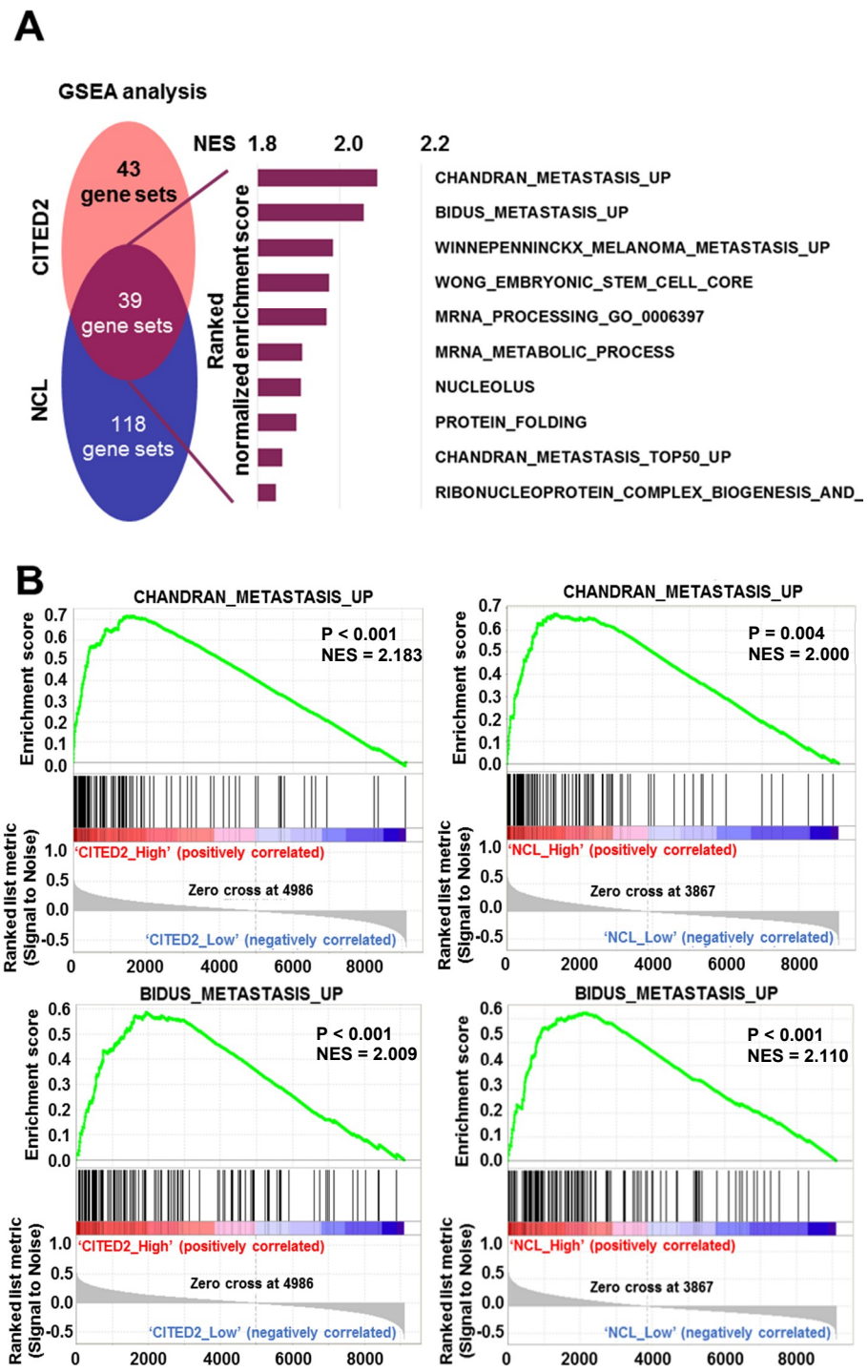

Figure 27. Metastasis related gene sets commonly associated with CITED2 and nucleolin.

Figure 27. Metastasis related gene sets commonly associated with CITED2 and nucleolin.

(A) Gene Set Enrichment Analysis (GSEA). Venn diagram depicts 39 gene sets upregulated ($P < 0.05$ and $FDR < 0.30$) commonly by CITED2 and nucleolin expression. Of them, top 10 gene sets are listed. (B) Representative enrichment plots of the metastasis-related gene set which positively correlate with CITED2 (left panel) or nucleolin (right panel).

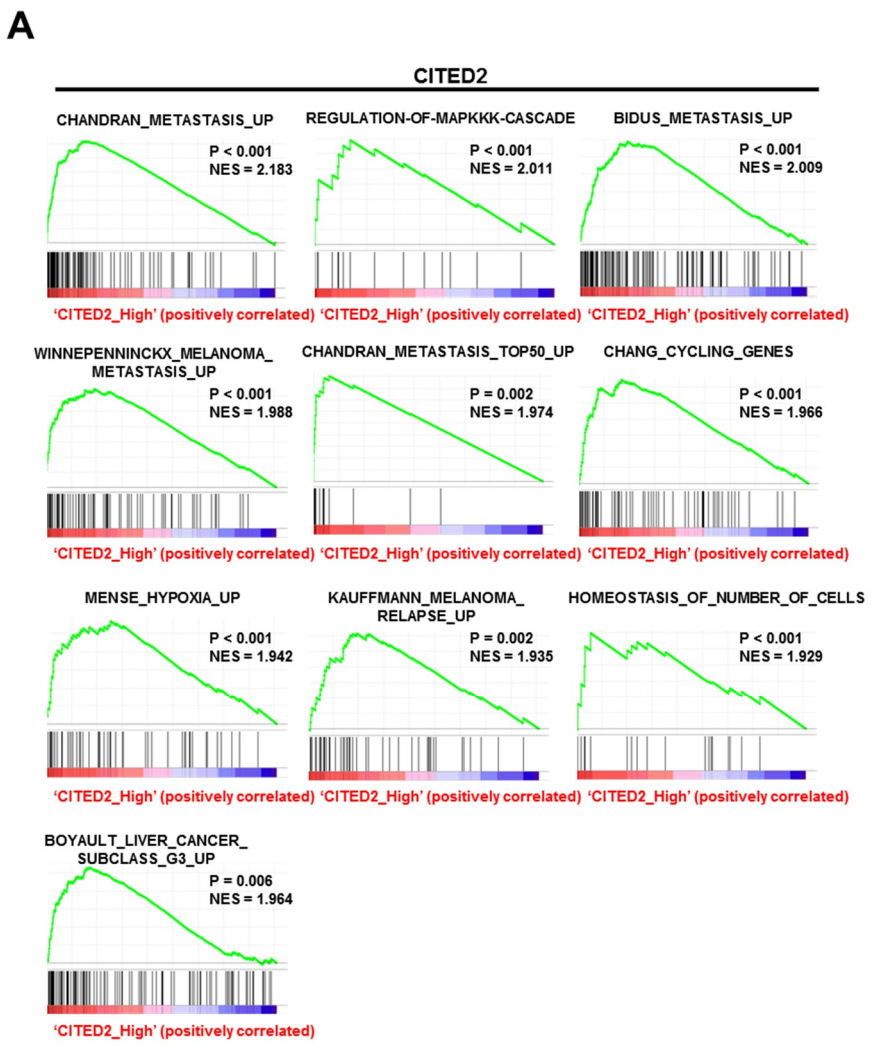

Figure 28. The enrichment profiles of gene sets associated with CITED2 and nucleolin expression.

B

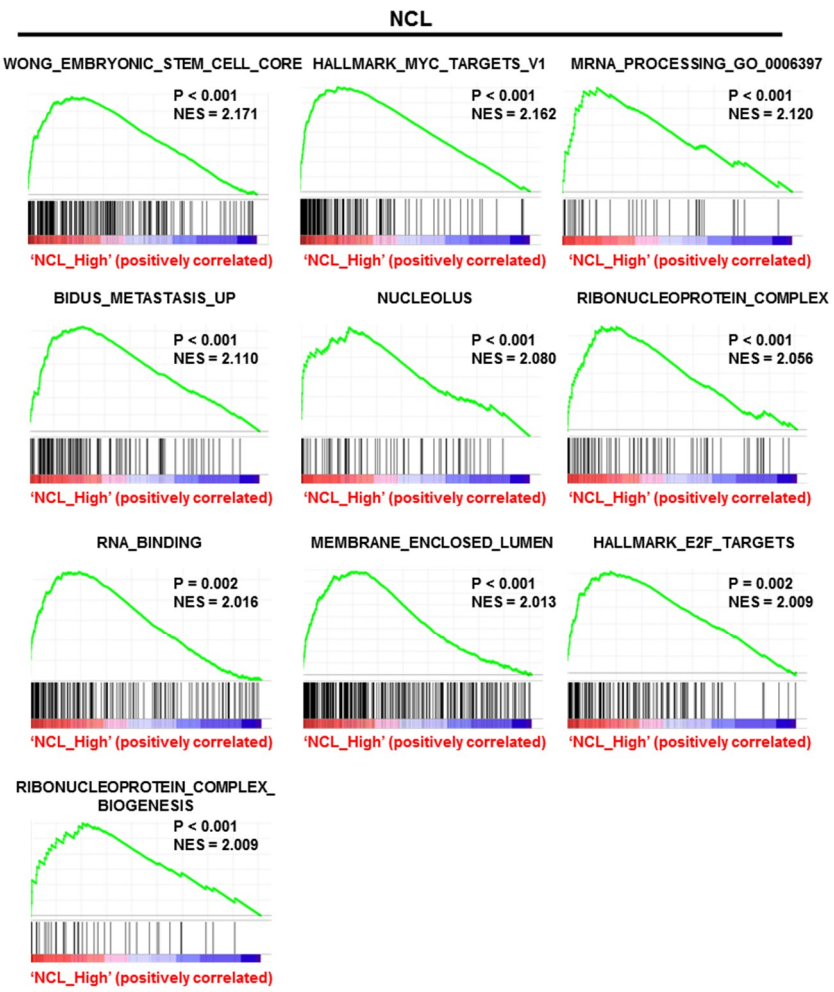

Figure 28. The enrichment profiles of gene sets associated with CITED2 and nucleolin expression.

Figure 28. The enrichment profiles of gene sets associated with CITED2 and nucleolin expression.

(A) Enrichment plots of the top 10 gene sets that were positively correlated with CITED2 expression with $P < 0.05$ and FDR < 0.30. (B) Enrichment plots of the top 10 gene sets that were positively correlated with nucleolin expression with $P < 0.05$ and FDR < 0.30.

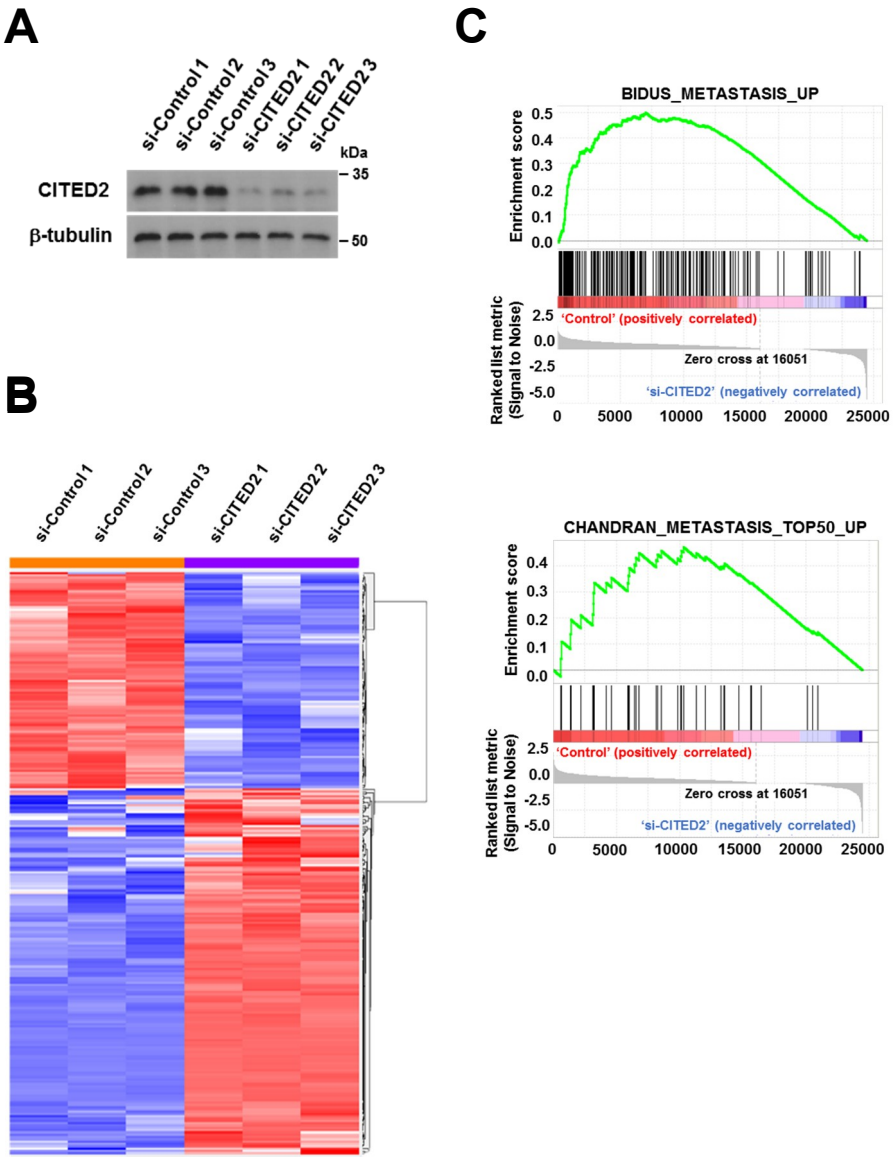

Figure 29. CITED2 promotes metastasis-related gene sets in PC3 cells.

Figure 29. CITED2 promotes metastasis-related gene sets in PC3 cells.

(A) PC3 cells were transfected with control or CITED2-targeting siRNA. Total RNAs were extracted using Trizol and subjected to RNA-sequencing analyses. The experiments were performed three times independently. CITED2 was immunoblotted to verify knockdown. (B) Heat map of genes that were differentially expressed in si-Control group (n = 3) and si-CITED2 group (n = 3) with P-value < 0.05 and Fold change > 2. (C) The graphs show representative enrichment plots of the metastasis-related gene set which positively correlate with CITED2 in PC3 cell.

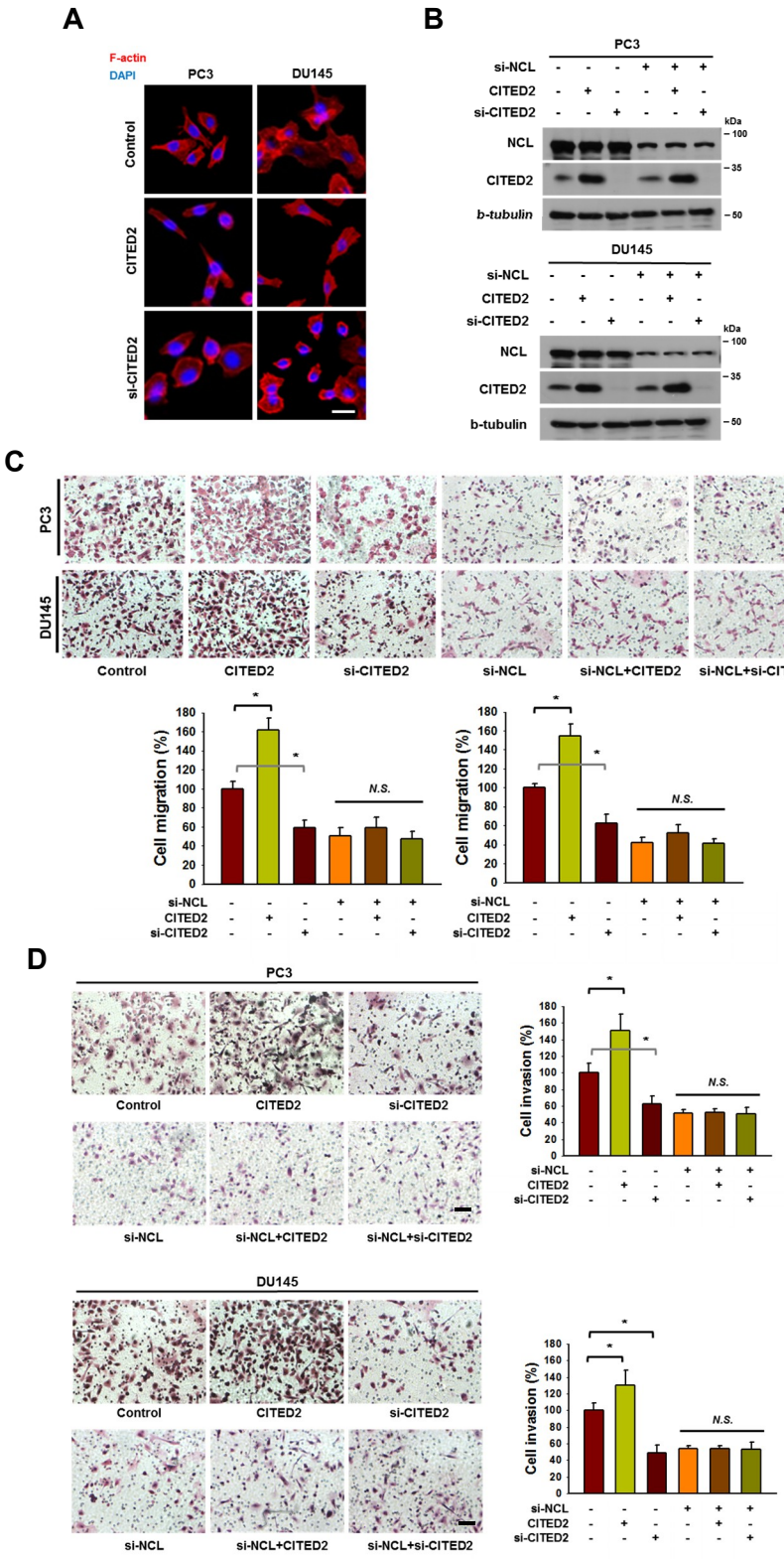
A
F-actin
DAPI
PC3
DU145
Control
CITED2
si-CITED2
B
PC3
si-NCL
CITED2
si-CITED2
kDa
NCL
CITED2
b-tubulin
100
35
50
DU145
si-NCL
CITED2
si-CITED2
kDa
NCL
CITED2
b-tubulin
100
35
50
C
PC3
DU145
Control
CITED2
si-CITED2
si-NCL
si-NCL+CITED2
si-NCL+si-CITED2
Cell migration (%)
N.S.
si-NCL
CITED2
si-CITED2
Cell migration (%)
N.S.
si-NCL
CITED2
si-CITED2
D
PC3
Control
CITED2
si-CITED2
si-NCL
si-NCL+CITED2
si-NCL+si-CITED2
Cell invasion (%)
N.S.
si-NCL
CITED2
si-CITED2
DU145
Control
CITED2
si-CITED2
si-NCL
si-NCL+CITED2
si-NCL+si-CITED2
Cell invasion (%)
N.S.
si-NCL
CITED2
si-CITED2

Figure 30. CITED2 promotes prostate cancer cell migration and invasion nucleolin-dependently.

(A) PC3 and DU145 cells were transfected with CITED2 or si-CITED2, and stained with rhodamine phalloidin (red) and DAPI (blue). The scale bar represents 20μm. (B) CITED2 and nucleolin were immunoblotted to verify knockdown and overexpression. (C) Cell migration was analyzed using a trans-well chamber. PC3 and DU145 cells ($1x10^4$/well), which had been transfected as indicated, were placed on the upper chamber. After 12 h, cells passing through the interface membrane were stained (top) and counted (bottom). Each bar represents the mean + s.d. (n=3). The scale bar represents 25μm. (C) Representative trans-well membrane pictures of invasion assay. The transfected PC3 and DU145 cells (1x104 per well) were loaded in the upper chamber of the trans-well culture dish. After 12 h, cells passing through a Matrigel-coated interface membrane were stained (left) and counted (right). Cells were stained and counted, which are presented as bar graphs. The scale bar represents 25 μm. * denotes $P < 0.05$ versus the control group and N.S. does 'not significantly different' among the groups by Student's t-test.

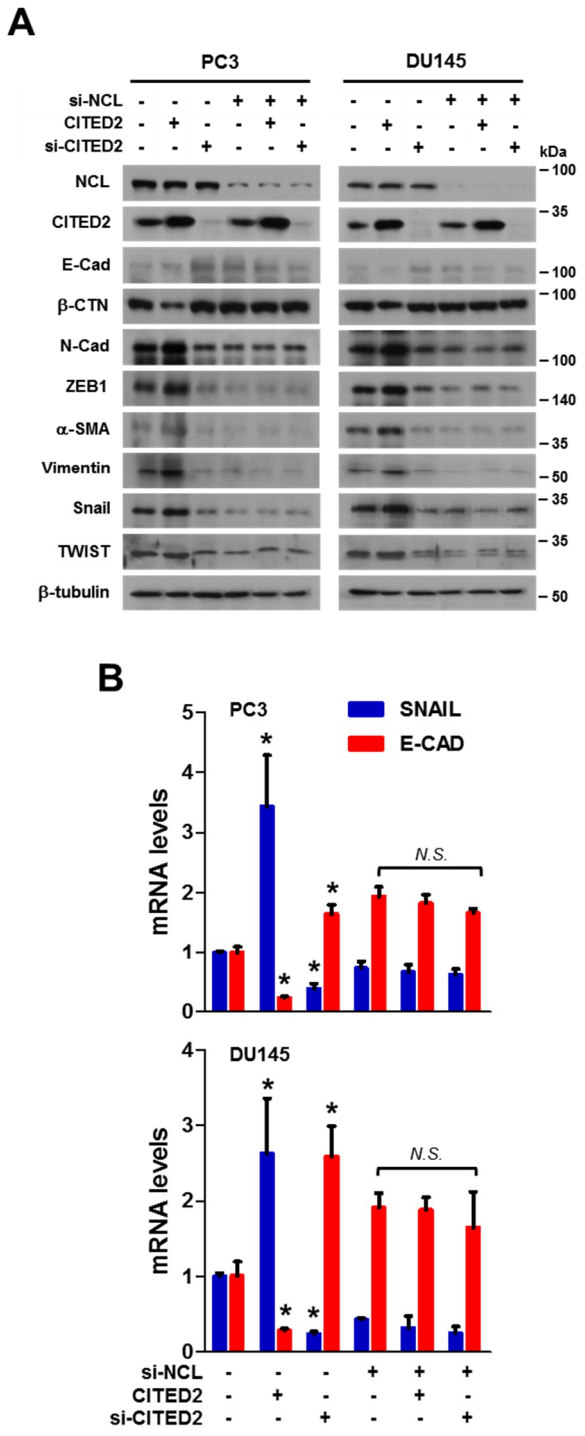

Figure 31. CITED2 increased the protein and mRNA levels of mesenchymal markers but decreased those of epithelial markers.

Figure 31. CITED2 increased the protein and mRNA levels of mesenchymal markers but decreased those of epithelial markers. (A) PC3 and DU145 cells were transfected with CITED2 or si-CITED2, and/or si-nucleolin. Representative EMT markers were immunoblotted. (B) RNAs were extracted from PC3 or DU145 cells which were transfected with CITED2 or si-CITED2 and/or si-nucleolin. The *SNAIL* and *E-CAD* mRNA levels were measured by RT-qPCR. Each bar represents the mean + s.d. (n=3). * denotes $P < 0.05$ versus the control group and N.S. does 'not significantly different' among the groups by Student's t-test.

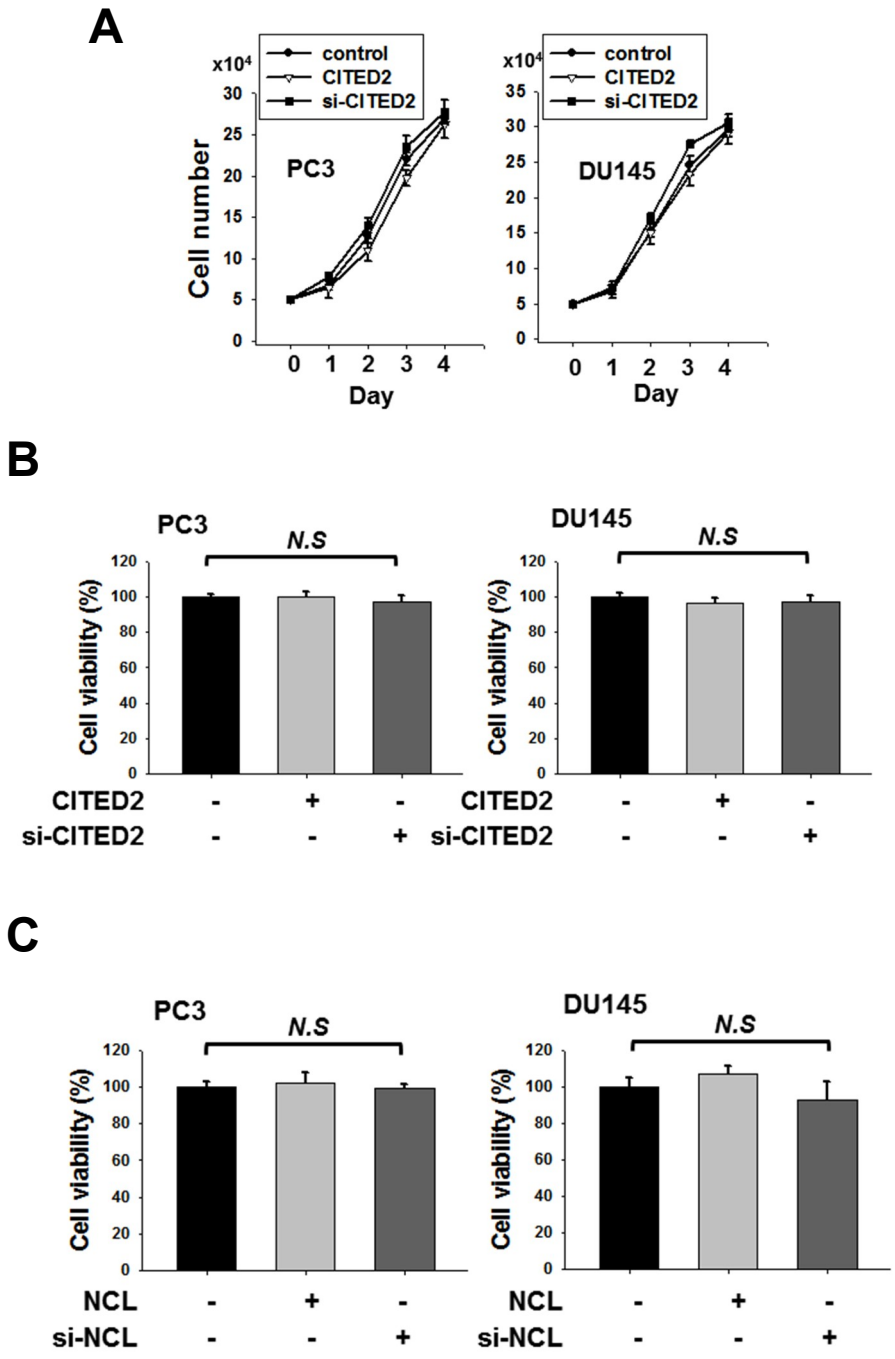

Figure 32. CITED2 or nucleolin expression did not affect cell growth or viability in prostate cancer cells.

Figure 32. CITED2 or nucleolin expression did not affect cell growth or viability in prostate cancer cells.

(A) Cell growth curves. PC3 or DU145 cells, which had been transfected with CITED2 or si-CITED2, were plated in 24-well culture dishes (5×10^4 per well) and counted at the indicated time. (B) Cell viabilities were measured using MTT. (C) Cell viabilities were measured using MTT. All results in the above graphs are presented as the means ± s.d. from three independent experiments and * denotes $P < 0.05$ versus the indicated control groups by Student's t-test and N.S. does 'not significantly different' among the groups.

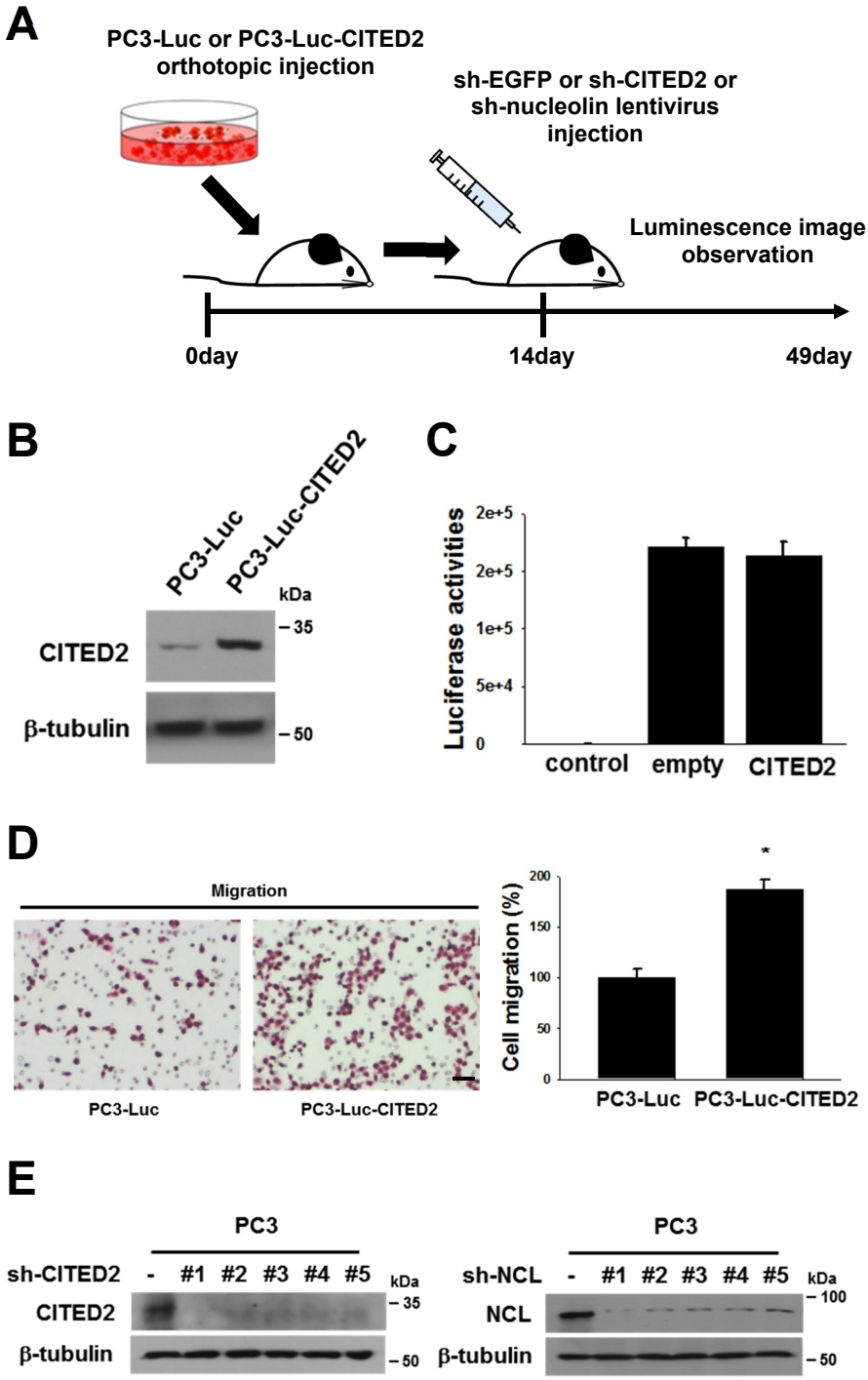

Figure 33. Schematic diagram of *in vivo* mouse model and verification of PC3 stable cell lines.

Figure 33. Schematic diagram of *in vivo* mouse model and verification of PC3 stable cell lines.

(A) Schematic diagram of *in vivo* prostate metastasis model. (B) CITED2 proteins were immunoblotted in a PC3 stable cell line transfected with Luc-CITED2. (C) The luciferase activities in PC3 stable cell lines were measured using a luminometer. Each bar represents the mean + s.d., from 3 experiments. (D) Representative pictures of trans-well membrane migration assays in PC3-Luc and PC3-Luc-CITED2 stable cell lines (left). Migrated cells were stained and counted (right). Each bar represents the mean + s.d., from 3 experiments. * denotes $P < 0.05$ versus the indicated control groups by Student's t-test. The scale bar represents 25 μm. (E) Efficacies of five different sequence shRNAs (#1 - #5) targeting CITED2 or nucleolin in PC3 cell lysates. Cell lystaes were immunoblotted with anti-CITED2 or anti-nucleolin antibody. The shCITED2 #4 and the shnucleolin #1 were used in xenograft experiments.

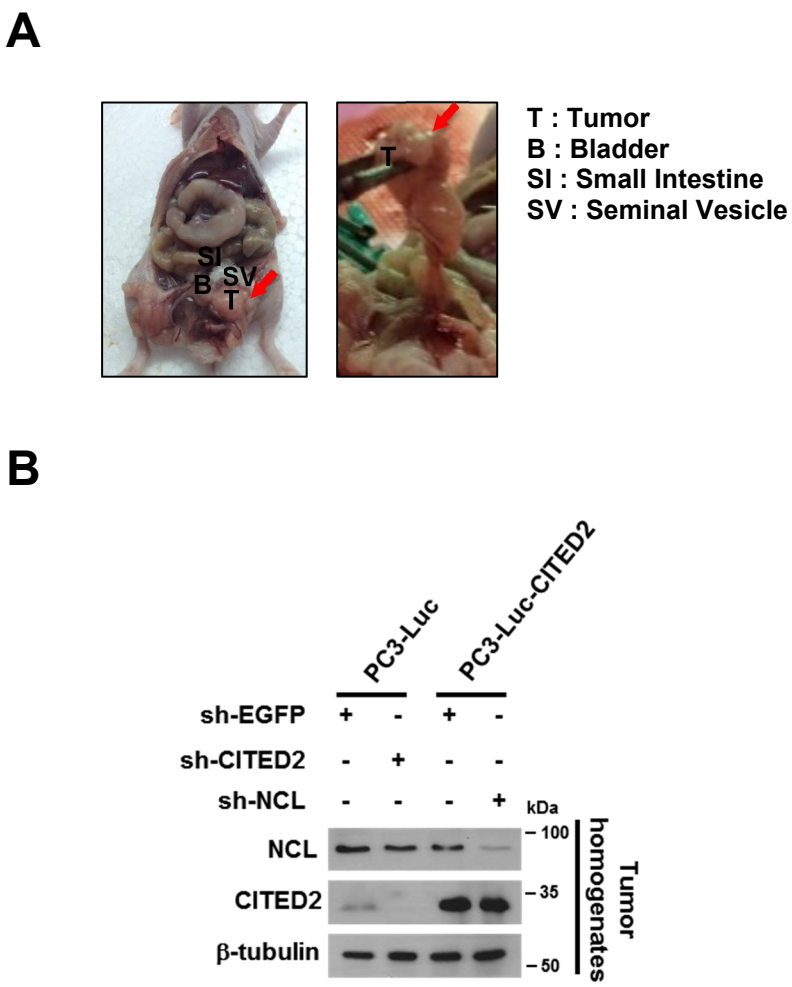

Figure 34. Verification of xenografted tumors and protein expressions.

(A) Representative photographs of prostate tumors 10 weeks after cell implantation. The luciferase-expressing PC3 cells (0.5 x 10^6) were suspended in 20 μL of sterile PBS and injected into the prostates of Balb/cSlc-nu/nu mice. (B) CITED2 and nucleolin proteins were immunoblotted in tumor homogenates from mice.

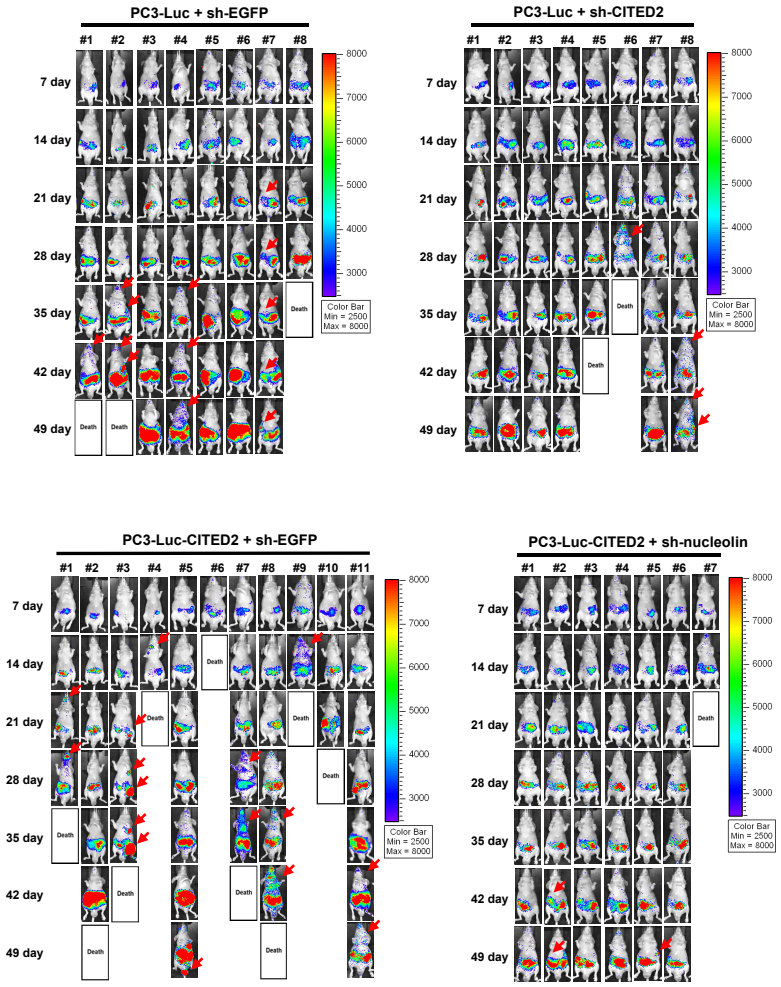

Figure 35. Bioluminescence images of mice having orthotopically grafted prostate cancer.

Luciferase-expressing PC3 stable cell lines were injected into the prostates of mice. Bioluminescence images of live mice were monitored using Xenogen IVIS® Lumina 100 weekly for 7 weeks. Red arrows indicate metastasis tumors. Color scale bars represent uminescence intensity from purple (low) to red (high).

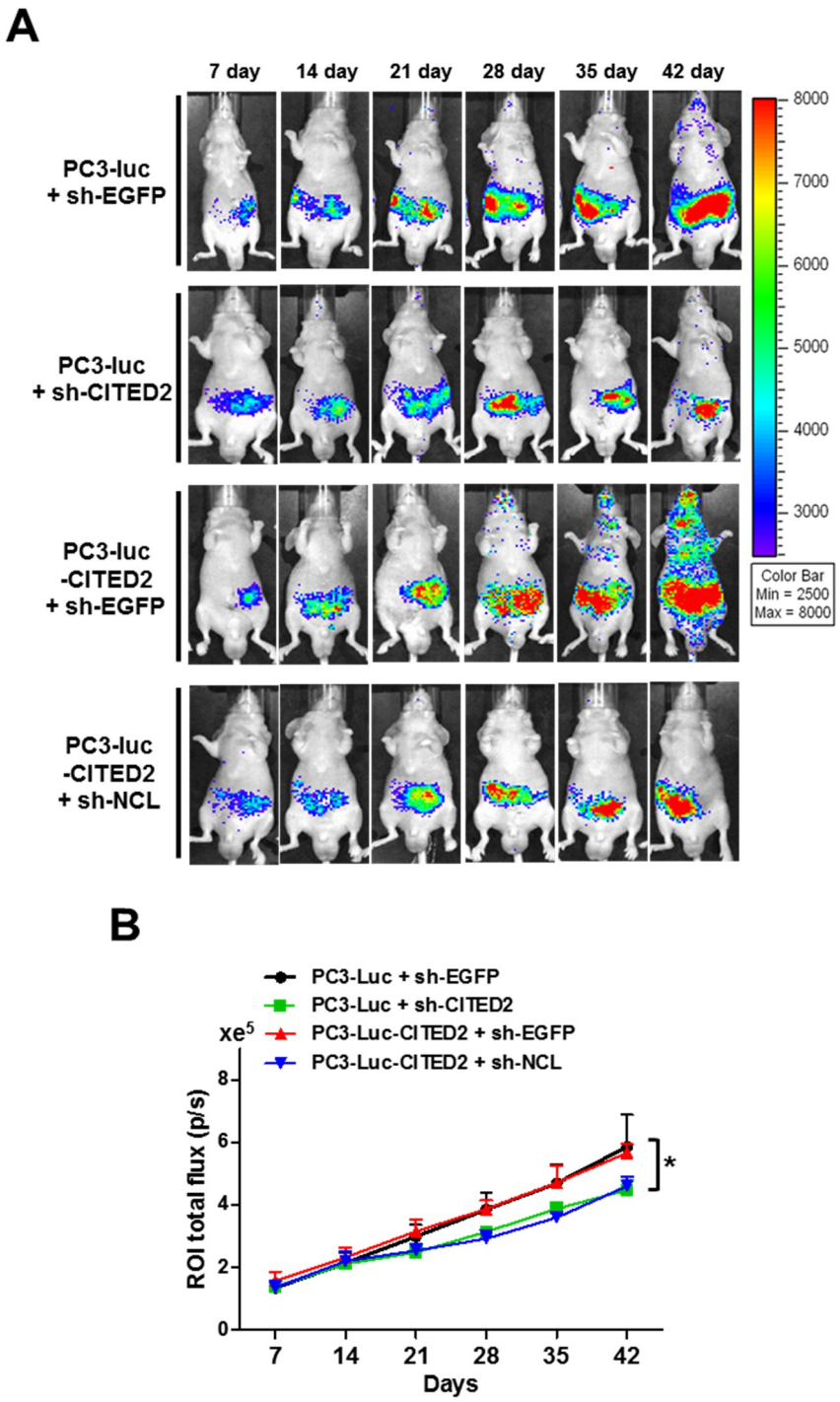

Figure 36. CITED2 promotes metastasis effect *in vivo* model.

Figure 36. CITED2 promotes metastasis effect *in vivo* model.

(A) Bioluminescent images of primary tumors and metastases were monitored using Xenogen IVIS® Lumina 100. Color scale bars represent tumor intensity from purple (low) to red (high). (B) Growth curves of primary tumors were plotted based on bioluminescence intensities. Data are presented as the mean + s.d., and * denotes $P < 0.05$ between two groups by Mann–Whitney statistical analysis. Mouse numbers are 8 in the sh–EGFP group, 8 in the sh–CITED2 group, 11 in the CITED2 + sh–EGFP, and 7 in the CITED2 + sh–nucleolin group.

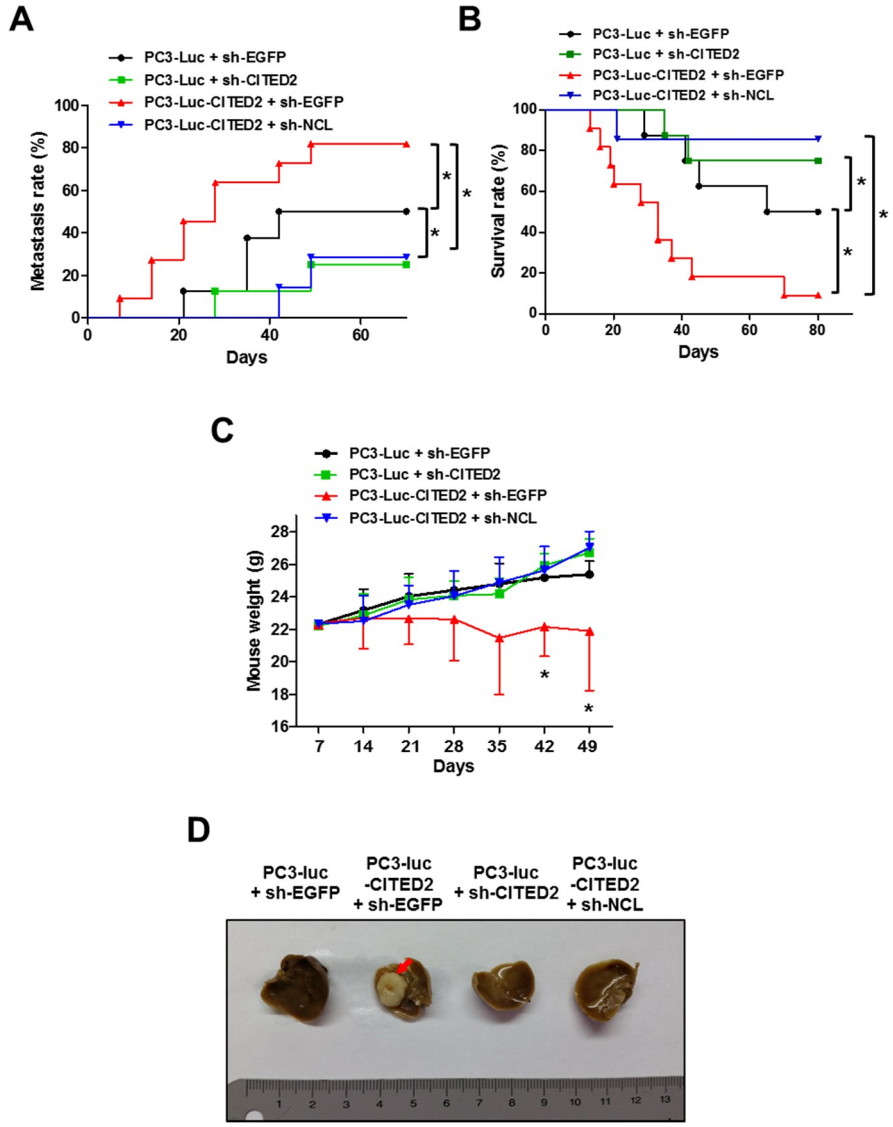

Figure 37. The CITED2–nucleolin axis induce prostate cancer metastasis *in vivo*.

Figure 37. The CITED2-nucleolin axis induce prostate cancer metastasis *in vivo.*

(A) Metastasis rate was retrieved according to the Kaplan-Meier method and * denotes P < 0.05 between two groups. Metastasis was defined as ROI flux value was larger than 1.0 x e5. (B) Kaplan-Meier overall survival rate analyses were followed up until 80 days after xenograft and * denotes P < 0.05 between two groups. (C) Tumor-bearing mice were weighed in the indicated times. Data are presented as the mean + s.d., and * denotes P < 0.05 between two groups by Mann-Whitney statistical analysis. (D) Representative photographs of livers with metastatic carcinoma nodules (indicated by arrow).

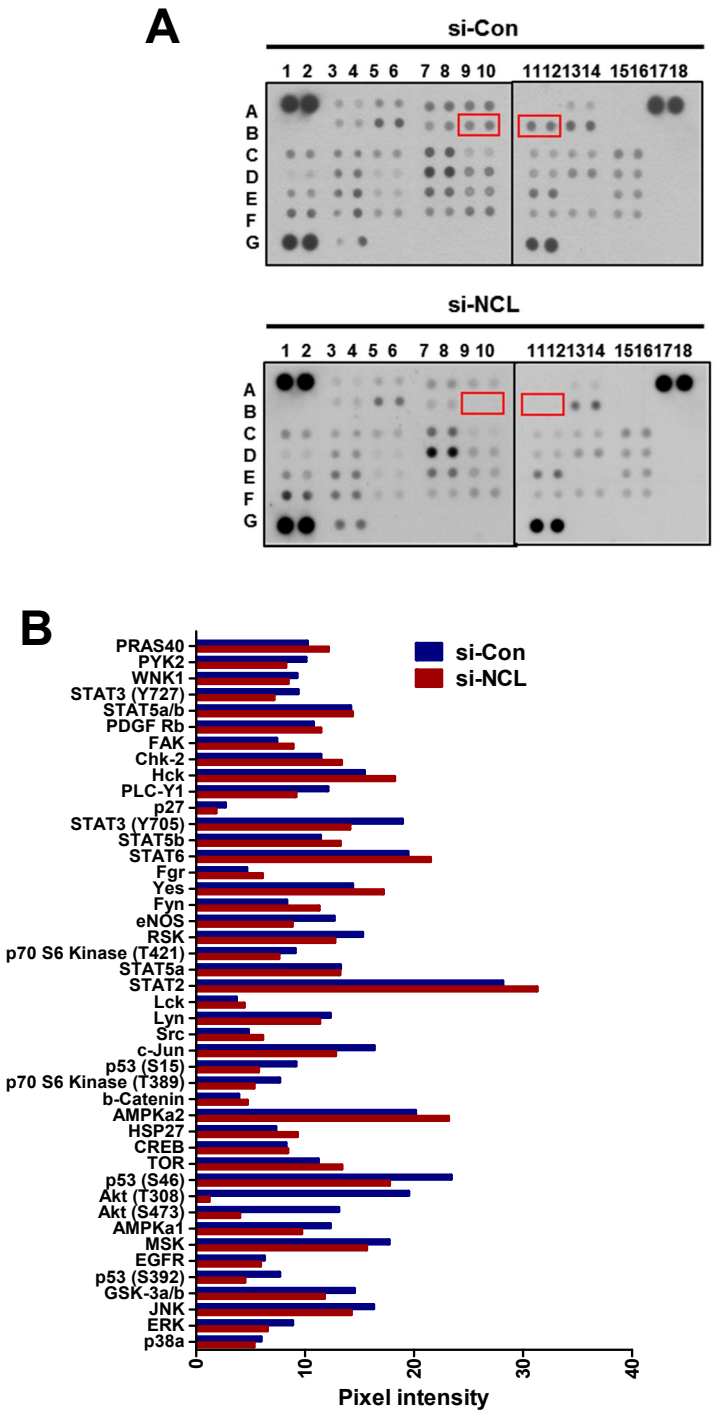

Figure 38. Phospho-AKT was reduced most in nucleolin-knockdown cells.

Figure 38. Phospho-AKT was reduced most in nucleolin-knockdown cells.

(A) PC3 cells were transfected with si-Con or si-nucleolin, and the cell lysates were subjected to the Proteome Profiler™ phospho-kinase array kit. The red boxes indicate blots of AKT phosphorylated at T308 and S473. (B) The blot spot pixel densities were analyzed by the ImageJ program.

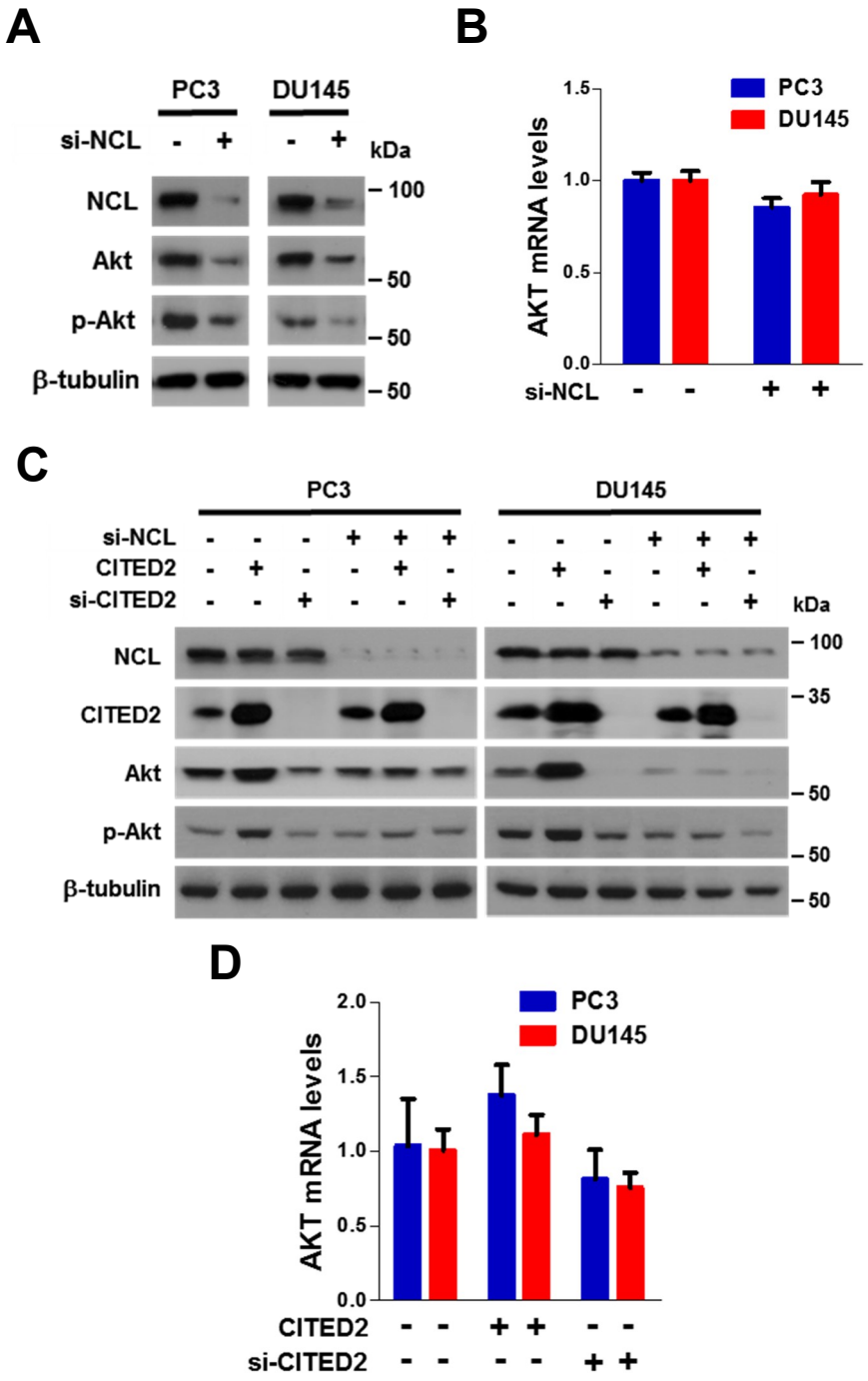

Figure 39. The CITED2−nucleolin axis was shown to affect the protein levels of AKT and phospho−AKT.

Figure 39. The CITED2-nucleolin axis was shown to affect the protein levels of AKT and phospho-AKT.

(A) Immunoblotting of nucleolin, AKT, p-AKT and β-tubulin in PC3 and DU145 cells that were transfected with si-Con or si-nucleolin. (B) The AKT mRNA levels in PC3 and DU145 cells were measured by RT-qPCR. (C) Immunoblotting of nucleolin, CITED2, AKT, p-AKT and β-tubulin in cells that were transfected with CITED2 or si-CITED2 and si-nucleolin. (D) The AKT mRNA levels in cells were measured by RT-qPCR.

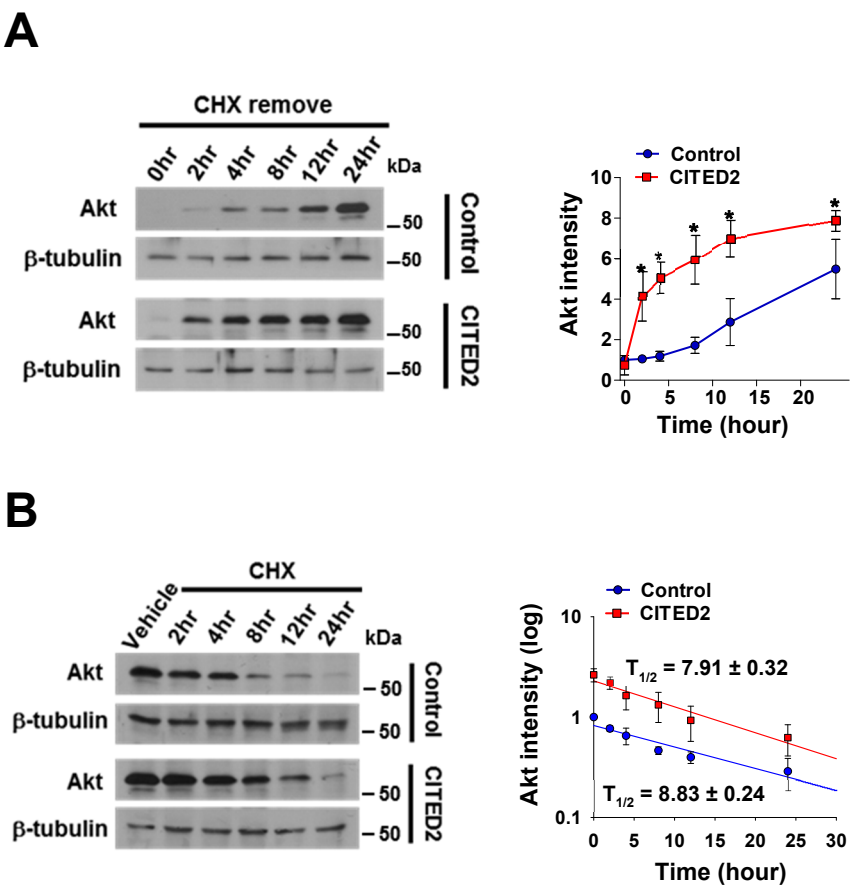

Figure 40. CITED2 facilitated de novo synthesis of the AKT protein.

Figure 40. CITED2 facilitated de novo synthesis of the AKT protein.

(A) DU145 cells, which had been transfected with pcDNA or CITED2, were pretreated with 100 μM cycloheximide for 12 h. After washing out cycloheximide, cells were incubated for the indicated times. AKT synthesis levels were detected by Western blotting and quantified using ImageJ. Each point represents the mean ± s.d. (n=3) (B) DU145 cells, which had been transfected with pcDNA or CITED2, were treated with 100 μM cycloheximide, and then cells were incubated for the indicated times. AKT levels were detected by Western blotting and quantified using ImageJ.

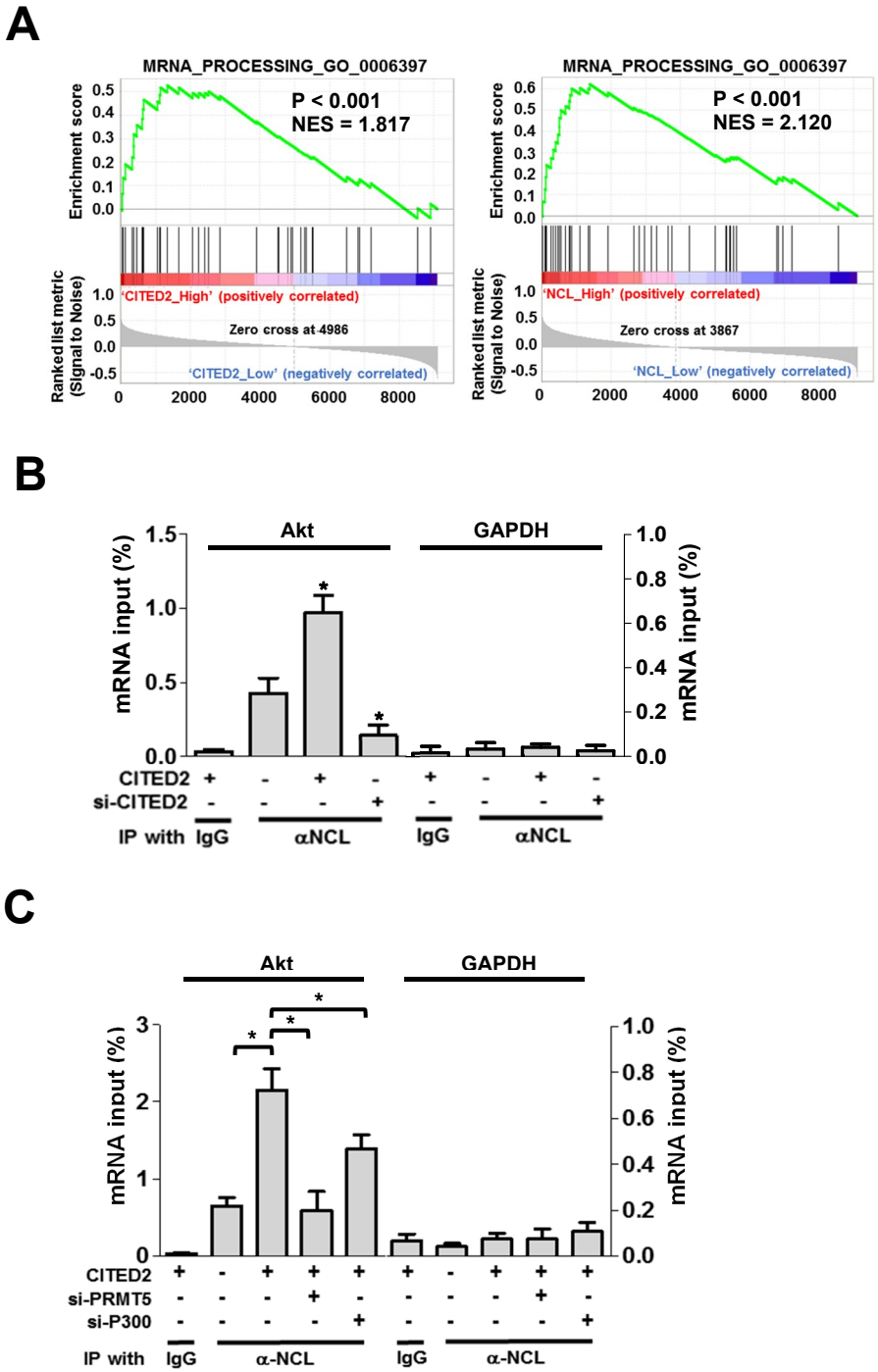

Figure 41. The CITED2–nucleolin axis regulates the translation of AKT mRNA.

Figure 41. The CITED2-nucleolin axis regulates the translation of AKT mRNA.

(A) Representative enrichment plots of the mRNA processing gene set which commonly correlates with CITED2 (left) and nucleolin (right). (B-C) RNA-IP was performed to analyze the nucleolin binding to AKT mRNA. DU145 cells were transfected as indicated and the cell lysates were immunoprecipitated with anti-nucleolin or IgG. The co-precipitated AKT or GAPDH (a negative control) mRNA was quantified using RT-qPCR. Results (the mean ± s.d., n=3) were represented as percentages of IP signal/input signal (% input).

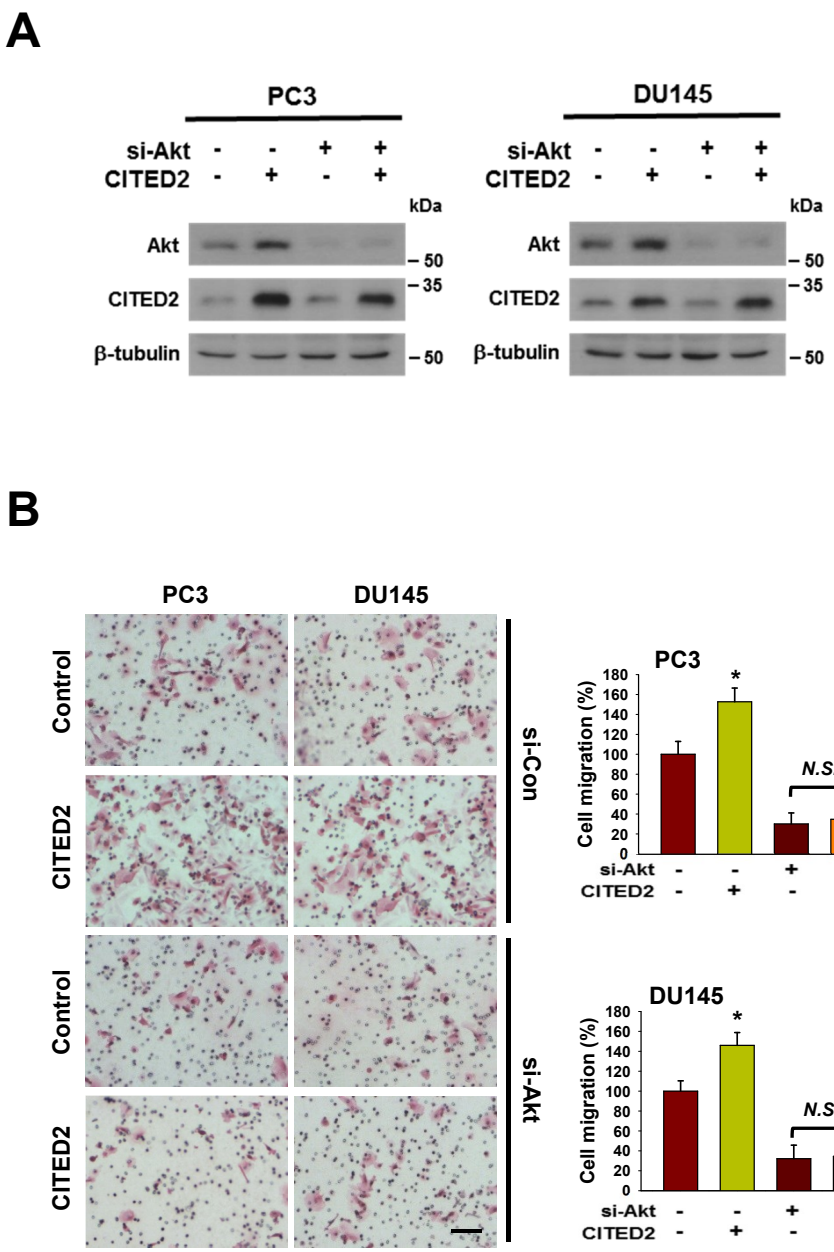

Figure 42. CITED2 overexpression increased cell migration through AKT pathway.

Figure 42. CITED2 overexpression increased cell migration through AKT pathway.

(A) AKT and CITED2 proteins were immunoblotted to verify knockdown and overexpression. (B) Cells had been transfected with CITED2, and/or si-AKT, were subjected to cell migration assay. Cells passing through the interface membrane were stained and counted. The relative cell migration is presented as a bar graph (the mean + s.d., n=3) and * denotes $P < 0.05$ versus the control group and N.S. does 'not significantly different' among the groups by Student's t-test. The scale bar represents 25μm.

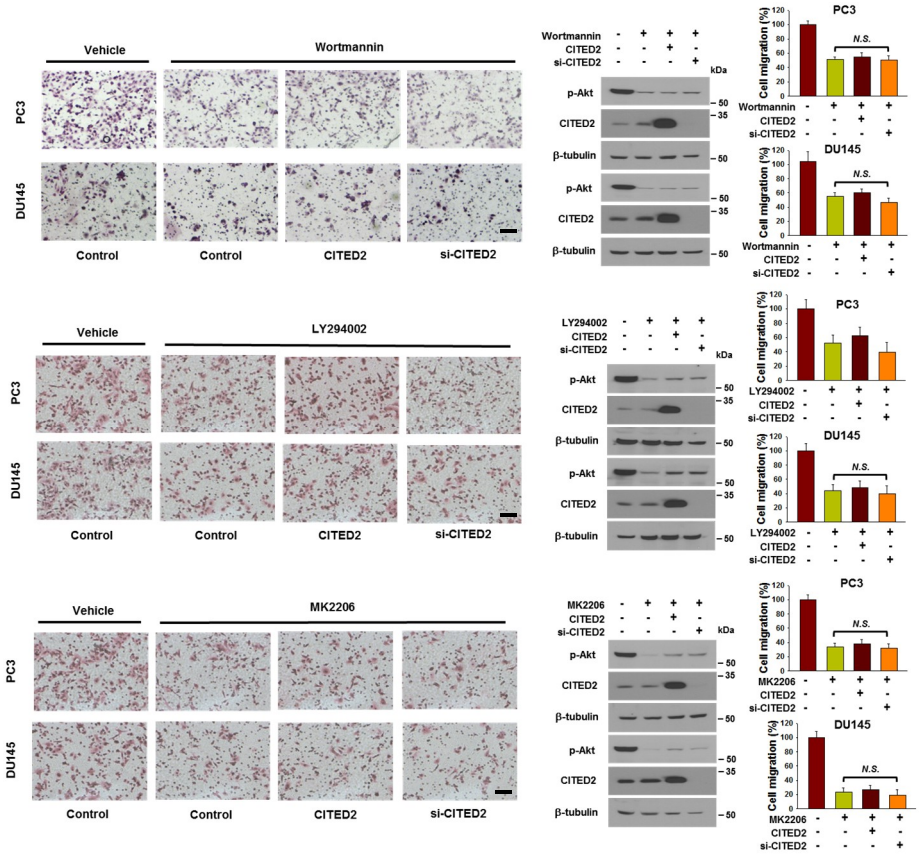

Figure 43. CITED2-dependent cell migration was attenuated by PI3K inhibitors.

Figure 43. CITED2-dependent cell migration was attenuated by PI3K inhibitors.

CITED2-activated nucleolin promotes the AKT-driven cell migration. Representative pictures of trans-well migration assays. The transfected cells were subjected to the cell migration assay in the presence of wortmannin (200 nM), LY294002 (25 μM), or MK2206 (2 μM). CITED2 and phospho-AKT levels were analyzed by Western blotting. Migrated cells were stained and counted, which are presented as bar graphs (means + s.d., n=3). N.S. represents 'not significantly different' among the indicated groups by Student's t-test. The scale bar represents 25 μm.

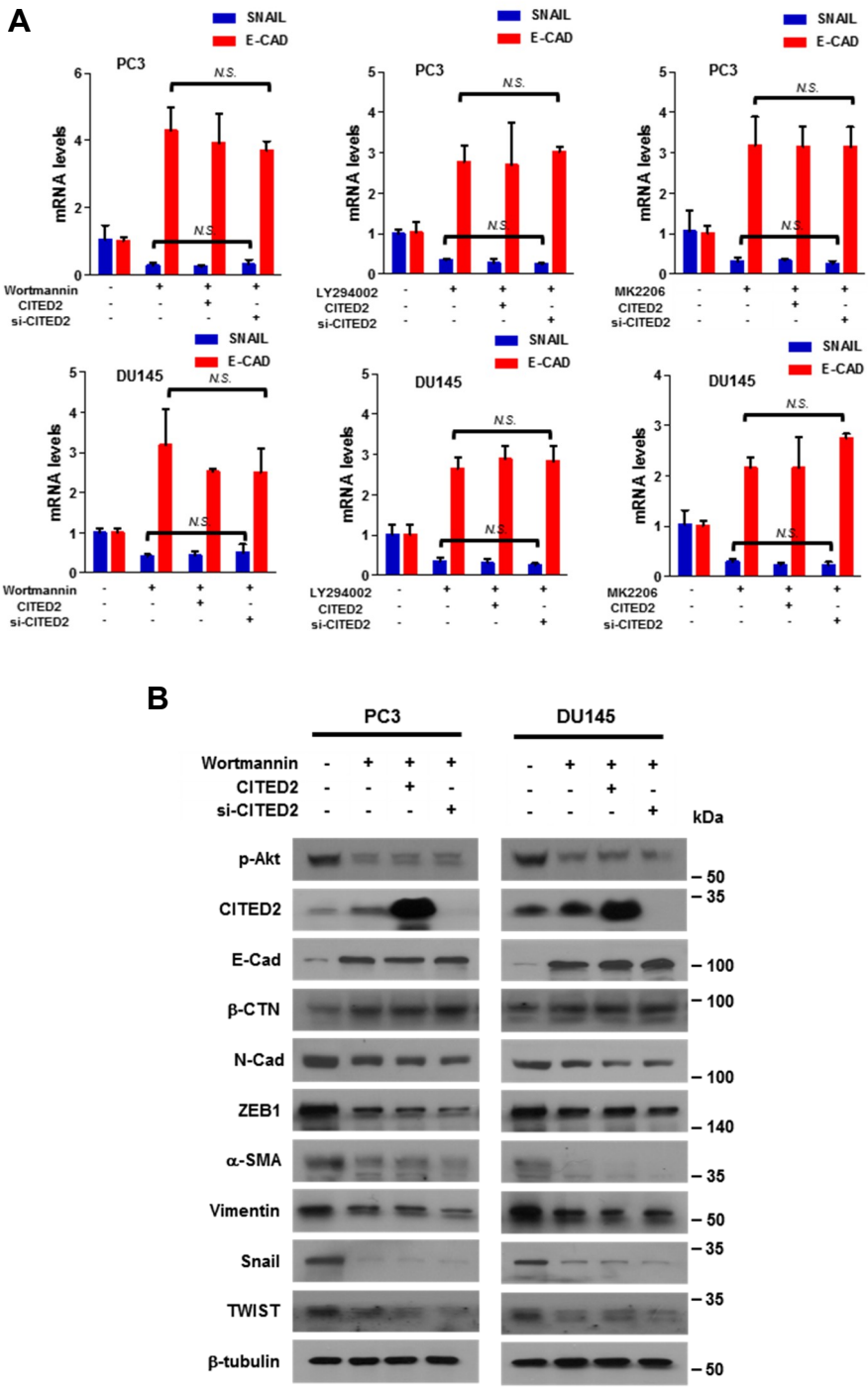

Figure 44. CITED2-dependent EMT marker alteration was attenuated by PI3K inhibitors.

Figure 44. CITED2-dependent EMT marker alteration was attenuated by PI3K inhibitors.

(A) PC3 and DU145 cells, which had been transfected with CITED2 or si-CITED2, were treated with wortmannin (200 nM), LY294002 (25 μM), or MK2206 (2 μM). The *SNAIL* and *E-CAD* mRNA levels (means + s.d., n=3) were measured by RT-qPCR. N.S. represents 'not significantly different' among the indicated groups by Student's t-test. (B) EMT markers were immunoblotted in PC3 and DU145 cells that were transfected with CITED2 or si-CITED2 and treated with wortmannin (200 nM).

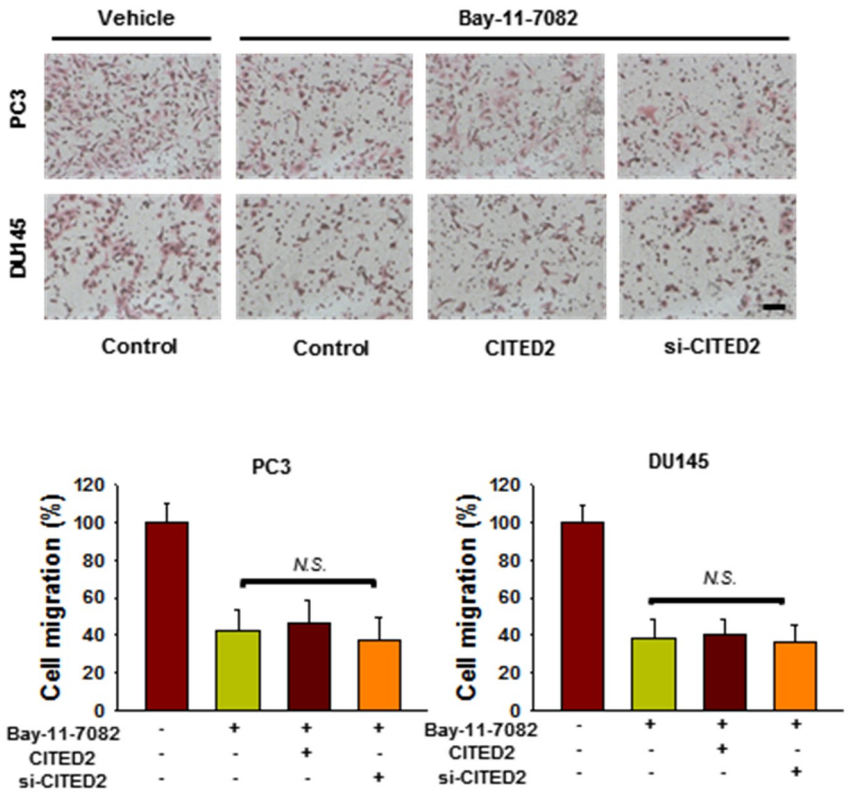

Figure 45. CITED2 regulates cell migration via the NF-kB pathway.

Representative pictures of trans-well migration assays. The transfected cells were subjected to the cell migration assay in the presence of Bay 11-7082 (10 μM). Migrated cells were stained and counted, which are presented as bar graphs (means + s.d., n=3). N.S. represents 'not significantly different' among the indicated groups by Student's t-test. The scale bar represents 25 μm.

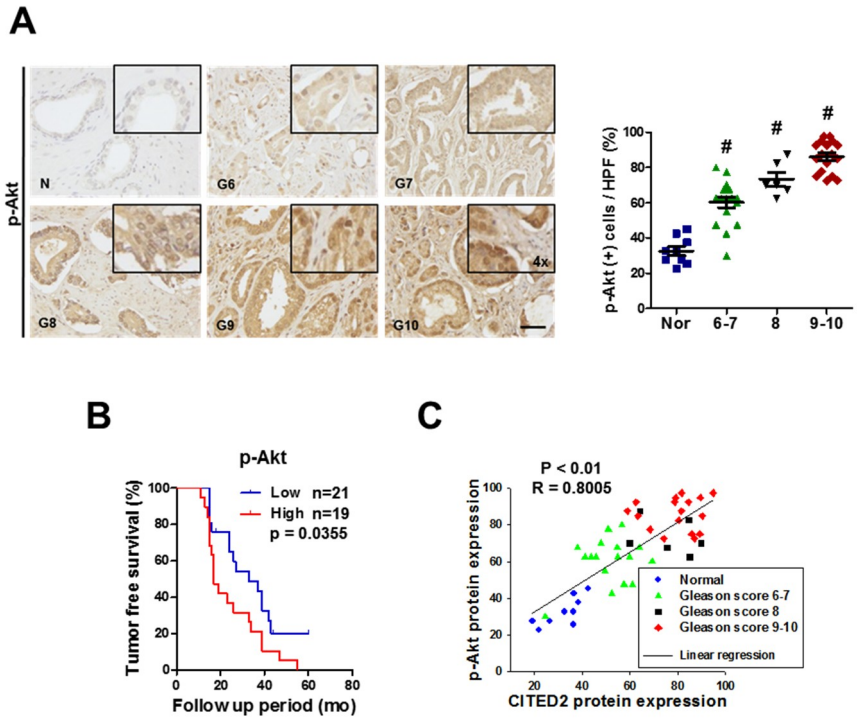

Figure 46. Phospho-AKT expression is associated with poor prognosis of prostate cancer patients.

Figure 46. Phospho-AKT expression is associated with poor prognosis of prostate cancer patients.

(A) Representative images of human prostate adenocarcinoma tissues immunostained with anti-phospho-AKT antibody. Abbreviations at the left bottoms of images: N, normal prostate tissue (blue squares); G6~10 (6-7, green triangles; 8, black inverted triangles; 9-10, red diamond) Gleason scores 6~10 of prostate cancer (left panel). The immunostaining scores were calculated by counting stained cells and presented as dot plots (right panel). The horizontal lines in dot plot represent the means ± s.e.m. and # denotes $P < 0.05$ versus the normal group by Mann-Whitney statistical analysis. The scale bar represents 50μm. (B) Kaplan-Meier tumor-free survival analysis of prostate cancer patients. P-value was calculated by Log-rank test. (C) Scatter diagrams for p-AKT expression versus CITED2 expression. R value means the Pearson's correlation coefficient.

Protein	Score	MW	Accession	Peptide
actin, gamma 1 propeptide	30.19	41765.8	4501887	3
actin, gamma 1 propeptide	20.15	41765.8	4501887	2
albumin preproprotein	160.30	69321.6	4502027	32
albumin preproprotein	70.27	69321.6	4502027	9
apolipoprotein A-I preproprotein	40.22	30758.9	4557321	4
apolipoprotein A-I preproprotein	10.14	30758.9	4557321	1
apolipoprotein D precursor	30.23	21261.8	4502163	4
apolipoprotein D precursor	10.15	21261.8	4502163	1
apolipoprotein E precursor	30.23	36131.8	4557325	3
apolipoprotein E precursor	10.18	36131.8	4557325	1
apolipoprotein H precursor	20.18	38272.7	153266841	3
apolipoprotein H precursor	10.14	38272.7	153266841	1
apolipoprotein L1 isoform c precursor	10.21	42132.0	211938442	2
apolipoprotein L1 isoform c precursor	10.14	42132.0	211938442	1
astrotactin 2 isoform d	10.15	44532.1	38016949	1
astrotactin 2 isoform d	10.13	44532.1	38016949	1
ATP-dependent DNA helicase II	10.12	82652.4	10863945	1
ATP-dependent DNA helicase II	10.12	82652.4	10863945	1
ATP-dependent DNA helicase II, 70 kDa subunit	10.18	69799.2	4503841	1
ATP-dependent DNA helicase II, 70 kDa subunit	20.13	69799.2	4503841	2
carbamoylphosphate synthetase 2/aspartate transcarbamylase	10.15	242827.1	18105007	1
carbamoylphosphate synthetase 2/aspartate transcarbamylase	130.24	242827.1	18105007	13
chaperonin	10.13	61016.5	41399285	1
chaperonin	20.17	61016.5	41399285	2
chloride channel, nucleotide-sensitive, 1A	10.19	26198.9	4502891	1
chloride channel, nucleotide-sensitive, 1A	10.20	26198.9	4502891	1
complement component 3 precursor	260.28	187029.3	115298678	32
complement component 3 precursor	20.14	187029.3	115298678	2
complement component 4B preproprotein	90.26	192629.6	178557739	10
complement component 4B preproprotein	10.12	192629.6	178557739	1
CREB binding protein isoform a	30.20	265180.1	119943104	3
CREB binding protein isoform a	100.26	265180.1	119943104	11
DEAD (Asp-Glu-Ala-Asp) box polypeptide 1	20.16	82379.9	4826686	2
DEAD (Asp-Glu-Ala-Asp) box polypeptide 1	20.12	82379.9	4826686	2
DEAD (Asp-Glu-Ala-Asp) box polypeptide 4 isoform 2	10.13	75773.2	216548263	1
DEAD (Asp-Glu-Ala-Asp) box polypeptide 4 isoform 2	10.13	75773.2	216548263	1
DEAD (Asp-Glu-Ala-Asp) box polypeptide 5	20.16	69104.8	4758138	2
DEAD (Asp-Glu-Ala-Asp) box polypeptide 5	20.15	69104.8	4758138	2
dynein heavy chain domain 3	10.13	507374.4	75677365	1
dynein heavy chain domain 3	10.12	507374.4	75677365	1
E1A binding protein p300	50.16	263988.7	50345997	5
E1A binding protein p300	230.27	263988.7	50345997	29
eukaryotic translation elongation factor 1 alpha 1	40.18	50109.2	4503471	5
eukaryotic translation elongation factor 1 alpha 1	30.20	50109.2	4503471	4
eukaryotic translation elongation factor 1 gamma	20.20	50087.2	4503481	2
eukaryotic translation elongation factor 1 gamma	20.20	50087.2	4503481	2
glutamyl-prolyl tRNA synthetase	10.12	170482.3	62241042	1
glutamyl-prolyl tRNA synthetase	10.14	170482.3	62241042	1
haptoglobin isoform 2 preproprotein	70.20	38427.3	186910296	9
haptoglobin isoform 2 preproprotein	30.18	38427.3	186910296	3
heat shock 70kDa protein 1A	100.22	70009.2	194248072	11
heat shock 70kDa protein 1A	170.24	70009.2	194248072	24
heat shock 70kDa protein 1-like	10.21	70331.5	124256496	1
heat shock 70kDa protein 1-like	10.25	70331.5	124256496	1
heat shock 70kDa protein 8 isoform 2	80.23	53484.5	24234686	9
heat shock 70kDa protein 8 isoform 2	140.25	53484.5	24234686	17
heat shock 70kDa protein 9 precursor	10.17	73634.8	24234688	1
heat shock 70kDa protein 9 precursor	50.21	73634.8	24234688	5
heat shock protein 90kDa alpha (cytosolic), class A member 1 isoform 2	10.17	84606.7	154146191	1
heat shock protein 90kDa alpha (cytosolic), class A member 1 isoform 2	30.17	84606.7	154146191	3
heterogeneous nuclear ribonucleoprotein H2	30.24	49232.3	74099697	5
heterogeneous nuclear ribonucleoprotein H2	30.22	49232.3	74099697	3
heterogeneous nuclear ribonucleoprotein K isoform a	20.20	50996.4	14165439	2
heterogeneous nuclear ribonucleoprotein K isoform a	30.18	50996.4	14165439	3
heterogeneous nuclear ribonucleoprotein U isoform a	30.14	90528.0	74136883	3
heterogeneous nuclear ribonucleoprotein U isoform a	20.16	90528.0	74136883	2
hypothetical protein LOC51493	10.15	55175.0	7657015	1
hypothetical protein LOC51493	10.12	55175.0	7657015	1
influenza virus NS1A binding protein	30.18	71682.9	24475847	3
influenza virus NS1A binding protein	10.14	71682.9	24475847	1
inter-alpha (globulin) inhibitor H4	40.25	103293.2	31542984	6
inter-alpha (globulin) inhibitor H4	10.22	103293.2	31542984	1
interleukin enhancer binding factor 3 isoform e	10.12	76454.2	212549555	1
interleukin enhancer binding factor 3 isoform e	20.12	76454.2	212549555	2

LINE-1 type transposase domain containing 1	10.12	98788.5	157694505	1
LINE-1 type transposase domain containing 1	10.12	98788.5	157694505	1
mesotrypsin isoform 1 preproprotein	10.16	32478.0	170296790	1
mesotrypsin isoform 1 preproprotein	10.15	32478.0	170296790	1
nucleolin	60.18	76568.5	55956788	6
nucleolin	40.14	76568.5	55956788	4
phosphoribosyl pyrophosphate synthetase-associated protein 2	10.17	40899.4	4506133	1
phosphoribosyl pyrophosphate synthetase-associated protein 2	10.16	40899.4	4506133	1
PREDICTED: similar to 22kDa peroxisomal membrane protein-like	10.17	41420.8	169205662	1
PREDICTED: similar to 22kDa peroxisomal membrane protein-like	10.18	41420.8	169205662	2
PREDICTED: similar to BCL2-associated transcription factor 1 isoform 1	10.17	79930.8	169218322	1
PREDICTED: similar to BCL2-associated transcription factor 1 isoform 2	10.16	100079.5	169218320	1
protein arginine methyltransferase 5 isoform a	10.22	72637.7	20070220	2
protein arginine methyltransferase 5 isoform a	10.21	72637.7	20070220	3
protein arginine methyltransferase 5 isoform b	160.27	71275.1	88900507	25
protein arginine methyltransferase 5 isoform b	100.27	71275.1	88900507	15
protein phosphatase 1B isoform 3	10.16	20740.1	29558099	1
protein phosphatase 1B isoform 3	10.17	20740.1	29558099	1
protein phosphatase 1B isoform 5	70.20	42059.5	75813620	12
protein phosphatase 1B isoform 5	50.23	42059.5	75813620	5
pyruvate kinase, muscle isoform M1	10.12	58025.1	33286422	1
pyruvate kinase, muscle isoform M1	10.15	58025.1	33286422	1
replication protein A1, 70kDa	10.14	68095.4	4506583	1
replication protein A1, 70kDa	20.17	68095.4	4506583	2
ribosomal protein L11	10.16	20239.7	15431290	1
ribosomal protein L11	10.13	20239.7	15431290	1
ribosomal protein L23a	10.12	17684.1	17105394	1
ribosomal protein L23a	10.17	17684.1	17105394	1
ribosomal protein P0	10.12	34251.8	16933546	1
ribosomal protein P0	10.12	34251.8	16933546	1
ribosomal protein S3	20.13	26671.4	15718687	2
ribosomal protein S3	20.16	26671.4	15718687	2
RIO kinase 1 isoform 1	10.14	65541.8	23510356	1
RIO kinase 1 isoform 1	20.13	65541.8	23510356	2
RIO kinase 1 isoform 2	10.18	38019.1	23510358	1
RIO kinase 1 isoform 2	10.19	38019.1	23510358	2
RNA binding motif protein 10 isoform 1	10.13	103469.3	20127479	1
RNA binding motif protein 10 isoform 1	10.12	103469.3	20127479	1
RNA binding motif protein 10 isoform 2	20.13	94312.2	23111018	2
RNA binding motif protein 10 isoform 2	10.15	94312.2	23111018	1
S100 calcium-binding protein A9	10.13	13233.5	4506773	1
S100 calcium-binding protein A9	10.15	13233.5	4506773	1
serine proteinase inhibitor, clade A, member 1	60.30	46707.1	189163542	12
serine proteinase inhibitor, clade A, member 1	50.27	46707.1	189163542	5
serine/threonine kinase 38	20.16	54155.4	6005814	2
serine/threonine kinase 38	10.12	54155.4	6005814	1
small nuclear ribonucleoprotein polypeptide D3	10.15	13907.3	4759160	1
small nuclear ribonucleoprotein polypeptide D3	10.15	13907.3	4759160	1
sodium channel, voltage-gated, type X, alpha	10.14	220481.8	110835710	2
sodium channel, voltage-gated, type X, alpha	10.12	220481.8	110835710	2
splicing factor 3b, subunit 1 isoform 1	30.16	145738.0	54112117	3
splicing factor 3b, subunit 1 isoform 1	10.12	145738.0	54112117	1
splicing factor 3b, subunit 3	50.15	135491.9	54112121	5
splicing factor 3b, subunit 3	10.15	135491.9	54112121	1
splicing factor proline/glutamine rich	10.14	76101.8	4826998	1
splicing factor proline/glutamine rich	10.15	76101.8	4826998	1
transferrin	160.26	76999.7	4557871	18
transferrin	10.14	76999.7	4557871	1
tripartite motif-containing 10 isoform 1	10.15	55001.7	157426898	1
tripartite motif-containing 10 isoform 1	10.13	55001.7	157426898	1
tubulin, alpha 1a	70.29	50103.7	17986283	7
tubulin, alpha 1a	90.29	50103.7	17986283	14
tubulin, alpha, ubiquitous	10.17	50119.6	57013276	1
tubulin, alpha, ubiquitous	20.16	50119.6	57013276	2
tubulin, beta	50.20	49639.0	29788785	7
tubulin, beta	70.20	49639.0	29788785	7
tubulin, beta 4	10.23	49553.9	21361322	1
tubulin, beta 4	20.24	49553.9	21361322	2
tubulin, beta, 4	70.23	50400.3	50592996	10
tubulin, beta, 4	120.24	50400.3	50592996	17
WD repeat domain 77	80.29	36701.1	13129110	11
WD repeat domain 77	40.31	36701.1	13129110	6
zinc finger, CCHC domain containing 11 isoform a	10.12	185134.4	57863248	1
zinc finger, CCHC domain containing 11 isoform a	10.13	185134.4	57863248	2

Table 1. List of CITED2-interacting proteins.

HEK293T cells were transfected with Flag/SBP-CITED2 and proteins in cell lysates were precipitated by anti-Flag or streptavidin affinity beads. Co-precipitated proteins were identified using LC-MS/MS. The proteins commonly precipitated by both affinity beads are listed.

Gene	Direction	Nucleotide Sequence
E-CADHERIN	Forward	5′-ACAACAAGCCCGAATTCACCCA-3′
	Reverse	5′-TCACAGCTGTTGCTGTTGTGCT-3′
SNAIL	Forward	5′-CCCAATCGGAAGCCTAACTA-3′
	Reverse	5′-CAGGACAGAGTCCCAGATGAG-3′
GAPDH	Forward	5′-TGTGGTCATGAGTCCTTCCA-3’
	Reverse	5’-CGAGATCCCTCCAAAATCAA-3’
CITED2	Forward	5’-ACCCACCTCCCTTATGTAGT-3’
	Reverse	5’-CCAACTAATGCAATTTTTCC-3’
AKT	Forward	5’-GCCATGAAGATCCTCAAGAA-3’
	Reverse	5’-GTACTCCATGACAAAGCAGA-3’
TMPRSS2-ERG	Forward	5’-CAGGAGGCGGAGGCGGA-3’
	Reverse	5’-GGCGTTGTAGCTGGGGGTGAG-3’
CITED2-P1	Forward	5’-CACTGCCCTGATCTTTCTAA-3’
	Reverse	5’-TGGGGTAGAAAATGTATGGC-3’
CITED2-P2	Forward	5’-GACTAGGAAAAGACAGAGGG-3’
	Reverse	5’-ACTCGATAGCCATTGAAGAC-3’
CITED2-P3	Forward	5’-ATGAAAACACAAAGGCACAG-3’
	Reverse	5’-TTTCTCACTCGGTTCACCTA-3’

Table 2. Sequences of primers used in PCR and ChIP.

No.	Age	Sex	Organ	Diagnosis	Gleason score	Stage	Residual tumor	Follow-up month	Live	PSA (ng/ml)
1	60	Male	Prostate	adenocarcinoma	9	3	no	60	alive	11.2
2	64	Male	Prostate	adenocarcinoma	7	2b	no	60	alive	30
3	71	Male	Prostate	adenocarcinoma	9	3	yes	55	alive	60.4
4	64	Male	Prostate	adenocarcinoma	10	3	yes	47	alive	7.4
5	59	Male	Prostate	adenocarcinoma	9	3	yes	44	alive	9.8
6	65	Male	Prostate	adenocarcinoma	8	3	yes	43	alive	34.9
7	73	Male	Prostate	adenocarcinoma	7	2b	yes	42	alive	48.1
8	69	Male	Prostate	adenocarcinoma	7	2b	no	42	alive	10.6
9	62	Male	Prostate	adenocarcinoma	7	2b	yes	39	alive	37.3
10	66	Male	Prostate	adenocarcinoma	9	3	yes	39	alive	1.2
11	60	Male	Prostate	adenocarcinoma	9	3	yes	39	alive	40
12	66	Male	Prostate	adenocarcinoma	7	3	yes	39	alive	8.4
13	70	Male	Prostate	adenocarcinoma	7	3	yes	37	alive	7
14	65	Male	Prostate	adenocarcinoma	9	3	yes	23	dead	17.5
15	67	Male	Prostate	adenocarcinoma	9	3	yes	34	alive	13.1
16	69	Male	Prostate	adenocarcinoma	7	3	yes	33	alive	1.1
17	63	Male	Prostate	adenocarcinoma	9	3	yes	33	alive	11.8
18	69	Male	Prostate	adenocarcinoma	7	3	yes	27	alive	17.6
19	70	Male	Prostate	adenocarcinoma	7	3	yes	26	alive	9
20	58	Male	Prostate	adenocarcinoma	9	3	no	26	alive	5.8
21	58	Male	Prostate	adenocarcinoma	7	3	yes	24	alive	15.8
22	71	Male	Prostate	adenocarcinoma	7	2b	yes	24	alive	31.4
23	70	Male	Prostate	adenocarcinoma	7	3	yes	19	alive	14.4
24	59	Male	Prostate	adenocarcinoma	6	2a	no	18	alive	18.3
25	63	Male	Prostate	adenocarcinoma	9	3	yes	17	alive	16.6
26	72	Male	Prostate	adenocarcinoma	9	3	yes	16	alive	.
27	66	Male	Prostate	adenocarcinoma	8	2	yes	17	dead	10.8
28	70	Male	Prostate	adenocarcinoma	6	3	yes	16	alive	10.8
29	70	Male	Prostate	adenocarcinoma	7	2b	no	15	alive	.
30	68	Male	Prostate	adenocarcinoma	8	3	yes	15	alive	26.9
31	63	Male	Prostate	adenocarcinoma	10	3	yes	15	alive	.
32	57	Male	Prostate	adenocarcinoma	7	3	yes	15	alive	25
33	72	Male	Prostate	adenocarcinoma	8	2b	yes	15	alive	16.8
34	70	Male	Prostate	adenocarcinoma	8	3	yes	15	alive	0.5
35	75	Male	Prostate	adenocarcinoma	9	3	yes	15	alive	98
36	62	Male	Prostate	adenocarcinoma	9	3	yes	15	alive	.
37	63	Male	Prostate	adenocarcinoma	9	3	yes	14	alive	91
38	53	Male	Prostate	adenocarcinoma	9	3	yes	17	dead	161
39	63	Male	Prostate	adenocarcinoma	8	3	yes	13	alive	13
40	44	Male	Prostate	adenocarcinoma	7	3	yes	11	alive	.
41	69	Male	Prostate	normal	.	.	.	.	.	.
42	62	Male	Prostate	normal	.	.	.	.	.	.
43	66	Male	Prostate	normal	.	.	.	.	.	.
44	65	Male	Prostate	normal	.	.	.	.	.	.
45	69	Male	Prostate	normal	.	.	.	.	.	.
46	70	Male	Prostate	normal	.	.	.	.	.	.
47	70	Male	Prostate	normal	.	.	.	.	.	.
48	63	Male	Prostate	normal	.	.	.	.	.	.
49	44	Male	Prostate	normal	.	.	.	.	.	.

Table 3. Clinical information on prostate cancer patients.

DISCUSSION

The current treatments for prostate cancer include surgery, irradiation, and androgen deprivation, but none of these treatments are effective for metastatic castration-resistant prostate cancer (CRPC). Docetaxel is currently used to treat CRPC, because it prolongs the median survival by 3 months (37), and abiraterone is an emerging anti-CRPC drug capable of increasing the survival by 4 months (38). Unfortunately, the anticancer effects of these drugs are very limited because of the development of drug resistance (39, 40). In this study, CITED2 was found to be uniquely overexpressed in prostate cancer cells, in which it promoted metastasis by activating the nucleolin-AKT signaling pathway. I therefore propose that CITED2 may be a potential target for treating metastatic prostate cancer.

ERG is an important factor that contributes to prostate cancer progression (4, 5). It is not expressed in normal prostate epithelium but is markedly amplified in prostate cancer because of its gene fusion to the androgen-driven promoter TMPRSS2 (41). Other ETS gene family members, such as *ETV1, ETV4, ETV5*, and *FLI1*, can also fuse to TMPRSS2, but these fusion

events display much lower frequencies compared with ERG (42-44). The significance of ERG gene fusion was demonstrated by its correlation with the clinical phase of patients. ERG expression was positively correlated with the Gleason score in prostate cancer tissues, and it was associated with prostate cancer metastasis and poor patient prognoses (45). Many follow-up studies have been conducted to understand how ERG promotes prostate cancer. For example, one study reported that ERG reorganizes actin filaments by activating vimentin and upregulating matrix metalloproteinases, leading to cell invasion (46). ERG was also reported to facilitate cell movement by inducing the EMT (47). However, the downstream signaling pathway responsible for ERG-driven metastasis remains unclear. I identified ERG as a transcription factor regulating expression of the *CITED2* gene, which is specifically overexpressed in prostate cancer, and further clarified the ERG-CITED2 axis as the downstream pathway involved in prostate cancer.

Because nucleolin exists in a complex with PRMT5 and p300, I tested the possibility that nucleolin is post-translationally co-modified by PRMT5 and p300. Although arginine methylation does not significantly affect the overall charge of nucleolin, steric

hindrance or hydrogen bonds around arginine could be altered. Thus, methylation can modify intermolecular interactions (48–50). In proteins containing the RNA–binding RGG domain, alterations of protein–RNA interactions by methylation have been reported previously (51). Because nucleolin is also an RNA–binding protein with a RGG motif (52), I tested the possibility that nucleolin binding to AKT mRNA is regulated by the PRMT5–mediated arginine dimethylation of nucleolin. Methylation enhanced the interaction between nucleolin and AKT mRNA, thereby facilitating de novo synthesis of AKT translationally. However, lysine acetylation of nucleolin has not been investigated comprehensively. A previous study reported that p300–mediated lysine acetylation stabilized nucleolin (53). However, I observed no change in the level of nucleolin after overexpressing or knocking–down p300. According to another study, acetylation may influence the binding between nucleolin and nucleic acids. Lysine acetylation is essential for STAT3 or p53 binding to DNA (54, 55). In a similar manner, I speculate that nucleolin acetylation by P300 can affect mRNA polysome formation. This possibility needs to be confirmed by additional studies.

Notably, I found that the nucleolin complex was present mainly in the nucleus, but nucleolin was bound to AKT mRNA in the cytoplasm. The difference in the location of nucleolin suggests that nucleolin is post-translationally modified in the nucleus and then transported to the cytoplasm. Because the entire nucleolin complex was too large to pass through the nuclear membrane, it is reasonable to assume that the modified nucleolin is released from the complex and then translocated to the cytoplasm. Consistent with these possibilities, a study demonstrated translocation of nucleolin from the nucleus to the cytoplasm and the plasma membrane after phosphorylation (56). However, no study has reported the translocation of nucleolin after acetylation or methylation, which suggests a mechanism underlying nucleolin translocation.

Although CITED2 has no special functional domain, it can participate in important biological processes as a scaffolding protein. CITED2 is comprised of three CR(1-3) and one SRJ domains (57, 58). Because each domain provides a docking site for protein interactions, CITED2 with multiple domains may act as a central scaffold recruiting different proteins. For example, CR2 interacts with transcription factors such as TFAP2, HNF4a,

PPARa/r, and Smad 2/3 and enhances gene expression by recruiting CBP/p300 (6, 10, 59, 60). CR1 interacts with the GCN5 acetyltransferase, thereby inhibiting the GCN5-mediated acetylation of PGC-1α (61). CR3 binds to the homeobox protein LHx2 and increases expression of glycoprotein hormone α-subunit (62). Because I am intrigued by the numerous functions of CITED2, which depend on its binding molecule, I investigated its potential role in tumorigenesis. Previous studies have reported that CITED2 increases cancer progression. It has been reported that CITED2 promotes MYC-mediated transactivation of the *E2F3* gene by recruiting p300 to stimulate lung cancer progression (16). However, little is known about the role of CITED2 in cancer metastasis. I thus conducted a screening in patients to identify the cancer type most affected by CITED2 expression and found that CITED2 was most elevated in metastatic prostate cancer. However, considering that a kind of cytokine storm occurs in tumor microenvironment, CITED2 could be differentially expressed in primary and metastatic tumors because they grow with distinct stromal cells. Indeed, various growth factors and cytokines have been reported to increase CITED2 expression(8). Therefore, I cannot rule out the

possibility that CITED2 is overexpressed in metastatic tumor milieu. Nonetheless, our cellular and animal experiments support our notion that ERG-induced CITED2 promotes prostate cancer metastasis. According to this scenario, CITED2 could be a potential target to prevent prostate cancer metastasis. Since the complete inhibition of CITED2 has been reported to induce acute bone marrow failure (14), the anti-CITED2 strategy should be carefully optimized before clinical application.

Because AKT is involved in important oncogenic pathways, most studies have emphasized its role in survival and the cell cycle. AKT activates the mTOR pathway, which increases cyclin D1 translation to promote cell cycle progression (63), and stimulates CREB activity to induce survival genes such as *Bcl-2* (64). Many recent studies have also characterized the roles of AKT in EMT and cell migration. AKT not only increases SNAIL expression by activating NF-kB (36), but also stabilizes the SNAIL protein by inactivating GSK-3β (65). Moreover, AKT enhances transcription of the *SNAIL* and *SLUG* genes by phosphorylating β-catenin (66). According to past studies, the AKT pathway is aberrantly activated in cancers because of *AKT* gene amplification and the *PTEN* gene deletion (67). Our study

suggests a mechanism involving AKT activation in prostate cancer. The CITED2 stimulation of AKT translation strengthens AKT signaling to promote EMT and eventually cancer metastasis.

In this study, I identified a pathway related to metastasis, involving ERG, CITED2, nucleolin, and AKT pathway, in prostate cancer. This metastasis-promoting mechanism may be particularly important in prostate cancer overexpressing ERG due to gene fusion events involving ERG. I also identified CITED2 and nucleolin as target molecules for preventing prostate cancer metastasis in an orthotopic xenograft animal model. Overall, this study provides a basis for future concept studies to develop the next generation of prostate cancer treatments.

REFERENCES

1. Attard G, *et al.* (2016) Prostate cancer. *Lancet* 387(10013):70-82.
2. Hwang C (2012) Overcoming docetaxel resistance in prostate cancer: a perspective review. *Ther Adv Med Oncol* 4(6):329-340.
3. Tomlins SA, *et al.* (2005) Recurrent fusion of TMPRSS2 and ETS transcription factor genes in prostate cancer. *Science* 310(5748):644-648.
4. Tomlins SA, *et al.* (2008) Role of the TMPRSS2-ERG gene fusion in prostate cancer. *Neoplasia* 10(2):177-188.
5. Vanaja DK, Cheville JC, Iturria SJ, & Young CY (2003) Transcriptional silencing of zinc finger protein 185 identified by expression profiling is associated with prostate cancer progression. *Cancer Res* 63(14):3877-3882.
6. Bamforth SD, *et al.* (2001) Cardiac malformations, adrenal agenesis, neural crest defects and exencephaly in mice lacking Cited2, a new Tfap2 co-activator. *Nat Genet* 29(4):469-474.
7. Bhattacharya S, *et al.* (1999) Functional role of p35srj, a novel p300/CBP binding protein, during transactivation by HIF-1. *Genes Dev* 13(1):64-75.
8. Sun HB, Zhu YX, Yin T, Sledge G, & Yang YC (1998) MRG1, the product of a melanocyte-specific gene related gene, is a cytokine-inducible transcription factor with

transformation activity. *Proc Natl Acad Sci U S A* 95(23):13555-13560.

9. Li Q, Ramirez-Bergeron DL, Dunwoodie SL, & Yang YC (2012) Cited2 gene controls pluripotency and cardiomyocyte differentiation of murine embryonic stem cells through Oct4 gene. *J Biol Chem* 287(34):29088-29100.

10. Qu X, *et al.* (2007) Cited2, a coactivator of HNF4alpha, is essential for liver development. *EMBO J* 26(21):4445-4456.

11. Xu B, *et al.* (2008) Cited2 is required for fetal lung maturation. *Dev Biol* 317(1):95-105.

12. Yin Z, *et al.* (2002) The essential role of Cited2, a negative regulator for HIF-1alpha, in heart development and neurulation. *Proc Natl Acad Sci U S A* 99(16):10488-10493.

13. Chen Y, *et al.* (2008) Cited2 is required for the proper formation of the hyaloid vasculature and for lens morphogenesis. *Development* 135(17):2939-2948.

14. Kranc KR, *et al.* (2009) Cited2 is an essential regulator of adult hematopoietic stem cells. *Cell Stem Cell* 5(6):659-665.

15. Korthuis PM, *et al.* (2015) CITED2-mediated human hematopoietic stem cell maintenance is critical for acute myeloid leukemia. *Leukemia* 29(3):625-635.

16. Chou YT, *et al.* (2012) CITED2 functions as a molecular switch of cytokine-induced proliferation and quiescence. *Cell Death Differ* 19(12):2015-2028.

17. Bai L & Merchant JL (2007) A role for CITED2, a CBP/p300 interacting protein, in colon cancer cell invasion. *FEBS Lett* 581(30):5904-5910.
18. van Agthoven T, *et al.* (2009) CITED2 and NCOR2 in anti-oestrogen resistance and progression of breast cancer. *Br J Cancer* 101(11):1824-1832.
19. Aprelikova O, Wood M, Tackett S, Chandramouli GV, & Barrett JC (2006) Role of ETS transcription factors in the hypoxia-inducible factor-2 target gene selection. *Cancer Res* 66(11):5641-5647.
20. Patki M, *et al.* (2013) The ETS domain transcription factor ELK1 directs a critical component of growth signaling by the androgen receptor in prostate cancer cells. *J Biol Chem* 288(16):11047-11065.
21. Greasley PJ, Bonnard C, & Amati B (2000) Myc induces the nucleolin and BN51 genes: possible implications in ribosome biogenesis. *Nucleic Acids Res* 28(2):446-453.
22. Pichiorri F, *et al.* (2013) In vivo nucleolin targeting affects breast cancer aggressiveness through miRNA regulation. *J Exp Med* 210(5):951-968.
23. Grinstein E, *et al.* (2006) Cell cycle-controlled interaction of nucleolin with the retinoblastoma protein and cancerous cell transformation. *J Biol Chem* 281(31):22223-22235.
24. Erard MS, Belenguer P, Caizergues-Ferrer M, Pantaloni A, & Amalric F (1988) A major nucleolar protein, nucleolin, induces chromatin decondensation by binding to histone H1. *Eur J Biochem* 175(3):525-530.
25. Escande-Geraud ML, Azum MC, Tichadou JL, & Gas N

(1985) Correlation between rDNA transcription and distribution of a 100 kD nucleolar protein in CHO cells. *Exp Cell Res* 161(2):353-363.

26. Ginisty H, Amalric F, & Bouvet P (1998) Nucleolin functions in the first step of ribosomal RNA processing. *EMBO J* 17(5):1476-1486.
27. Sipos K & Olson MO (1991) Nucleolin promotes secondary structure in ribosomal RNA. *Biochem Biophys Res Commun* 177(2):673-678.
28. Abdelmohsen K, *et al.* (2011) Enhanced translation by Nucleolin via G-rich elements in coding and non-coding regions of target mRNAs. *Nucleic Acids Res* 39(19):8513-8530.
29. Caizergues-Ferrer M, *et al.* (1987) Phosphorylation of nucleolin by a nucleolar type NII protein kinase. *Biochemistry* 26(24):7876-7883.
30. Peter M, Nakagawa J, Doree M, Labbe JC, & Nigg EA (1990) Identification of major nucleolar proteins as candidate mitotic substrates of cdc2 kinase. *Cell* 60(5):791-801.
31. Das S, *et al.* (2013) Characterization of nucleolin K88 acetylation defines a new pool of nucleolin colocalizing with pre-mRNA splicing factors. *FEBS Lett* 587(5):417-424.
32. Guderian G, *et al.* (2011) RioK1, a new interactor of protein arginine methyltransferase 5 (PRMT5), competes with pICln for binding and modulates PRMT5 complex composition and substrate specificity. *J Biol Chem*

286(3):1976-1986.

33. Edge SB & Compton CC (2010) The American Joint Committee on Cancer: the 7th edition of the AJCC cancer staging manual and the future of TNM. *Ann Surg Oncol* 17(6):1471-1474.

34. Clark JP & Cooper CS (2009) ETS gene fusions in prostate cancer. *Nat Rev Urol* 6(8):429-439.

35. Han B, Liu N, Yang X, Sun HB, & Yang YC (2001) MRG1 expression in fibroblasts is regulated by Sp1/Sp3 and an Ets transcription factor. *J Biol Chem* 276(11):7937-7942.

36. Julien S, *et al.* (2007) Activation of NF-kappaB by Akt upregulates Snail expression and induces epithelium mesenchyme transition. *Oncogene* 26(53):7445-7456.

37. Tannock IF, *et al.* (2004) Docetaxel plus prednisone or mitoxantrone plus prednisone for advanced prostate cancer. *N Engl J Med* 351(15):1502-1512.

38. Ryan CJ, *et al.* (2013) Abiraterone in metastatic prostate cancer without previous chemotherapy. *N Engl J Med* 368(2):138-148.

39. Richards J, *et al.* (2012) Interactions of abiraterone, eplerenone, and prednisolone with wild-type and mutant androgen receptor: a rationale for increasing abiraterone exposure or combining with MDV3100. *Cancer Res* 72(9):2176-2182.

40. Cai C, *et al.* (2011) Intratumoral de novo steroid synthesis activates androgen receptor in castration-resistant prostate cancer and is upregulated by treatment with CYP17A1 inhibitors. *Cancer Res* 71(20):6503-6513.

41. Deramaudt TB, Remy P, & Stiegler P (2001) Identification of interaction partners for two closely-related members of the ETS protein family, FLI and ERG. *Gene* 274(1-2):169-177.
42. Tomlins SA, *et al.* (2007) Distinct classes of chromosomal rearrangements create oncogenic ETS gene fusions in prostate cancer. *Nature* 448(7153):595-599.
43. Berger MF, *et al.* (2011) The genomic complexity of primary human prostate cancer. *Nature* 470(7333):214-220.
44. Rubin MA, Maher CA, & Chinnaiyan AM (2011) Common gene rearrangements in prostate cancer. *J Clin Oncol* 29(27):3659-3668.
45. Hagglof C, *et al.* (2014) TMPRSS2-ERG expression predicts prostate cancer survival and associates with stromal biomarkers. *PLoS One* 9(2):e86824.
46. Becker-Santos DD, *et al.* (2012) Integrin-linked kinase as a target for ERG-mediated invasive properties in prostate cancer models. *Carcinogenesis* 33(12):2558-2567.
47. Leshem O, *et al.* (2011) TMPRSS2/ERG promotes epithelial to mesenchymal transition through the ZEB1/ZEB2 axis in a prostate cancer model. *PLoS One* 6(7):e21650.
48. McBride AE & Silver PA (2001) State of the arg: protein methylation at arginine comes of age. *Cell* 106(1):5-8.
49. Bedford MT, *et al.* (2000) Arginine methylation inhibits the binding of proline-rich ligands to Src homology 3, but

not WW, domains. *J Biol Chem* 275(21):16030-16036.

50. Friesen WJ, Massenet S, Paushkin S, Wyce A, & Dreyfuss G (2001) SMN, the product of the spinal muscular atrophy gene, binds preferentially to dimethylarginine-containing protein targets. *Mol Cell* 7(5):1111-1117.

51. Rajpurohit R, Paik WK, & Kim S (1994) Effect of enzymic methylation of heterogeneous ribonucleoprotein particle A1 on its nucleic-acid binding and controlled proteolysis. *Biochem J* 304 (Pt 3):903-909.

52. Raman B, *et al.* (2001) N(omega)-arginine dimethylation modulates the interaction between a Gly/Arg-rich peptide from human nucleolin and nucleic acids. *Nucleic Acids Res* 29(16):3377-3384.

53. Ko CY, Lin CH, Chuang JY, Chang WC, & Hsu TI (2017) MDM2 Degrades Deacetylated Nucleolin Through Ubiquitination to Promote Glioma Stem-Like Cell Enrichment for Chemotherapeutic Resistance. *Mol Neurobiol*.

54. Yuan ZL, Guan YJ, Chatterjee D, & Chin YE (2005) Stat3 dimerization regulated by reversible acetylation of a single lysine residue. *Science* 307(5707):269-273.

55. Tang Y, Zhao W, Chen Y, Zhao Y, & Gu W (2008) Acetylation is indispensable for p53 activation. *Cell* 133(4):612-626.

56. Wu DM, *et al.* (2014) Phosphorylation and changes in the distribution of nucleolin promote tumor metastasis via the PI3K/Akt pathway in colorectal carcinoma. *FEBS Lett* 588(10):1921-1929.

57. Shioda T, Fenner MH, & Isselbacher KJ (1997) MSG1 and its related protein MRG1 share a transcription activating domain. *Gene* 204(1-2):235-241.
58. Chen CM, *et al.* (2012) Functional significance of SRJ domain mutations in CITED2. *PLoS One* 7(10):e46256.
59. Chou YT, Wang H, Chen Y, Danielpour D, & Yang YC (2006) Cited2 modulates TGF-beta-mediated upregulation of MMP9. *Oncogene* 25(40):5547-5560.
60. Tien ES, Davis JW, & Vanden Heuvel JP (2004) Identification of the CREB-binding protein/p300-interacting protein CITED2 as a peroxisome proliferator-activated receptor alpha coregulator. *J Biol Chem* 279(23):24053-24063.
61. Sakai M, *et al.* (2012) CITED2 links hormonal signaling to PGC-1alpha acetylation in the regulation of gluconeogenesis. *Nat Med* 18(4):612-617.
62. Glenn DJ & Maurer RA (1999) MRG1 binds to the LIM domain of Lhx2 and may function as a coactivator to stimulate glycoprotein hormone alpha-subunit gene expression. *J Biol Chem* 274(51):36159-36167.
63. Nicholson KM & Anderson NG (2002) The protein kinase B/Akt signalling pathway in human malignancy. *Cell Signal* 14(5):381-395.
64. Du K & Montminy M (1998) CREB is a regulatory target for the protein kinase Akt/PKB. *J Biol Chem* 273(49):32377-32379.
65. Zhou BP, *et al.* (2004) Dual regulation of Snail by GSK-3beta-mediated phosphorylation in control of epithelial-

mesenchymal transition. *Nat Cell Biol* 6(10):931-940.

66. Fang D, *et al.* (2007) Phosphorylation of beta-catenin by AKT promotes beta-catenin transcriptional activity. *J Biol Chem* 282(15):11221-11229.

67. Osaki M, Oshimura M, & Ito H (2004) PI3K-Akt pathway: its functions and alterations in human cancer. *Apoptosis* 9(6):667-676.

국문 초록

전립선암 전이를 치료하기 위해 그 동안 호르몬 치료와 화학적 요법을 개발하여 많은 시도가 이루어져 왔다. 하지만 효과적인 치료 방법은 개발되지 못했고 전립선암 전이 조절 기작은 완전히 밝혀지지 않았다. 본 연구는 CITED2가 전립선암 조직에서 특이적으로 과발현 되어 있는 것을 주목하였고 이러한 발현량은 전립선암 환자의 예후와 관련이 있었다. ETS 관련 유전자 (ERG)는 전립선암 환자의 약 30% 이상 유전자 융합이 이루어져 있으며 그로 인해 ERG는 전립선암에서 과발현 되었다. 본 논문을 통해 ERG는 CITED2의 전사 인자로 작용하며 이를 기전으로 CITED2가 전립선암에서 증가된 원인을 제시하였다. ERG로 인해 과활성화된 CITED2는 PRMT5와 P300을 뉴클레오린으로 안내하여 각각 이중 메틸화와 아세틸화를 시킴으로써 뉴클레오린을 활성화시킨다. 전립선암은 PTEN 유전자의 소실로 인해 AKT가 활성화되어 있다. 하지만 앞선 기전 말고는 AKT 활성화에 대해 완전히 밝혀지지 않았다. 놀랍게도, 활성화된 뉴클레오린은 핵에서 세포질로 이동하게 되고 세포질에서 AKT mRNA의 번역을 촉진시킨다. 이를 통해 AKT의 합성이 증가되었고 증가된 AKT로 인해 활성화 형태인 p-AKT의 양 또한 증가된다. 본 논문은 전립선암 조직 중 전이 조직에서 CITED2의 발현이 높은 것에 착안하여 전립선암세포의 전이에 CITED2가 관여할 것이라 가설을 세웠다. 암세포에 CITED2를 과발현하게 되면 암세포에서 강력한 상피-중간엽 전환이 일어났으며 이러한 효과는 뉴클레오린을 억제 했을 때 상쇄되었다. 더욱이 이러한 현상이 전립선암세포주를

이식한 설치류 실험에서도 CITED2 과발현 세포주에서 암 전이가 높았으며 CITED2를 억제할 시 전이가 낮아졌고 CITED2의 하위인자인 뉴클레오린을 억제하게 되면 CITED2가 높아도 전이가 촉진되지 않음을 증명하였다.

이를 통해 CITED2-뉴클레오린 기전이 AKT를 활성화 시킴으로써 전립선암세포의 상피-중간엽 전환을 촉진시켰고 이를 기반으로 전립선암 전이가 촉진되는 것을 세포수준부터 설치류 실험과 나아가 환자 조직에서 CITED2가 전립선암 전이를 촉진시킴을 밝혔다. CITED2는 전립선암 전이 치료에 있어서 새로운 중요한 표적이 될 수 있을 것이라 기대한다.

주요어: 전립선암, 전이, CITED2, AKT, ETS 관련 유전자, PRMT5, P300, 번역 후 변형

학 번 : 2013-21776